MARTIN OLAV SABO PEDESTRIAN BRIDGE
Cable Diaphragm Plate Fracture Investigation
Minneapolis Bridge #6925, State Bridge #27B35

Minneapolis, Minnesota

Final Report
June 28, 2012
WJE No. 2012.0901

Prepared for:
Ms. Debra Brisk
Assistant County Administrator
Public Works
Hennepin County
A-2303 Government Center
300 South Sixth Street
Minneapolis, Minnesota 55487

Ms. Heidi Hamilton
Deputy Director, Public Works
City of Minneapolis
350 S. 5th Street, Rm 127
Minneapolis, Minnesota 55415

Prepared by:
Wiss, Janney, Elstner Associates, Inc.
330 Pfingsten Road
Northbrook, Illinois 60062
847.272.7400 tel | 847.291.4813 fax

WJE

MARTIN OLAV SABO PEDESTRIAN BRIDGE
Cable Diaphragm Plate Fracture Investigation
Minneapolis Bridge #6925, State Bridge #27B35

Minneapolis, Minnesota

Brian J. Santosuosso, S.E.
Senior Associate and Project Manager

Gary J. Klein, S.E.
Senior Principal and Project Advisor

Mark R. Chauvin, P.E.
Licensed Professional Engineer
Minnesota No. 42769

I hereby certify that this plan, specification, or report was prepared by me or under my direct supervision and that I am a duly Licensed Professional Engineer under the laws of the State of Minnesota.

Print Name: Mark Chauvin

Signature:

Date: 6/28/12 License # 42769

Final Report
June 28, 2012
WJE No. 2012.0901

Prepared for:
Ms. Debra Brisk
Assistant County Administrator
Public Works
Hennepin County
A-2303 Government Center
300 South Sixth Street
Minneapolis, Minnesota 55487

Ms. Heidi Hamilton
Deputy Director, Public Works
City of Minneapolis
350 S. 5th Street, Rm 127
Minneapolis, Minnesota 55415

Prepared by:
Wiss, Janney, Elstner Associates, Inc.
330 Pfingsten Road
Northbrook, Illinois 60062
847.272.7400 tel | 847.291.4813 fax

EXECUTIVE SUMMARY

Cable Diaphragm Plate 9 of the Martin Olav Sabo Pedestrian Bridge over Hiawatha Avenue fractured on the evening of Sunday February 19, 2012. The fracture was oriented so as to allow the portion of the plate connected to the two stay cables to fall to the ground, with the cables still attached. Upon review, fractures and cracks were also discovered in Cable Diaphragm Plate 8. The Diaphragm Plate 8 damage left each of the associated stay cables connected to the pylon. Winds were reported to be out of the south-southeast at 6 mph to 13 mph for several hours prior to the incident. The temperature was approximately 23 degrees Fahrenheit.

In response to this incident, Wiss, Janney, Elstner Associates, Inc. (WJE) was retained by Hennepin County and the City of Minneapolis to perform the following tasks: assist on site during stabilization of the structure; inspect the remaining in-service diaphragm plates using nondestructive test methods; determine the cause of the cable diaphragm plate failures; perform an independent review of the bridge design for Spans 1 through 3; and develop retrofit options to address any noted deficiencies.

During the investigation, nondestructive testing of the sixteen remaining in-service diaphragm plates revealed welding defects or cracks in two plates. A welding defect was removed from one plate, and a temporary redundancy fixture was installed over the other to provide load path redundancy. The other fourteen cable diaphragm plates were found to not contain cracks.

Samples from Cable Diaphragm Plates 8 and 9 were removed from the structure and analyzed to determine the cause of cracking and fracture. In addition, materials tests for physical, chemical, and toughness properties were performed. The plate samples were found contain evidence of extensive fatigue cracking prior to fracture. The steel plate material was found to be consistent with the requirements of the project specifications. It should also be noted that the cable diaphragm plate assembly geometry contains welded details that provide poor fatigue resistance.

An instrumentation program was developed and implemented to determine stresses and other structural responses to wind-induced cable vibrations. Wind speed and direction was recorded to correlate wind effects to this data. Low to moderate wind speeds with a direction approximately transverse to the structure alignment result in cable vibrations that induce damaging stress cycles at the fatigue sensitive details of the cable diaphragm plates. These vibrations occur at high frequency, resulting in a large accumulation of stress cycles over short periods of wind-induced vibration.

An independent review of the original bridge design was performed. The results from an independent finite element model revealed that the primary bridge elements were adequately designed for the reported loads. The effects of wind-induced cable vibrations were not included in the original design calculations package. However, a monitoring program was implemented following bridge construction to determine if stay cable vibrations were problematic. The results of the monitoring work indicated that stay cable vibrations were not a structural concern.

Failure of Cable Diaphragm Plates 8 and 9 occurred due to fatigue cracking that initiated at weld toes with low fatigue resistance. These welds connected the 3/4 inch thick diaphragm plates to the pylon flanges, and to the reinforcing ring plates used at the cable connection points. The fatigue cracks extended to critical size in both plates due to wind-induced cable vibrations that resulted in unstable fractures. Retrofit options to upgrade the cable diaphragm plate connections are presented.

WJE ENGINEERS ARCHITECTS MATERIALS SCIENTISTS

TABLE OF CONTENTS

Executive Summary ..... ES-i
1.0 Introduction 1
2.0 Background 1
  2.1 Structure Description 1
  2.2 Parties Involved in the Design and Construction 2
  2.3 Summary of Diaphragm Plate Failures and Structure Stabilization 2
3.0 Scope of Work 3
4.0 Nondestructive Testing 3
  4.1 Nondestructive Test Methods 3
  4.2 Nondestructive Test Results 4
5.0 Physical Measurements 5
  5.1 Cable Diaphragm Plate Alignment 5
  5.2 Pylon Flange Plastic Rotation at Cable Diaphragm Plate 8 5
6.0 Fracture Investigation 6
  6.1 Summary of Dr. Fisher's Assessment 6
  6.2 Summary of Dr. Fisher's Findings 6
7.0 Instrumentation and Monitoring Program 7
  7.1 Instruments and Installation Locations 7
  7.2 Data Acquisition System 8
  7.3 Pluck Tests 8
  7.4 Monitoring Period 9
  7.5 Effective Stress Range Calculation 10
8.0 Peer Review of Original Bridge Design 11
9.0 Review of Wind-Induced Stay Cable Vibration Phenomena 13
10.0 Structural Analysis of Diaphragm Plates 14
  10.1 Stresses Due to Cable Vibrations 14
  10.2 Stresses Due to Plate Misalignment 14
11.0 Discussion 15
12.0 Conclusions and Recommendations 17
  12.1 Conclusions and Items for Further Study 17
  12.2 Cable Diaphragm Plate Retrofit Options 17

Appendix A - John W. Fisher Report
Appendix B - Instrumentation Plan Drawings
Appendix C - Effective Stress Range Histograms
Appendix D - Preliminary Retrofit Drawings

MARTIN OLAV SABO PEDESTRIAN BRIDGE
Cable Diaphragm Plate Fracture Investigation

Minneapolis, Minnesota

1.0 INTRODUCTION

The main span of the Martin Olav Sabo Pedestrian Bridge is a cable-stayed structure consisting of a reinforced concrete deck supported by eighteen stay cables arranged in nine pairs and extending from the main pylon to deck anchorages placed along the 215 foot span. During the evening of Sunday, February 19, 2012, the diaphragm plate connecting Cables 9L and 9R fractured, disconnecting the cables from the pylon. Both cable clevises remained attached to the portion of the plate that separated from the pylon, and therefore, the cable ends descended together, landing in a grassy area east of Hiawatha Avenue. Assessment of the pylon cable connection was made by City forces immediately following discovery that Cables 9L and 9R had detached from the pylon. The City inspectors discovered that the diaphragm plate connecting Cables 8L and 8R was also cracked and fractured into two segments. However, both segments remained attached to the pylon.

Following these events, Hennepin County and the City of Minneapolis jointly engaged Wiss, Janney, Elstner Associates, Inc. (WJE) to investigate the cause of the failure and provide engineering services needed to return the structure to service. This report describes the investigation into the cause of the failure and summarizes the findings of an independent peer review of the structural design. Also, the results of WJE's inspection of the remaining diaphragm plates are presented along with preliminary options for retrofitting the cable-to-pylon connections.

2.0 BACKGROUND

2.1 Structure Description

The Martin Olav Sabo Pedestrian Bridge consists of a total of ten spans and extends over a total length of 686 feet 8 inches. An overall view of the bridge, looking northeast, is shown in Figure 1. Located southeast of downtown Minneapolis, the structure carries the Midtown Greenway and Hiawatha Bike Trail over Minnesota Trunk Highway 55 (Hiawatha Avenue) and two sets of light rail train tracks. The main span of the bridge (Span 3), oriented in an approximate east-west direction, is 215 foot long and is a cable-stayed structure. The remaining nine spans consist of conventional reinforced concrete deck and substructures that vary in length from 51 to 55 feet.

The bridge deck for the cable-stayed unit (Spans 1 through 3) was constructed using conventionally reinforced concrete construction, varying in thickness from 8 inches to 2 feet. A 2-foot thick curb section is also present along each edge of the concrete deck. A typical deck section is 18 feet wide, between curbs, and flares out to approximately 30 feet wide over Pier 2. An overall plan drawing of the bridge deck for Spans 1 to 3 is shown in Figure 2.

The reinforced concrete deck in Span 3 is supported by nine pairs stay cables (fore stays) that are attached to deck anchorages placed along the 215 foot span. Each stay cable is manufactured using multiple wires to achieve a diameter of 1 1/2 or 2 inches. At their upper end, each stay cable is attached to cable diaphragm plates at the east side of the steel pylon set on Pier 2. An additional nine pairs of stay cables (back stays) are attached to the west side of the steel pylon, using similar cable diaphragm plates. These back stays are attached to ground anchorages adjacent to Span 1, and are used to balance the fore stay

loads applied to the opposite side of the pylon. Typical cable attachments at the concrete deck, pylon, and earth anchorage are shown in Figures 3, 4, and 5, respectively.

The cable diaphragm plate anchorages are identified as Cable Diaphragm Plates 1 through 9 (bottom to top) on the east side of the pylon, and Cable Diaphragm Plates 10 through 18 (bottom to top) on the west side of the pylon, as shown in Figure 6. Each stay cable is identified by the cable diaphragm plate to which it attaches, and its position within the structure; the left side (L) of the structure is taken as north and the right side (R) of the structure is taken as south.

The pylon was constructed at a 20 degree angle from vertical and was fabricated as a built-up section using Grade HPS 70W steel for the flange and web plates. Tab plates were fillet welded to the edge of each pylon flange along the majority of its height to provide a connection for pylon screening panels.

Each cable diaphragm plate attached to the pylon was cut from 3/4 inch thick steel plate conforming to ASTM A572 Grade 50, and was welded to the inside surfaces of the 1 1/2 inch thick pylon flanges using 3/8 inch fillet welds around the entire perimeter of each interface. Holes for the clevis pins are reinforced by ring plates on each side of the diaphragm plate. Each ring plate was fillet welded (1/4 inch fillet) to the diaphragm plate all around its outside edge. A typical cable diaphragm plate is shown in Figure 7.

The concrete deck in Span 3 acts as a compression strut to resist the horizontal compression forces between the fore stays and the pylon. Compression struts were also constructed between Pier 2 and the earth anchorage blocks to resist the horizontal compression forces generated between Pier 2 and the backstay cables.

2.2 Parties Involved in the Design and Construction

Design and construction of the Martin Olav Sabo Pedestrian Bridge was commissioned by Hennepin County and the City of Minneapolis. URS Corporation (URS) designed the structure, provided review of shop drawings, and was retained by Hennepin County to provide contract and construction administration duties. Ames Construction, Inc. (Ames) was awarded the construction project and acted as General Contractor. Fabrication of the pylon and other steel components was subcontracted to PDM Bridge, LLC. Shop inspection of the steel portions of the structure was performed by the Minnesota Department of Transportation (MnDOT). Since construction, the City of Minneapolis has carried out maintenance and inspection operations.

2.3 Summary of Diaphragm Plate Failures and Structure Stabilization

The diaphragm plate connecting Cables 9L and 9R to the pylon fractured on the evening of Sunday, February 19, 2012. During their immediate response to the incident, City forces discovered that the diaphragm plate connecting Cables 8L and 8R to the pylon was also cracked, and had fractured into two segments. In addition, the left flange of the pylon had rotated out of alignment in the vicinity of the connection for Cables 8L and 8R. This rotation caused the force in Cables 8L and 8R to be reduced somewhat. Winds at the nearest major airport (MSP) were reported to be out of the south-southeast at 6 mph to 13 mph for several hours prior to the incident. The temperature was approximately 23 degrees F. No personal injuries were reported as a result of this incident.

The immediate response to stabilize the structure included erection of shoring towers underneath the reinforced concrete deck of Span 3 to support the deck in the area where Cables 8 and 9 were connected. Following installation of adequate shoring, the remaining tension in Cables 8L and 8R was released using

a hydraulic jacking system and winch system. The cables were then disconnected from the fractured diaphragm plate at the pylon.

Following these operations, the pylon screening panels in the vicinity of the cable diaphragm plates were removed to allow access for detailed nondestructive testing of the remaining in-service diaphragm plates. Defects or cracks were located in Cable Diaphragm Plates 7 and 5. The defect in Cable Diaphragm Plate 7 was removed. However, two cracks observed in Cable Diaphragm Plate 5 prompted the design and installation of a temporary redundancy fixture to provide load path redundancy for the cracked diaphragm plate.

3.0 SCOPE OF WORK

WJE was retained by Hennepin County and the City of Minneapolis to perform the following tasks:

1. Assist on site during stabilization of the structure.
2. Inspect the remaining in-service diaphragm plates using nondestructive test methods.
3. Determine the cause of the cable diaphragm plate failures.
4. Perform an independent review of the bridge design for Spans 1 through 3.
5. Develop retrofit options to address any noted deficiencies.

This report describes the investigation into the cause of the failure and summarizes the findings of the peer review of the structural design. Also, the results of WJE's inspection of the remaining diaphragm plates are presented along with preliminary options for retrofitting the cable-to-pylon connections. The assignment of fault for any party responsible for the design, fabrication, erection, or maintenance of the structure is beyond this scope of work.

4.0 NONDESTRUCTIVE TESTING

Various nondestructive test methods were used to assess the sixteen remaining in-service cable diaphragm plates to determine if these plates contained unknown welding defects or cracks. These examinations took place between February 23 and 25, 2012.

4.1 Nondestructive Test Methods

Visual, magnetic particle, and ultrasonic test methods were used for condition evaluation of all cable diaphragm plates, except for Cable Diaphragm Plates 8 and 9 where fractures had already occurred. Visual examinations and magnetic particle testing (MT) were aided by flashlights for illumination of dark areas and a mirror for observation in areas with restricted viewing access. MT was limited due to constraints of access. The upper sides of all plates were sufficiently accessible for MT examination, but portions of lower sides of many plates were not accessible. This condition was most prevalent at the west side of the pylon, where lower plate surfaces were inaccessible except for visual examinations.

MT was performed in accordance with the provisions of ASTM E-709. An alternating current yoke was used for the induction of magnetic fields, in conjunction with application of an inspection medium of red dry particles for examinations of welded joints and diaphragm plate regions. Magnetic fields were oriented to the fullest possible extent for detection of cracks or defects, although ideal positioning of the yoke was not always possible due to the constraints of the assembly. Figure 8 shows a typical application

for evaluation by MT of a fillet welded joint. All examinations were performed with paint coatings in place, except for local removal where indications were detected.

Ultrasonic testing (UT) was performed using conventional pulse echo equipment. Calibrations of the test apparatus followed the provisions of AWS D1.1 for linearity and sensitivity. A scanning plan was implemented for detection of potential crack initiations using multiple probe angles and orientations. Ultrasonic scans were directed toward the toes of all fillet welded joints, as well as toward respective regions of the diaphragm plates along the fracture surfaces exhibited by Cable Diaphragm Plates 8 and 9. In general, all scans were introduced from the top surface of the subject diaphragm plate. Figure 9 shows UT in progress, scanning the diaphragm plate toward the fillet welded joint connecting a representative ring plate.

A summary of primary equipment used in nondestructive examinations is provided in Table 1.

4.2 Nondestructive Test Results

Examinations of the cable diaphragm plates emphasized detection of crack initiations. Use of multiple nondestructive methods facilitated complete coverage of potential crack initiation sites by at least one method, and in many instances confirmed the assessment based on the complimentary methods. The magnetic particle method is sensitive to surface cracks and may enhance detection of cracks that are too fine for visual observation. In addition, the penetrating nature of ultrasonic waves permitted volumetric examination through the thickness of the subject plates.

The fabricated edges of the diaphragm plates resulted in a variation of gaps at the connection, with a wider gap at the lower side of the plates. In general, the fillet welded joints appeared to be of uniform size and profile, although no actual sizing of the fillets was carried out using gages. UT indicated additional, but inconsistent fusion below the theoretical root in portions of some joints. In many instances, a fillet welded joint for attachment of the pylon screen tab plate intersects with the termination of the diaphragm plate fillet weld completion around the pylon flange tip.

Discontinuities were detected in two of the in-service cable diaphragm plates. In Cable Diaphragm Plate 7, a crack was detected at the right flange tip by MT, as shown in Figure 10. This defect was removed by grinding less than 1/4 inch of material with a die grinder. This discontinuity appeared to be the result of non-fusion within the welded joint, but was located in a prime location for crack initiation. In addition, cracks originating in Cable Diaphragm Plate 5 near the toe of the diaphragm plate-to-pylon flange welds were detected. These cracks extended along the bottom plate surface and exhibited lengths of 3/4 inches and 1 1/2 inches at the right and left pylon flange tips, respectively. These defects are shown in Figures 11 and 12, respectively. Removal of the painted coating revealed a slight length increase in comparison with the initial observations. UT corroborated these findings and confirmed that no further extension was present.

Embedded discontinuities and cracks were generally discernible with UT, except for very small indications at the pylon flange tips. These could not be distinguished from the component geometry using UT methods. In these flange tip locations, MT provided an adequate evaluation. With the volumetric penetration of UT, and MT aided by visual inspection of accessible areas, virtually all regions of potential crack initiation were examined.

5.0 PHYSICAL MEASUREMENTS

Measurements were taken to define the approximate alignment for each cable diaphragm plate and to define the extent of plastic pylon flange deformations of the left flange plate at its connection to Cable Diaphragm Plate 8.

5.1 Cable Diaphragm Plate Alignment

WJE carried out three independent methods of measurement to define the cable diaphragm plate alignments with respect to the pylon web plate. The first method included use of a tape measure (direct measurements) to determine the distance from the face of the pylon web to the top and bottom corners of the subject cable diaphragm plate, or use of a protractor type measurement device. The direct measurements, if used, were used to create a scaled drawing of the plate alignment in AutoCAD from which the alignment angle was reported.

As an alternate measurement method, a Bosch Model DAF220 digital miter finder was used to directly report the angle between the top of each cable diaphragm plate and the pylon web plate. This instrument has a digital output that reports the angle to the nearest 0.1 degrees.

Lastly, a Stabila Type 96 digital level was used to measure the absolute attitude of each cable diaphragm plate and the pylon web adjacent to each plate. The plate alignment angle was then calculated using these values. The Stabila instrument has a digital output that reports the angle of the instrument to the nearest 0.1 degrees.

The results of the three forms of cable diaphragm plate alignment measurement are included in Table 2. For reference, the cable diaphragm plate alignments included in the design and shop drawings for each plate and deviations from these values are included in the table. It should be noted that the accuracy of the reported measurements is anticipated to be within 0.5 degrees due to geometric constraints of the structure, paint thickness or debris in the vicinity of the measurement locations, and limitations of the measurement devices. Design alignment values were given as the angle between the center of the pylon web and the center of the cable diaphragm plate to a precise value including degrees, minutes, and seconds. For example, the intended alignment of Cable Diaphragm Plate 9 was given as 49°21’34” on both the design and shop drawing sets.

All but three of the eighteen cable diaphragm plates were found to be aligned within about 0.5 degrees of the design alignment values. Cable Diaphragm Plates 6, 9, and 10 were determined to out of alignment by about 2.87 degrees, 4.46 degrees, and -4.56 degrees, respectively. (Positive values of misalignment represent rotation up.) Review of the allowable fabrication tolerances that make up the cable diaphragm plate alignment indicates that an acceptable plate alignment would be within about ±1 degree of that specified in the design drawings.

5.2 Pylon Flange Plastic Rotation at Cable Diaphragm Plate 8

The distance between the pylon flange tips was measured at several locations in the vicinity of Cable Diaphragm Plate 8 following fracture. It was determined that the outstanding edge of the 1 1/2 inch thick left pylon flange had been deformed out if its original alignment by a maximum of about 7/8 inches. This deformation took place over an approximate distance of 19 inches along the flange in the vicinity of the cable diaphragm plate connection.

6.0 FRACTURE INVESTIGATION

An in-depth assessment was carried out for the fracture surfaces of Cable Diaphragm Plates 8 and 9. The plate segment from Cable Diaphragm Plate 9 that separated from the pylon was sent to WJE's subconsultant, John W. Fisher and Associates, Inc. Dr. Fisher indicated upon initial review of the plate segment that the fracture surfaces had been damaged during the fall to the ground. In addition, the fracture path for each plate was different. A segment of Cable Diaphragm Plate 9 including the ring plates and cable clevises separated from the pylon, as shown in Figures 13 and 14. The Cable Diaphragm Plate 8 fracture path included the right side plate connection weld to the pylon flange tip and the back of the right ring plates. This fracture then extended up through the center section of the plate, as shown in Figure 15. This fracture path allowed Cables 8 to remain connected to the pylon. However, the left pylon flange was plastically deformed out of plane as shown in Figure 16.

WJE developed and implemented a fracture sample removal plan to recover the remaining portion of Cable Diaphragm Plate 9 and the two attached segments of Cable Diaphragm Plate 8 from the pylon. This removal plan included coring the pylon flange tips to completely remove and preserve the end of the weld terminations connecting the cable diaphragm plates to the pylon flanges. The removed segments of Cable Diaphragm Plates 8 and 9 are shown shortly after removal in Figures 17 and 18, respectively. All fracture samples were sent to Dr. Fisher for fractographic assessment. A summary of Dr. Fisher's evaluation and findings is included below. The complete report document, titled "Report on the cracking that developed in the Cable Stay diaphragm plates of the Martin Olav Sabo Pedestrian Bridge," authored by John W. Fisher and Eric J. Kaufmann, and dated May 24, 2012 (John W. Fisher Report), is included as Appendix A.

6.1 Summary of Dr. Fisher's Assessment

Dr. Fisher performed a visual examination of each fracture surface; a fractographic evaluation of selected areas of the fracture surfaces from each of Cable Diaphragm Plates 8 and 9; materials tests for physical, chemical, and toughness properties of the cable diaphragm plate material; a fractographic assessment of selected fracture surfaces using a scanning electron microscope (SEM); a review of the fatigue resistance of the welded details; and a metallographic assessment of a representative set of ring plate-to-diaphragm plate welds.

6.2 Summary of Dr. Fisher's Findings

A summary of the findings from the John W. Fisher Report are provided below.

- The welded details used on the cable diaphragm plates provide low fatigue resistance, consistent with Category E or E´.
- Prior to its fracture, Cable Diaphragm Plate 8 sustained fatigue cracking with approximately 7 1/2 inches of stable growth occurring at the right side of the plate between the lower end of the pylon flange-to-diaphragm plate weld and the right ring plate-to-diaphragm plate weld, initiating in both locations. These two fatigue cracks coalesced and then extended in an unstable manner to intersect the top edge of the plate, dividing the plate into two pieces. A similar but shorter fatigue crack existed at the left side of the plate, initiating at the lower end of the pylon flange-to-diaphragm plate weld, but there were no signs of significant unstable crack extension.
- Cable Diaphragm Plate 9 sustained extensive fatigue cracking before it fractured. A stable crack extension of approximately 11 1/4 inches occurred at the right side of the plate between the pylon flange-to-diaphragm plate weld and the right ring plate-to-diaphragm plate weld, initiating in both

locations. A separate stable crack extension of about 9 inches was found at the left ring plate weld. These fatigue cracks in Cable Diaphragm Plate 9 extended in an unstable manner, separating the complete front section of the diaphragm plate, including the ring plates, from the remainder of the plate.

- The noted fatigue cracks initiated from the top surface of both cable diaphragm plates, indicating that the applied cable forces and plate geometry created some degree of initial bending in the plates.
- The noted fatigue cracks initiated and extended due to cyclic stresses caused by wind-induced cable vibrations.
- Welding defects including embedded slag and porosity existed in the portion of the fillet welded connection to the pylon flanges that wrapped around the lower end of the subject cable diaphragm plates. However, these welding defects did not influence the weld toe cracks that formed in the diaphragm plates.
- The steel plate material conformed to the design specifications and provided good toughness.

7.0 INSTRUMENTATION AND MONITORING PROGRAM

An instrumentation and monitoring program was developed and implemented to measure stresses, cable vibrations, and other structural responses at selected locations. The instrumentation measured the structural response to "pluck testing" of instrumented cables as well as ambient conditions over a monitoring period of about 18 days.

7.1 Instruments and Installation Locations

Accelerometers, strain gages, displacement transducers, thermocouples, and wind anemometers were used to determine structural responses to environmental and induced loadings. All sensors were installed during the week of April 16, 2012. A description of each type of sensor and its installation location is included below. Instrumentation plan drawing Sheets Si-1 through Si-5 are included as Appendix B.

Strain Gages. A total of 24 bondable strain gages, Type CEA-06-125UN-350 manufactured by Vishay Micro-Measurements, Inc., were used for this installation. Strain gages were installed on Cable Diaphragm Plates 7 and 6 back-to-back (top side and bottom side) at the locations shown on Sheets Si-2 and Si-3 in Appendix B, for a total of 12 strain gages on each plate. A typical strain gage is shown in Figure 19 prior to application of environmental protection for water resistance.

Accelerometers. Eight uniaxial accelerometers, Model 353B33 manufactured by PCB Piezotronics, Inc., were mounted on Cables 6L, 6R, 7L, and 7R. Two accelerometers were mounted on each cable using a mounting cube fastened to an aluminum ring used to clamp the stay cable, as shown in Figure 20. These accelerometers were positioned to measure lateral and vertical cable vibrations. The mounting locations along the cables were determined on-site during a period of cable vibrations. The accelerometers mounted on Cables 7 and Cables 6 were positioned approximately 9 feet and 7 1/2 feet from the pylon cable anchor point (measured from the center of the clevis pin), respectively.

Displacement Transducers. A total of two linear variable displacement transducers (LVDTs), Model 242-000, ±0.25 inch, manufactured by Trans-Tek, were used to monitor the displacement of the outstanding edge of Cable Diaphragm Plates 7 and 6. Special fixtures were fabricated for each installation location to allow the displacement transducer armature to be mounted to the bottom surface of the subject diaphragm plate near the tip of the plate as close as possible to the plate centerline, as shown in Figure 21.

Out-of-plane (up and down) displacements were measured at each location. Installation details are given on Sheets Si-4 and Si-5 in Appendix B.

Wind Speed and Direction. Two wind anemometers, Model 5103 manufactured by R. M. Young Co., were used to measure wind speed and direction at selected locations on the structure. One wind monitor was mounted 5 feet above the top of the pylon using a fixture attached to the pylon cap plate. The other wind monitor was mounted 10 feet above the top surface of the left curb between Cables 3L and 4L, as shown in Figure 22. For reference, project north (0 degrees) was taken as perpendicular left of the longitudinal centerline of Span 3. Increasing degrees were taken clockwise looking down like a compass.

Temperature. A total of three thermocouples were used to monitor the temperature of the concrete at the pylon base connection, the steel pylon web between Cable Diaphragm Plates 7 and 6, and the air temperature at the data acquisition enclosure. Type T thermocouple wire manufactured Omega was used for this installation.

7.2 Data Acquisition System

A CR9000X data logger manufactured by Campbell Scientific, Inc., was used to monitor responses from all instruments. This high speed data acquisition system provides precision measurements and is rugged for field use applications. The system was outfitted with eight I/O modules to accommodate the number of sensors used for this installation: one CR9050 Analog Input w/ RTD, one CR9060 Excitation Module, and six CR9052DC Filtered Analog Input Modules with DC excitation. This data logger was supplemented using a Model 483B07 ICP Signal Conditioner manufactured by PCB Piezotronics, Inc. to excite and pass signals from the accelerometers. The data acquisition equipment is shown in Figure 23.

The data acquisition system was installed in a steel tool box enclosure mounted on the bridge deck near the base of the steel pylon. All instrumentation wire was routed from the instruments to the data acquisition system and was attached to the structure using a combination of cable ties and beam clamps.

7.3 Pluck Tests

A total of four pluck tests were performed to determine structural responses to known loading. One pluck test was performed on each of Cables 7L, 7R, 6L, and 6R. For each pluck test, a 250 pound force was applied to the subject cable approximately perpendicular to the cable alignment in the vertical plane. A hydraulic tension ram was used in line with a load cell to apply the force into the cable. Following load application, a quick-release connector was used to instantaneously release the applied force, and the structural response was recorded. Cable vibrations due to ambient winds were minimal at the time the pluck tests were performed.

The loading equipment for the four pluck tests was attached to the subject cables as follows:

Cable	Total Cable Length (feet)	Approximate Pluck Test Location (feet from pylon anchor point)
6L	180.588	58
6R	180.664	38
7L	204.712	62
7R	204.782	42

Recorded stress ranges for the cable diaphragm plates in response to the pluck tests are included in Table 3. Note that the stress range values reported in Table 3 were taken from the first major stress cycle following load release. In general, the location of the highest stress range for each respective cable diaphragm plate and pluck test was similar. The highest stress ranges were recorded at the strain gages positioned perpendicular to the ring plate welds at the midpoint between the cable alignment and the weld wrap around where the plate is attached to the pylon flange on the same side of the plate where the loaded cable connects. These stress ranges were 3.1 ksi to 3.4 ksi for Cable Diaphragm Plate 7 and 3.3 ksi to 3.8 ksi for Cable Diaphragm Plate 6. Note that the digital strain measurements collected from each strain gage were converted to stress using the equation $S_r = \varepsilon_r \times E$, where ε_r is a strain range determined from the response of the gage and E is the modulus of elasticity for steel, which was taken as 30,000,000 psi. All stress readings were stored on the data acquisition equipment in units of pounds per square inch (psi). Representative stress data plots for these tests are included in Figures 24 through 31.

Accelerations recorded during the pluck test indicate that multiple modes of vibration participated in the cable response. Figure 32 includes a normalized Fast Fourier Transform (FFT) analysis plot of the vertical acceleration data from the pluck test performed on Cable 7L. This data was double-integrated to determine the magnitude of approximate displacements at the accelerometer locations. Figure 33 shows a plot of approximate displacements at the vertical accelerometer location for Cable 7L (Accelerometer Accel01) during the Cable 7L Pluck Test. The peak-to-peak displacement of the cable during this test was approximately 0.3 inches at the location of the accelerometer. No approximation of maximum cable amplitude or location for this maximum can be made using data from this one location along the cable due to the participation of multiple vibration modes.

7.4 Monitoring Period

The monitoring period consisted of a continuous 18 day period over which data was recorded to determine structural responses to ambient winds. During this time, data from all strain gages, displacement transducers, accelerometers, and wind anemometers was recorded during “triggered events”, when threshold values set in the data acquisition program were exceeded. In addition, the data acquisition system was used to perform real-time analysis of the stress range data to allow calculation of the effective stress range for each instrumented location.

About 225 triggered events were stored throughout the monitoring period. Each triggered event represents a period of about one minute during which stress data from selected strain gages exceeded set limits. The threshold was adjusted to capture events with large stress ranges without filling the data acquisition memory allotment.

Data from ten representative events was reduced and evaluated. A summary of the event number, time, average wind speed, average wind direction, maximum stress range, and corresponding plate tip displacement is included in Table 4. The wind direction values for these triggered events indicate that cable vibration is most active for the instrumented cables when the wind blows within 30 degrees of north (0 degrees) or south (180 degrees). The range of average wind speeds is 6 mph to 25 mph for these ten events. Note that no significant rain was reported during the occurrence any of the selected events. Maximum stress range values for the strain gage indicated in the table ranged from 5.9 ksi to 7.6 ksi. Note that the highest wind speed for this group occurred at the top of the pylon during Event 224 with a wind speed of 38 mph.

Selected stress data plots from Events 007 and 225 are included as Figures 34 and 35, respectively. As seen in the stress data presented, the vibration characteristics vary with wind speed and direction. The stress data presented for Event 007 is affected primarily by the 11th, 12th, and 14th modes of vibration of Cables 7, as shown in the normalized FFT of this stress data shown in Figure 36. Note that this FFT mode signature represents a superposition of mode shapes from both Cables 7L and 7R. Figures 37, 38, and 39 include FFT data for Cable 7L (Accelerometer Accel01), 7R (Accelerometer Accel03), and the superposition of these two, respectively. Note that the dominant mode signatures from Figures 36 and 39 are similar.

The stress data presented for Event 225 is affected primarily by the 7th mode of vibration of Cables 7. FFT data for Strain Gage SG11 (stress data presented in Figure 35 above) and the superposition of FFT data from Accelerometers Accel01 and Accel03 are shown in Figures 40 and 41, respectively. These two FFT data plots are similar.

Due to the dominance of cable mode 7 in the data presented for Event 225, the available accelerometer data for this event was double-integrated to produce a plot of approximate displacements at the accelerometer locations. Figures 42 and 43 are plots of approximate vertical displacements at Accelerometers Accel01 (Cable 7L) and Accel03 (Cable 7R). Maximum displacements at the accelerometer locations for Accel01 and Accel03 were 0.16 inches and 0.43 inches peak-to-peak, respectively. This data indicates that the high stress ranges shown in Figure 35 can be generated due to small displacements at higher modes of vibration. The higher vibration modes essentially shorten the length of the cable between nodes and therefore increase the rotation demand at the pylon anchorage for similar peak-to-peak displacements.

7.5 Effective Stress Range Calculation

The recorded stress data from each strain gage was analyzed to produce a stress histogram for each instrumented location. Rainflow analysis in accordance with ASTM E1049 was performed by the data acquisition system on-board and was used to produce stress histograms with stress bin sizes of 150 psi. A representative stress histogram for Strain Gage SG02 is shown in Figure 44. Stress histograms for all strain gages are included in Appendix C. Miner's Rule, given below, was then used to calculate the effective stress range, S_{re}, at each gage location. The purpose of the effective stress range calculation is to provide a "weighted" average of the amount of damage caused by a random loading pattern at a particular instrumented detail. The effective stress range provides a means of relating random variable stress cycles to constant amplitude stress cycle data.

Miner's Rule for a variable stress spectrum is as follows:

$$S_{re} = \left[\sum \gamma_i S_r^3\right]^{1/3}$$

where:
S_{re} is the effective stress range
γ_i is the ratio of the number of occurrences (counts) of S_r to the total number of stress cycles
S_r is the actual measured stress range at the detail under consideration

Calculation of the effective stress range at each location was performed using the stress histograms produced by the rainflow analysis with the bin cut-off set at 50 percent of the constant amplitude fatigue limit for the Category E details. This equates to a bin cut-off of 2.25 ksi. The fifty percent cutoff has been

recommended by Dr. Fisher and serves to eliminate the contribution of stress cycles that are smaller in magnitude.

A summary of the calculated effective stress range for all strain gaged locations over the 18 day monitoring period is included in Table 5. The S_{re} values ranged from 2.5 ksi to 3.9 ksi across all locations. It should be noted that cycle count data from the majority of the instrumented locations includes more than 0.01 percent of the total cycle counts greater than the constant amplitude fatigue limit (CAFL) for Category E details (4.5 ksi). In addition, about 2,000,000 stress cycles accumulated at strain gages SG02, SG05, and SG08 during the 18 day period.

8.0 PEER REVIEW OF ORIGINAL BRIDGE DESIGN

The tasks performed by WJE included a peer review of the original design for Spans 1 to 3 of the bridge structure. This task included a review of the structural calculations, prepared by URS, for the primary structural elements, including the cables, pylon, deck, and piers. The following documents were used for the basis of the peer review task:

- Design Drawings for Bridge No 27B35, Sheets B1 through B98, dated April 18, 2006
- 29th Street Greenway, Pedestrian Bridge Spans 1 to 3 Calcs, Volume 1 of 3, Dated 4-21-2006
- 29th Street Greenway, Pedestrian Bridge Spans 1 to 3 Calcs, Volume 2 of 3, Dated 4-21-2006
- 29th Street Greenway, Pedestrian Bridge Spans 1 to 3 Calcs, Volume 3 of 3, Dated 4-21-2006
- 29th Street Midtown Greenway Cable-Stayed Bridge, *Inspection and Maintenance Manual*, Version 1, February 2008
- "Response to WJE Project Summary of Evaluation of Sabo Bridge Cable Failure," authored by Dr. Steven L. Stroh of URS Corporation, transmitted to WJE on June 25, 2012

The original structural design drawings and applicable portions of the calculations were reviewed for general compliance with the structural requirements with the design standards. Sheet B1 of the original design drawings indicates that the following design standards were used:

- American Association of State Highway and Transportation Officials (AASHTO), *Guide Specifications for Design of Pedestrian Bridges*, August 1997
- AASHTO, Standard Specifications for Highway Bridges, 2002 and Interims, Load Factor Design (LFD) Method
- CEB/FIP Model Code for Concrete Structures
- 1978 Post-Tensioning Institute (PTI), Recommendations for Stay Cable Design

The peer review effort focused on selected details for the primary structural elements. In addition, an independent finite-element analysis model was created and independent calculations were performed to verify the results of the original analysis and design. This review did not include a review of every detail or component of the design; therefore, in no way does this review relieve the designer of record from responsibility for the design. The peer review approach and findings are summarized in the following paragraphs.

WJE developed an independent finite-element model of Spans 1 through 3 to evaluate forces in the primary elements of the bridge structure. This finite-element model, shown in Figure 45, was created

using SAP2000 computer analysis software. Linear frame elements were used to represent the cables, pylon, and piers, while quadrilateral shell elements were used for the concrete deck. Each element in the model was assigned properties based on the properties of the corresponding member in the bridge structure.

The independent finite-element model considered dead loads (self-weight of the bridge elements) and staged construction modeling techniques were utilized to generate dead load cable forces as specified on the original design drawings. After the structural model was completed, an 85 pounds per square foot (psf) pedestrian live load was applied to the deck surface. Under certain loading scenarios, the pedestrian live load was reduced to 65 psf in accordance with the applicable design standards. In addition, H-10 vehicle loading was considered. Static forces resulting from wind and thermal loads were also evaluated.

The peer review focused on evaluating member forces and capacities for the as-designed bridge structure; however, the *Inspection and Maintenance Manual* for the structure states that "The stay cable anchorage brackets are not considered fracture critical elements since the failure of any one bracket will not jeopardize the stability of the bridge system." This Manual goes on to state that "the steel cable diaphragm plates are also not considered fracture critical elements since the loss of any one plate will not jeopardize the stability of the bridge." Therefore, the WJE analysis model assumed failure of a single cable or a pair of cables at various locations in order to determine the increase in force at the remaining cables. The cable failures in the analysis were considered when the bridge is subjected to the full design live load.

The results of the independent analysis model were summarized to determine forces in various primary structural members for the controlling load cases. The independently-calculated forces were used to verify forces reported in the original design calculations package. Once the forces were verified, a review of the original design calculations package was performed. This review concentrated on strength limit states of the bridge elements; however, selected serviceability limit states were also checked, such as live load deflections of the bridge deck and pedestrian-induces footfall vibrations on the bridge deck.

The peer review and independent analysis performed by WJE revealed the following:

- Forces in the primary structural elements determined from WJE's independent finite element analysis model are in general agreement with those reported in the original design calculations package.
- The design for static loads was in general accordance with the specified standards.
- The primary structural bridge elements are adequate for the reported design loads.
- Although adequately designed for strength, the member design was often efficient as there were not significant levels of reserve capacity.
- Under full live load, the deflections of the concrete deck were in the range of L/500.
- A modal analysis performed using the WJE independent finite-element model revealed the fundamental frequency of the bridge structure to be less than 3 Hz, which is not in accordance with the AASHTO Design Standards. URS considered several approaches to evaluate pedestrian-induced footfall vibrations of the bridge deck and found them to be acceptable.

- Wind-induced stay cable vibrations were not included in the original design calculations package, but they were considered in the original design[1].
- Failure of a single cable or pair of cables redistributes the dead and live loads to the remaining cables. The WJE independent analysis revealed that the adjacent cables have a significant increase in cable force. However, it should be noted that the adequacy of these adjacent cables was determined using a 33% increase in allowable stress as suggested by the project design standard authored by PTI.
- Checks of other members after a failure of a single cable or pair of cables, such as the pylon, pylon anchorage plates, deck anchorages, and the reinforced concrete deck did not appear to be included in the original design calculations package.

9.0 REVIEW OF WIND-INDUCED STAY CABLE VIBRATION PHENOMENA

Wind-induced stay cable vibration can be attributed to several phenomena. The four most prevalent phenomena to be considered during evaluation of stay cables are vortex shedding, excitation due to interactions of rain and wind, wake galloping of cable groups, and galloping of individual inclined cables[2]. A brief discussion of each is included below:

Vortex Shedding. During occurrence of this phenomenon, the shedding of alternating wind vortices occurs as air flows past the subject stay cable. This effect can cause a cable to resonate in one of its fundamental modes if the frequency of alternation of the wind vortices matches the fundamental frequency of the cable, which typically occurs when the wind flow is perpendicular to the cable alignment. The amplitude of cable vibrations in response to vortex shedding is typically small and occurs at low wind speeds. This phenomenon can typically be controlled with even a small amount of damping.

Rain-Wind Interaction. Rain-wind interaction occurs when moderate rainfall causes rivulets of water to form on the surfaces of cables. These water rivulets cause a change in the aerodynamic properties of the cable by fundamentally changing the overall shape of the cable as it is exposed to wind action. Moderate wind speeds have been documented to cause large amplitude cable vibrations due to this phenomenon. This phenomenon can typically be controlled by altering the surface roughness of the smooth cable to prevent water rivulet formation.

Wake Galloping of Cable Groups. This phenomenon occurs at high wind speeds and results in large amplitude cable oscillations when cables are in the wake of other elements, causing variations in drag and wind forces. This phenomenon is not typically a consideration for separated cable alignments.

Galloping of Individual Inclined Cables. The inclination of long stay cables can theoretically cause large amplitude vibrations due to high wind speed with appropriate direction. Recent wind tunnel testing performed to study this phenomenon indicates that a small amount of damping can prevent resulting cable vibrations.

---

[1] URS's "Response to WJE Project Summary of Evaluation of Sabo Bridge Cable Failure," dated June 25, 2012, indicates that URS considered wind-induced vibrations during design but deferred a final decision on providing a stay cable damping system until after construction. After periodically monitoring cable vibrations over a period of 30 days, URS concluded that the observed vibrations were acceptable and stay cable dampers were not necessary.

[2] Kumarasena, S., Jones, N., Irwin, P., Taylor, P., "Wind-Induced Vibration of Stay Cables", Publication No. FHWA-HRT-05-083, McLean, VA. : U.S. Dept. of Transportation, Federal Highway Administration, Research, Development, and Technology, Turner-Fairbank Highway Research Center, August 2007 (Citation applies for all of Section 9)

Other Phenomena. Stay cable vibrations can be attributed to the effects of other phenomena. These include live load effects, deck and stay cable interaction, and natural effects such as ice formation on the stays, which would alter the aerodynamic properties of the cable (similar to the effects of rain-wind interaction).

The effects of all wind related phenomena on the magnitude of stay cable vibration amplitudes are typically controlled by increasing the mass of the cable, increasing the damping of the cable system, providing cable cross-ties, and/or altering the cable surface roughness.

As discussed in Section 11, the observed stay cable vibrations are the result of vortex shedding.

10.0 STRUCTURAL ANALYSIS OF DIAPHRAGM PLATES

A finite element analysis (FEA) model of a cable diaphragm plate was developed and analyzed using SAP 2000, a proprietary software program developed for static and dynamic analysis of structures using finite elements. The FEA model was used to evaluate stresses due to cable vibrations and plate misalignment. A rendering of the FEA model is shown in Figure 46. The model was based on the dimensions of Cable Diaphragm Plate 7, which are similar to the dimensions of Cable Diaphragm Plates 8 and 9.

10.1 Stresses Due to Cable Vibrations

Wind-induced vibrations in the vertical plane cause cyclical bending moments in the diaphragm plates. The analysis focused on Event 225 (refer to section 7.4), which caused steady-state vibrations of Cables 7L and 7R in the seventh mode, with a zero-to-peak amplitude of 0.217 inches at a frequency of about 11 Hz. Note that the reported zero-to-peak amplitude value was for Cable 7R and this displacement was measured at the location of Accelerometer Accel03. The measured zero-to-peak stress is approximately 3.5 ksi at the location of Strain Gage SG11, as can be seen in Figure 35. The measured zero-to-peak deflection of the diaphragm plate was 0.006 inches.

To provide an independent correlation between the measured vibrations and diaphragm plate deflections, a bending moment was applied in the model at each clevis pin hole until the plate deflections matched the measurement of 0.006 inches. The resulting maximum bending stresses at the surface of the plate are plotted in Figure 47. The strain gage locations are also shown. As can be seen, the stress predicted by the model at Strain Gauge SG11 is approximately 2.1 ksi, which is comparable to but somewhat less than the measured stress. Note that the amplitude of vibration for Cables 7L and 7R during Event 225 was not equal although the vibrations were in phase. Therefore, direct comparison of the measured stresses to the results of an evenly loaded finite element model is somewhat difficult.

10.2 Stresses Due to Plate Misalignment

If the angle of the cable is not aligned with the diaphragm plate, cable tension will induce bending stresses in the diaphragm plate. The bending force is approximately equal to the tension force in the cable times the sin of the misalignment angle times the distance from the hole to the end of the clevis assembly. Diaphragm Plate 9 was misaligned by approximately 4.5 degrees, as shown in Table 2. The project drawings indicate a long-term dead load force of 79.8 kips in Cables 9L and 9R. The calculated bending moment due to the misalignment is 210 inch-kips. The resulting maximum bending stresses at the surface of the plate are plotted in Figure 48. As can be seen in this figure, there is a small region of relatively high stress near the end of the pylon flange, and the stresses approach or exceed the yield stress of 60 ksi

between the end of the pylon flange and back of the ring plate. The significance of the misalignment stresses is discussed in Section 11.

The project drawings also indicate a temperature force of 8.2 kips in Cables 9L and 9R, which is about 10 percent of the dead load force. (The live load force in Cables 9L and 9R is only 0.5 kips, according to the drawings.) Thus, the combination of misalignment and extreme temperature change results in stresses equal to about 10 percent of those plotted in Figure 48. Actual stresses over the last five years are somewhat less because temperatures in Minneapolis have been well within the design extreme temperatures of -30 degrees F and 120 degrees F. Regardless, thermal stresses are comparable to those measured and calculated due to wind-induced vibrations, but the number of cycles are less by several orders of magnitude.

11.0 DISCUSSION

The stay cable system used for the Martin Olav Sabo Pedestrian Bridge includes a total of eighteen cable diaphragm plates to connect the cables to the steel pylon. Two of the eighteen plates fractured, resulting in Cables 9L and 9R detaching from the pylon, and the need to relieve and remove Cables 8L and 8R. An additional two of the remaining sixteen in-service cable diaphragm plates were found to contain defects or cracks that had to be addressed following the discovery of the two fractured plates. At Cable Diaphragm Plate 7, the noted weld defect was removed by grinding to remove about 1/4 inch of material. A redundancy fixture was installed at Cable Diaphragm Plate 5 to provide load path redundancy around the cracks located at the edges of the plate.

The discontinuities discovered in Cable Diaphragm Plates 7 and 5 were located using appropriate nondestructive test methods. No other discontinuities of significance were detected in the other in-service diaphragm plates. Comprehensive evaluations of the cable diaphragm plates included visual, magnetic particle, and ultrasonic methods. The combined application of visual, magnetic particle, and ultrasonic examination methods includes overlapping and complimentary coverage, and extends confidence to these assessments.

The cable diaphragm plate assemblies include thick reinforcement rings that are fillet welded to the comparatively thin diaphragm plates. In turn, the diaphragm plates are fillet welded to the thick pylon flanges. These welded connection details provide poor fatigue resistance in conformance with Category E or E´.

Physical measurements of the alignment for all cable diaphragm plates were performed. The results of this work indicate that the majority of the cable diaphragm plates were installed within about 0.5 degrees of the alignment prescribed on the design drawings. The alignment of Cable Diaphragm Plates 6, 9, and 10 was found to be 2.87 degrees, 4.46 degrees, and -4.56 degrees away from the design alignment, respectively. These values are outside of the accepted tolerance of about ±1 degree.

A representative cable diaphragm plate was analyzed for the combined effects of misalignment and temperature change. This analysis considered the static effects on the stress field within the diaphragm plate due to the misalignment. Also considered was the calculated fluctuation in cable tension due to temperature fluctuations. The effects of these increased static stresses on the cable diaphragm plates over those which were anticipated during design may have attributed to the path along which fatigue cracks driven by wind-induced cable vibrations extended. Thermal stresses are comparable to those measured and calculated due to wind-induced vibrations, but the number of cycles are less by several orders of

magnitude. As such, thermal stresses are not considered an important contributing factor to the fatigue damage.

Examinations of the fracture surfaces for Cable Diaphragm Plates 8 and 9 revealed the presence of significant stable fatigue crack growth prior to fracture. Cable Diaphragm Plate 8 sustained fatigue cracking with approximately 7 1/2 inches of stable growth occurring at the right side of the plate between the lower end of the pylon flange-to-diaphragm plate weld and the right ring plate-to-diaphragm plate weld, initiating in both locations. These two fatigue cracks coalesced and then extended in an unstable manner to intersect the top edge of the plate, dividing the plate into two pieces. A similar but shorter fatigue crack existed at the left side of the plate, initiating at the lower end of the pylon flange-to-diaphragm plate weld, but there were no signs of significant unstable crack extension.

Cable Diaphragm Plate 9 also sustained extensive fatigue cracking before it fractured. A stable crack extension of approximately 11 1/4 inches occurred at the right side of the plate between the pylon flange-to-diaphragm plate weld and the right ring plate-to-diaphragm plate weld, initiating in both locations. A separate stable crack extension of about 9 inches was noted at the left ring plate weld. These fatigue cracks extended in an unstable manner, separating the front section of the diaphragm plate, including the ring plates, from the remainder of the plate.

Materials tests for physical, chemical, and toughness properties performed on the diaphragm plate material indicate that it conformed to the design specifications. This material provided good toughness.

Embedded welding defects including slag and porosity existed in the portion of the fillet welded connection to the pylon flanges that wrapped around the lower end of Cable Diaphragm Plates 8 and 9. However, these defects did not influence the weld toe cracks that formed in the diaphragm plates.

An instrumentation program was implemented to determine the magnitude of stresses in representative cable diaphragm plates in response to wind-induced cable vibrations over an 18 day monitoring period. Cable accelerations, plate tip displacements, and wind speed and direction were also recorded. During the monitoring period, rainflow analysis of the stress data was performed to produce stress range histograms for the data from each strain gage. This information was recorded continuously. The effective stress range (S_{re}) calculated for instrumented regions of the cable diaphragm plates adjacent to the terminations of the pylon flange-to-diaphragm plate welds, and ring plate-to-diaphragm plate welds is in the range of 2.5 ksi to 3.9 ksi for the ambient events monitored. The number of stress range cycles accumulated over the 18 day monitoring period was as high as 2,000,000 at some locations.

In addition, selected structural responses to wind events resulting in high stress ranges were recorded. The stress data reported for the individual events indicates that stress ranges on the order of 5.9 ksi to 7.6 ksi are generated in response to wind events with average wind speeds ranging from 6 mph to 25 mph. The wind direction for these recorded events was primarily transverse to the bridge alignment. The measured structural responses are the result of wind-induced cable vibrations consistent with the phenomenon of vortex shedding.

Stress data correlated to wind speed and direction, plate tip displacement, and accelerometer displacement data calculated by double-integrating accelerations was presented for Event 225. For this event, the average wind speed and direction was 7 mph to 8 mph and 25 degrees to 30 degrees, respectively. Maximum accelerometer displacements were on the order of 0.16 inches to 0.43 inches peak-to-peak. In addition, steady state cable vibration in the 7th mode at about 11 Hz was apparent. It is evident that low

wind speeds with appropriate direction can induce high stress range cycles at high frequency in the cable diaphragm plates due to low amplitude cable displacements.

An independent peer review of the original bridge design was performed for Spans 1 through 3 of the structure. The model was used to verify forces reported in the original design calculations package. Structural checks for strength and serviceability limit states were performed for selected primary structural elements, including the steel pylon, the cables, the bridge deck, and the piers. A review of the original design calculations package and the design drawings was also performed. Forces in the primary structural elements determined from WJE's independent finite element analysis model are in general agreement with those reported in the original design calculations package. In addition, the primary structural bridge elements are adequate for the reported design loads.

12.0 CONCLUSIONS AND RECOMMENDATIONS

12.1 Conclusions and Items for Further Study

The following conclusions and items for further study are drawn from this fracture investigation:

- The fracture of Cable Diaphragm Plates 8 and 9 resulted from extensive fatigue crack propagation that initiated at multiple sites. These fatigue cracks coalesced and led to sudden and unstable fracture.
- The cable diaphragm plates incorporate welded details that offer poor fatigue resistance and are sensitive to cyclic stresses due to wind-induced cable vibrations under ambient conditions. The stress ranges measured during the 18 day monitoring period are of sufficient magnitude to cause fatigue cracking.
- The diaphragm plate misalignment exceeded reasonable tolerances at three cable diaphragm plates and caused high static stresses within the plates. The misalignment influenced the location of the fatigue cracks in Cable Diaphragm Plate 9, but is not an important contributor to plate fracture.
- The fillet welded joint between Cable Diaphragm Plates 8 and 9 and the pylon flanges exhibited inclusions and other welding defects, but the defects did not initiate cracks or significantly diminish fatigue resistance.
- Other than the vulnerability of the cable diaphragm plates to fatigue damage from wind-induced vibration, the design is structurally adequate.
- The existing cable diaphragm plates should be retrofitted to enhance fatigue resistance, including the backstay plates.
- Cable damping systems should be considered to avoid user concerns and protect the cables themselves.
- The lower cable anchorages and sockets should be reviewed for fatigue susceptibility and damage.

12.2 Cable Diaphragm Plate Retrofit Options

Three retrofit options have been developed and should be considered to retrofit the pylon cable diaphragm connections. Retrofit detail Sheets S-0 through S-4 are included as Appendix D.

Option 1 - Mechanically Fastened Plates to the Existing Connection Plate and Pylon Flanges. Sheets S-1 and S-2 (or S-2A) detail this retrofit option complete with a Procedure for installation and General Notes. To allow the fit-up the additional plates, removal of the connection ring plates is required.

Placement of two 1 3/4 inch thick plates will provide the correct clevis connection dimension. The two new diaphragm plates will be fastened through the existing 3/4 inch thick plate using twelve 1 inch diameter ASTM A325 high strength bolts. Four angles will be used to connect the cable diaphragm plates to the pylon flange plates. Each connection angle is fastened with nine 1 inch diameter ASTM A325 high strength bolts. It should be noted that all faying surfaces for this option are prepared to Category B slip resistance. This retrofit provides a mechanically fastened connection to the pylon that eliminates welding, results in increased section properties, and provides built-in redundancy.

Option 2 - Mechanically Fastened Doubler Plates to Pylon Flanges to Complete Cable Connections. For installation of this retrofit the cable diaphragm plate will be removed and existing welds will be ground off the pylon flange plates. At each pylon flange, this new connection is made up of three bent plates consisting of a 1 1/2 inch thick fill plate and two 1 3/8 inch thick side plates. Sheet S-3 shows the retrofit connection installed on the pylon complete with General Notes. A two piece HP14x73 cut off section will be installed as a strut between the pylon flanges. In total, fifteen 1 inch diameter ASTM A325 high strength bolts connect the three bent plate group to each pylon flange. Fabricating this three bent plate group is considered to be difficult. In addition, this option includes modification of the original cable alignment and therefore may require modification to the distance between cable anchor points.

Option 3 - Mechanically Fastened Weldment to Pylon. For installation of this retrofit the cable diaphragm plate will be removed and existing welds will be removed by grinding. This two piece weldment is made up of multiple plates that are connected to the pylon flanges as shown on Sheet S-4. The main connection of the cables to the weldment uses two 4 3/8 inch thick plates. These plates will be installed vertically on the proper alignment of the cables. However, the cable clevis at the pylon has been rotated 90 degrees. Note that the weldment must be fabricated in two pieces to allow placement at any connection elevation without total removal of all cable diaphragm plates during installation. In total, sixteen 1 inch diameter ASTM A325 high strength bolts connect the weldment to the pylon.

It is recommended that any of the three retrofit options should be carried out by qualified and experienced machine type metal workers that have documented experience working closely with a fabricator that is qualified in accordance with MnDOT and AASHTO requirements to produce fracture critical bridge members. Although the cable diaphragm plates are not considered fracture critical, a fabricator with the stated qualifications is preferred. Construction period services and field inspection should be carried out by an engineering firm with documented experience in retrofit design and physical modification of fracture critical bridge details. Proper fit-up of each piece is of utmost importance and high quality workmanship is required.

Based on the retrofit options, the detail shown on Sheets S-1 and S-2 (or S-2A) is the preferred choice for the installation at this time. This detail can be installed at one location at a time with only one pair of cables removed from the pylon for the work period. In addition, Option 1 is the most adaptable and straight-forward connection that can be used to upgrade all 18 cable diaphragm plate connection locations.

WJE ENGINEERS ARCHITECTS MATERIALS SCIENTISTS

TABLES

Table 1. Primary Equipment for Nondestructive Examination of Cable Diaphragm Plates

Test Equipment	General Description	Primary Function
Ultrasonic test instrument *All ultrasonic scans*	G.E. Krautkramer USN 58 L Ultrasonic Flaw Detector	Production & detection of ultrasonic pulses
Transducer 1 *Straight Beam Scans*	G.E. - 1.00 inch diameter, 2.25 MHz - 0° (Longitudinal)	Initial straight beam scans
Transducer 2 *Straight Beam Scans*	G.E. - 0.50 inch diameter, 5.00 MHz - 0° (Longitudinal)	Straight beam scans
Transducer 3 *Shear Wave Scans*	G.E. - 0.50 inch diameter, 3.50 MHz - 45° (Shear)	Diaphragm Plates - Shear wave scans
Transducer 4 *Shear Wave Scans*	G.E. - 0.50 inch diameter, 2.25 MHz - 60° (Shear)	Diaphragm Fillet Weld - Shear wave scans
Transducer 5 *Shear Wave Scans*	G.E. - 0.50 inch diameter, 2.25 MHz -70° (Shear)	Ring Plate Fillet Weld - Shear wave scans
Calibration Standard	IIW Type 2 Ultrasonic Reference Standard	Horizontal linearity and transducer sensitivity
Couplant	Sonotech - Ultragel II (modified with windshield washing fluid to resist freezing)	Coupling for all scans
Magnetic Particle Yoke	Parker Research Model B310 Mini-Magnetic particle yoke	Induction of magnetic fields
Magnetic Examination Medium	Dry red particles	Enhanced exhibition of discontinuities

Table 2. Cable Diaphragm Plate Alignment Measurements

Cable Diaphragm Plate	Design Angle Value		Protractor and/or Direct Measurement (deg)		Bosch Instrument (deg)		Stabila Instrument (deg)		Avg Design Δ (deg)
	DMS	Deg	Value	Δ Design	Value	Δ Design	Value	Δ Design	
1	17° 35’ 02”	17.58	17.5	-0.08	17.0	-0.58	18.0	0.37	-0.10
2	28° 18’ 13”	28.30	28.3	0.00	28.3	0.00	28.6	0.25	0.08
3	34° 59’ 26”	34.99	35.0	0.01	34.9	-0.09	35.2	0.16	0.03
4	39° 27’ 00”	39.45	39.0	-0.45	39.6	0.15	39.5	0.05	-0.08
5	42° 36’ 01”	42.60	42.0	-0.60	42.5	-0.10	42.7	0.05	-0.22
6	44° 55’ 55”	44.93	47.5	2.57	47.9	2.97	48.0	3.07	2.87
7	46° 43’ 16”	46.72	46.5	-0.22	46.9	0.18	46.9	0.13	0.03
8	48° 17’ 55”	48.30	49.0	0.70	48.5	0.20	48.8	0.50	0.47
9	49° 21’ 34”	49.36	54.0	4.64	53.7	4.34	53.8	4.39	4.46
10	58° 24’ 18”	58.41	54.0	-4.41	53.6	-4.81	54.0	-4.46	-4.56
11	55° 36’ 29”	55.61	55.5	-0.11	55.7	0.09	56.1	0.44	0.14
12	52° 54’ 36”	52.91	53.0	0.09	53.0	0.09	53.4	0.44	0.21
13	50° 18’ 45”	50.31	50.5	0.19	50.6	0.29	50.9	0.59	0.35
14	47° 49’ 00”	47.82	47.5	-0.32	47.7	-0.12	48.2	0.33	-0.03
15	45° 25’ 09”	45.42	45.5	0.08	45.4	-0.02	45.8	0.38	0.15
16	43° 07’ 17”	43.12	43.0	-0.12	42.7	-0.42	43.2	0.03	-0.17
17	40° 55’ 15”	40.92	40.5	-0.42	40.7	-0.22	41.1	0.18	-0.15
18	38° 40’ 42”	38.68	39.0	0.32	38.7	0.02	39.2	0.47	0.27

Table 3. Summary of Pluck Test Data

Pluck Test Cable 7L				Pluck Test Cable 7R			
Gage	**Stress Range (psi)**	**Gage**	**Stress Range (psi)**	**Gage**	**Stress Range (psi)**	**Gage**	**Stress Range (psi)**
SG01	1,380	SG07	1,460	SG01	830	SG07	880
SG02	3,070	SG08	3,110	SG02	2,140	SG08	2,200
SG03	1,960	SG09	2,200	SG03	930	SG09	1,100
SG04	860	SG10	650	SG04	2,360	SG10	1,860
SG05	1,770	SG11	1,920	SG05	3,160	SG11	3,400
SG06	600	SG12	1,530	SG06	1,270	SG12	3,230
Wind Speed (mph)	6-10	Wind Direction (Deg)	98	Wind Speed (mph)	7-9	Wind Direction (Deg)	114
Pluck Test Cable 6L				**Pluck Test Cable 6R**			
Gage	**Stress Range (psi)**	**Gage**	**Stress Range (psi)**	**Gage**	**Stress Range (psi)**	**Gage**	**Stress Range (psi)**
SG13	980	SG19	2,490	SG13	620	SG19	1,540
SG14	3,670	SG20	3,300	SG14	2,610	SG20	2,340
SG15	2,500	SG21	2,650	SG15	1,270	SG21	1,350
SG16	1,210	SG22	1,240	SG16	2,770	SG22	2,490
SG17	2,260	SG23	2,370	SG17	3,550	SG23	3,770
SG18	1,190	SG24	1,930	SG18	2,200	SG24	3,470
Wind Speed (mph)	6-10	Wind Direction (Deg)	103	Wind Speed (mph)	6-10	Wind Direction (Deg)	108

Notes:

1. All pluck tests performed using a 250 lb load perpendicular (down) to the cable alignment.
2. Load applied at approximately 58 ft, 38 ft, 62 ft, and 42 ft from the top Anchor Point for Cable 6L, 6R, 7L, and 7R, respectively.
3. Load applied using tension ram and load cell to verify force.
4. Quick release equipment used to instantaneously release load.
5. Reported stress range is from first cycle following load release.
6. Reported wind speed and direction are average values throughout the test period.
7. Wind-induced cable vibration minimal during test period.
8. Wind direction reference is 0 Degrees perpendicular left (north) of the structure with increasing increments clockwise looking down.

Table 4. Representative Triggered Event Data

Event	Date/Time		Average Wind Speed (mph)	Average Wind Direction (deg)	Max Stress Range Gage	Max Stress Range (ksi)	Max Tip Displacement (inches)
007	4/21/12	9:34	10-14	195-200	2	6.2	0.009
014	4/21/12	17:27	10-13	175-190	11	6.8	0.013
067	4/22/12	16:18	6-9	5-15	11	7.6	0.015
072	4/27/12	17:11	6-8	20-35	11	7.1	0.014
076	5/1/12	09:35	13-14	180-185	2	6.3	0.009
123	5/1/12	11:40	12-13	190-205	2	5.9	0.012
150	5/1/12	15:54	19-23	180-185	11	6.0	0.012
223	5/1/12	19:46	16-19	190-205	2	7.5	0.014
224	5/1/12	20:04	20-25*	190-200	2	7.2	0.013
225	5/6/12	14:58	7-8	25-30	11	6.9	0.014

* max of 38 mph at pylon top

Table 5. Summary of Effective Stress Range Data

Gage	Total Counts	S_{re} (psi)	Comments	Percent of Counts for S_r Above 4.5 ksi
SG01	123,237	2,720		0.000%
SG02	2,058,369	3,660		0.965%
SG03	512,472	2,900		0.036%
SG04	939,634	3,060		0.179%
SG05	1,855,078	3,810		1.802%
SG06	79,735	2,560		0.000%
SG07	107,528	2,710		0.001%
SG08	1,988,854	3,320		1.734%
SG09	348,232	2,870		0.032%
SG10	-	-	No Data	-
SG11	1,244,034	3,900		3.100%
SG12	-	-	No Data	-
SG13	1	2,330	No Significant Data	0.000%
SG14	321,260	3,290		0.209%
SG15	62,359	2,710		0.001%
SG16	98,028	2,650		0.001%
SG17	326,342	3,050		0.060%
SG18	24,152	2,530		0.000%
SG19	85,642	2,790		0.003%
SG20	254,300	3,160		0.108%
SG21	-	-	No Data	-
SG22	30,881	2,560		0.000%
SG23	-	-	No Data	-
SG24	304,871	2,980		0.037%

WJE ENGINEERS ARCHITECTS MATERIALS SCIENTISTS

FIGURES

Figure 1. Side view of the Martin Olav Sabo Pedestrian Bridge looking northeast.

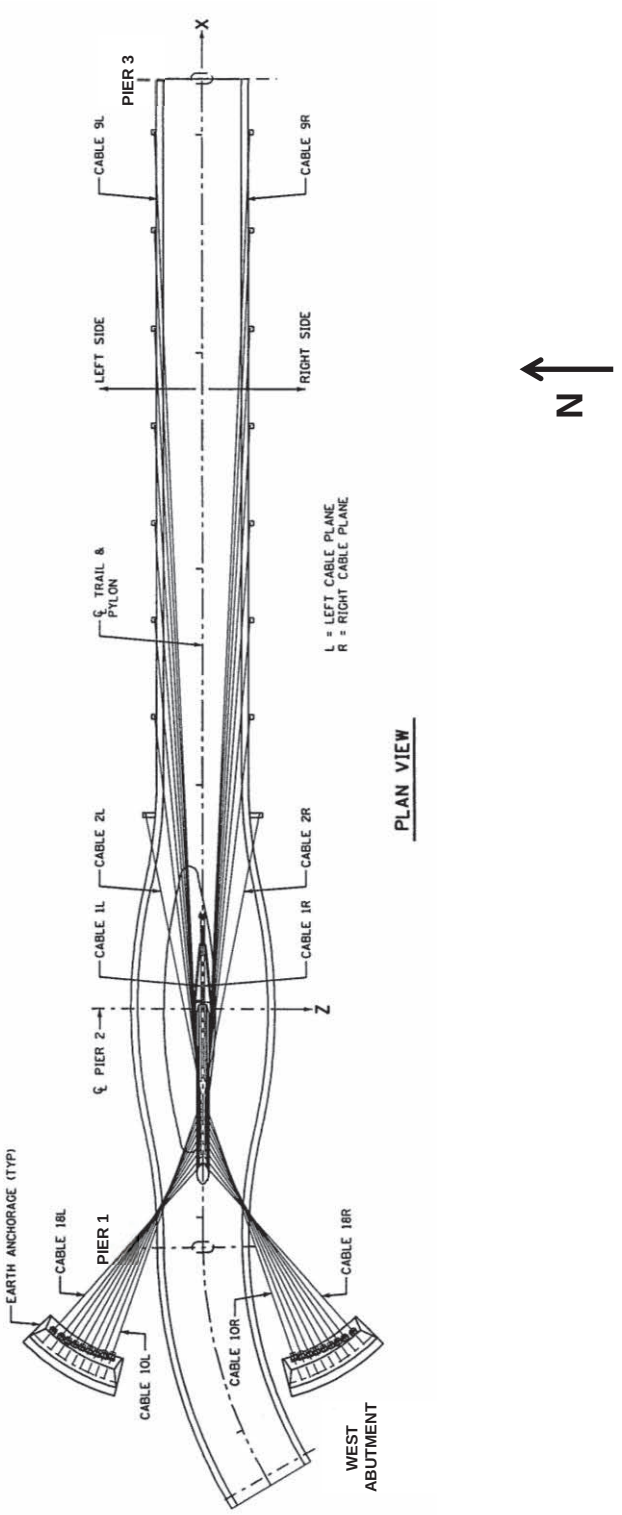

Figure 2. Overall plan drawing of Spans 1 through 3 taken from the original design drawings.

Figure 3. Typical cable anchorage assembly at the concrete deck.

Figure 4. Typical cable anchorage at the pylon showing the cable diaphragm plate and clevis pin connection.

Figure 5. Typical cable earth anchorages.

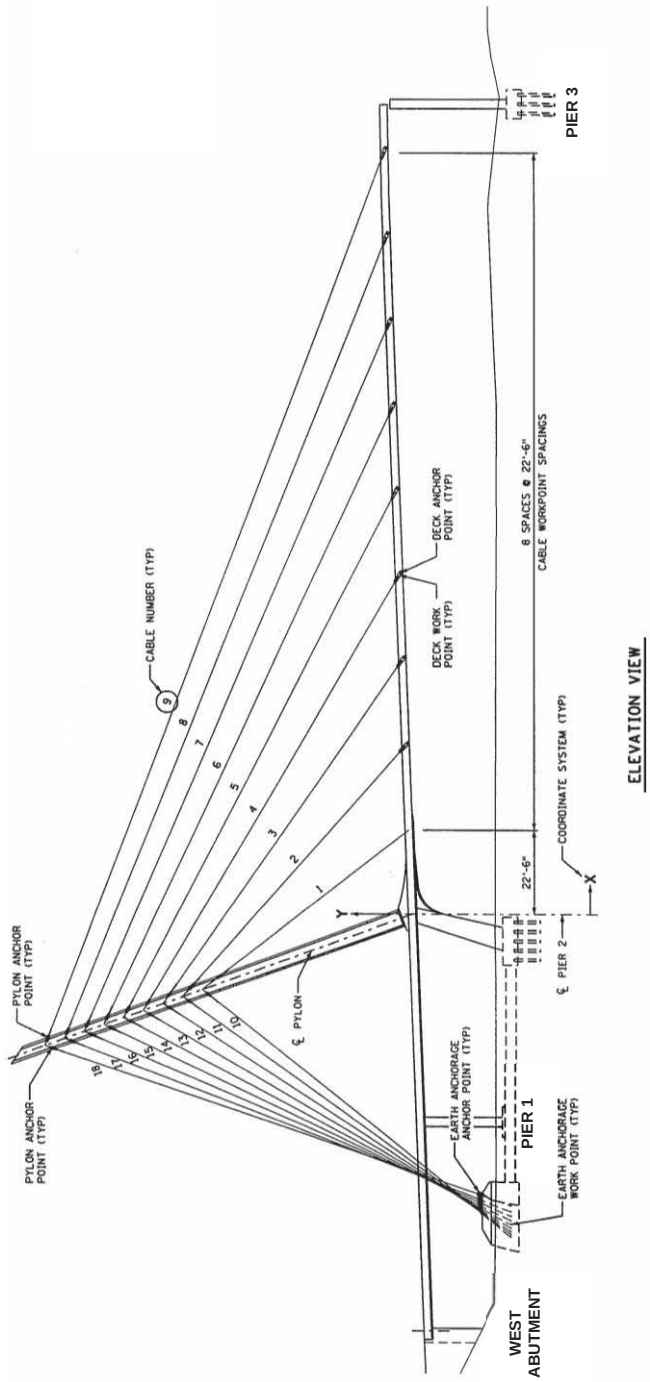

Figure 6. Elevation drawing of Spans 1 through 3 looking north taken from the original design drawings.

Figure 7. Typical cable diaphragm plate. Cable Diaphragm Plate 6 shown.

Figure 8. Magnetic particle testing (MT) in progress showing test equipment.

Figure 9. Ultrasonic testing (UT) in progress.

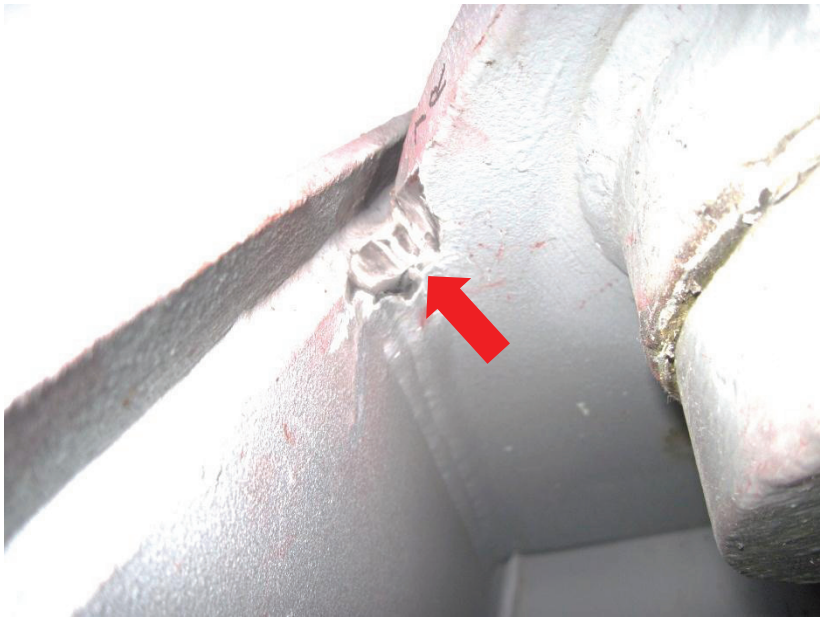

Figure 10. Area at the right side diaphragm plate-to-pylon flange weld wrap around for Cable Diaphragm Plate 7 showing the area from which the noted indication was removed.

Figure 11. Crack located in the bottom surface of Cable Diaphragm Plate 5 at the right side diaphragm plate-to-pylon flange weld. The crack is approximately 3/4 inches long. It is shown highlighted with red MT powder before chipping the paint off.

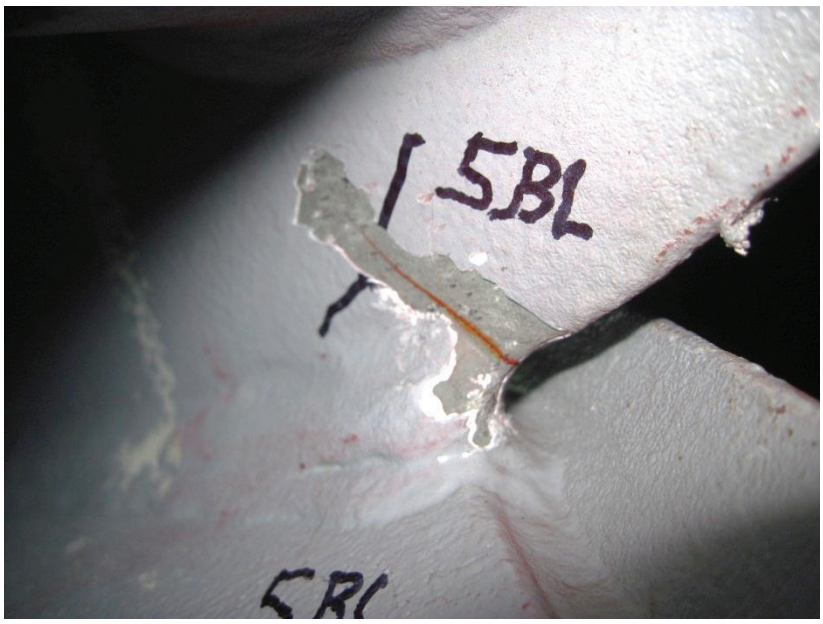

Figure 12. Crack located in the bottom surface of Cable Diaphragm Plate 5 at the left side diaphragm plate-to-pylon flange weld. The crack is approximately 1 1/2 inches long. It is shown highlighted by red MT powder after chipping the paint off.

Figure 13. View of Cable Diaphragm Plate 9 after fracture.

Figure 14. Segment of Cable Diaphragm Plate 9 that separated from the pylon following plate fracture.

Figure 15. View of Cable Diaphragm Plate 8 following fracture and removal of Cables 8L and 8R.

Figure 16.View of the left pylon flange alignment following local plastic rotation of the flange at the attachment elevation for Cable Diaphragm Plate 8.

Figure 17. Segments of Cable Diaphragm Plate 8 shown shortly after removal from the pylon.

Figure 18. Segment of Cable Diaphragm Plate 9 shown shortly after removal from the pylon.

Figure 19. Typical strain gage installation near a diaphragm plate-to-ring plate weld toe.

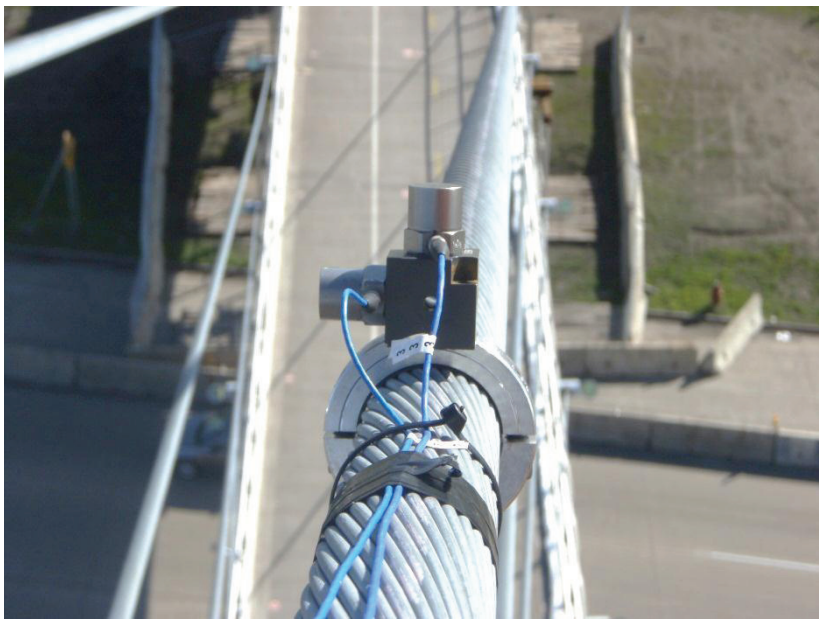

Figure 20. Typical accelerometer installation on a stay cable. The two accelerometers are attached to block surfaces normal to one another in order to measure vertical and lateral accelerations.

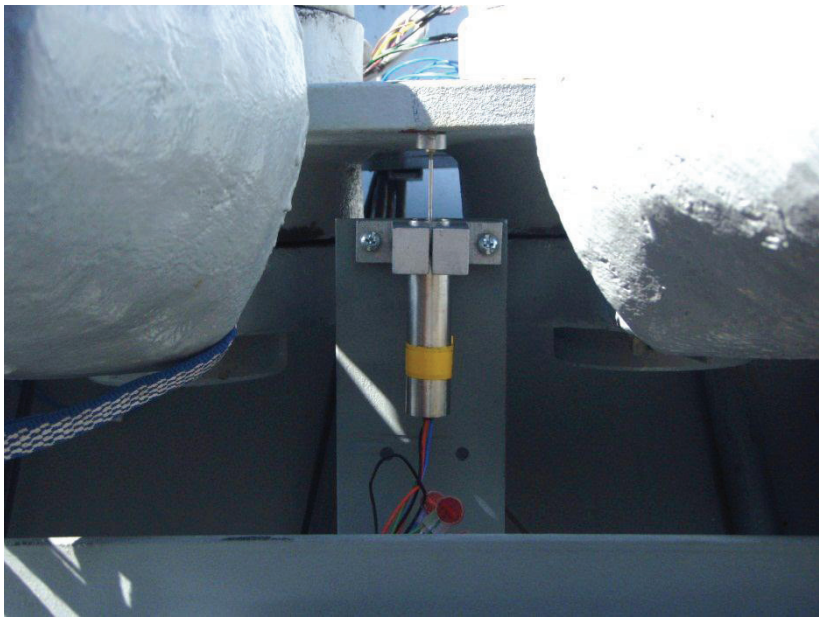

Figure 21. Typical LVDT installation at the tip of Cable Diaphragm Plate 7.

Figure 22. Wind monitor mounted 10 feet above the left curb between Cables 3L and 4L.

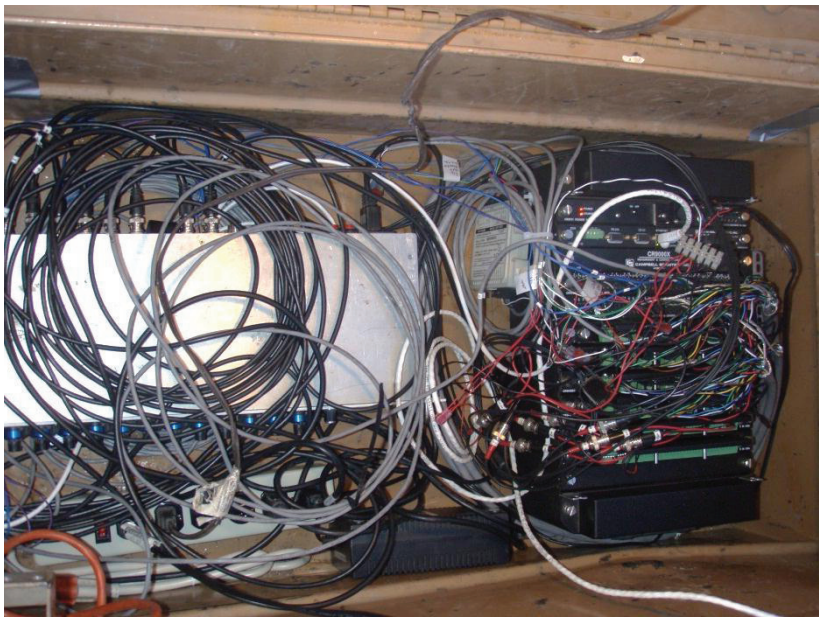

Figure 23. Data acquisition system shown after attachment of instrument wiring.

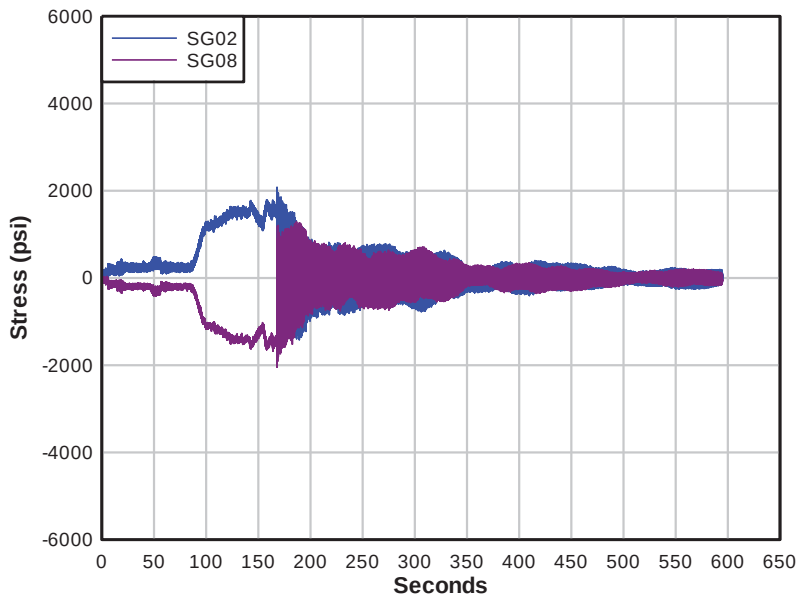

Figure 24. Plot of stress data from selected strain gages in response to the Cable 7L pluck test.

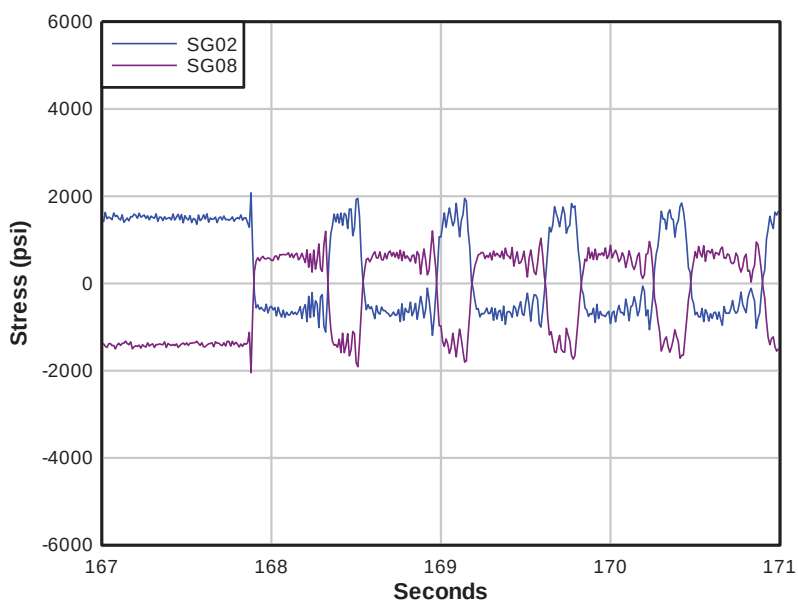

Figure 25. Zoom of stress data at load release for the data shown in Figure 24.

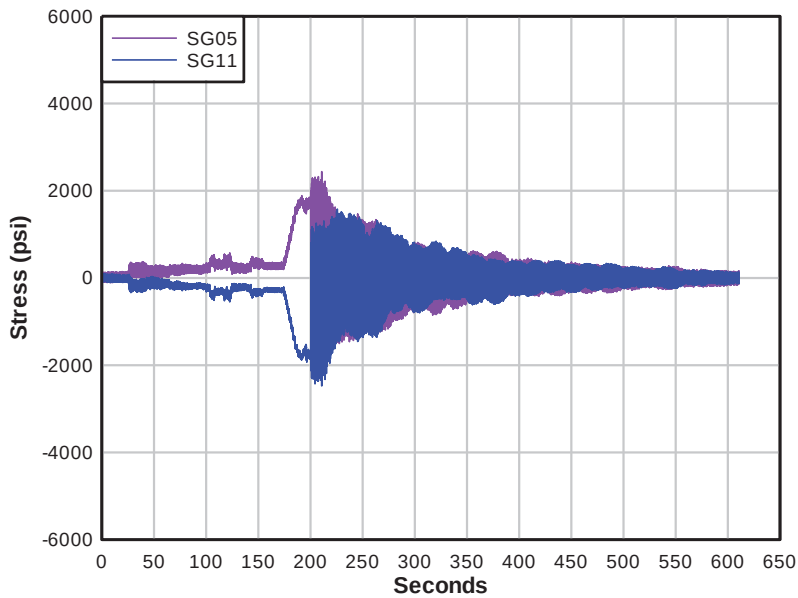

Figure 26. Plot of stress data from selected strain gages in response to the Cable 7R pluck test.

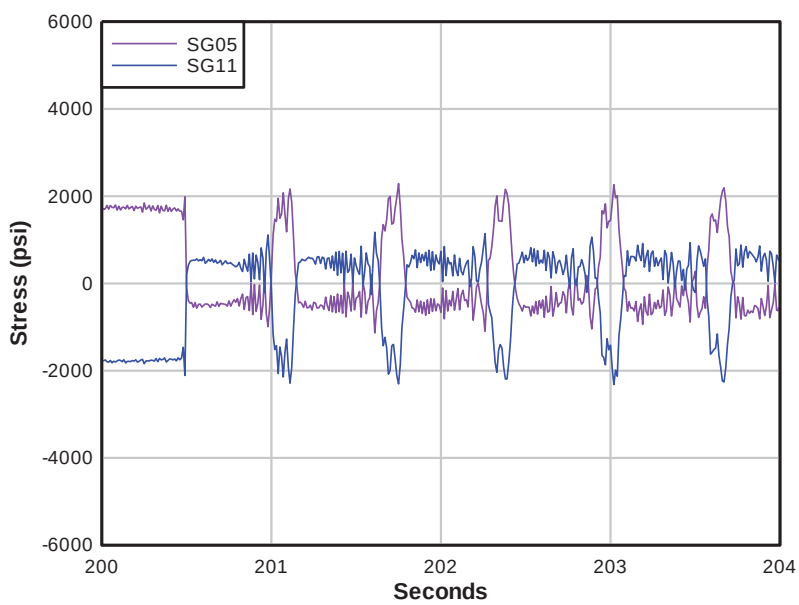

Figure 27. Zoom of stress data at load release for the data shown in Figure 26.

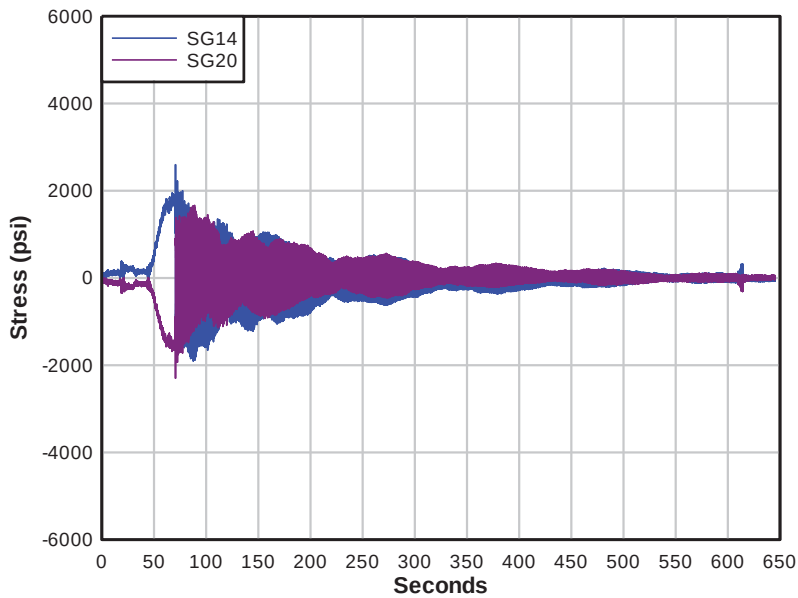

Figure 28. Plot of stress data from selected strain gages in response to the Cable 6L pluck test.

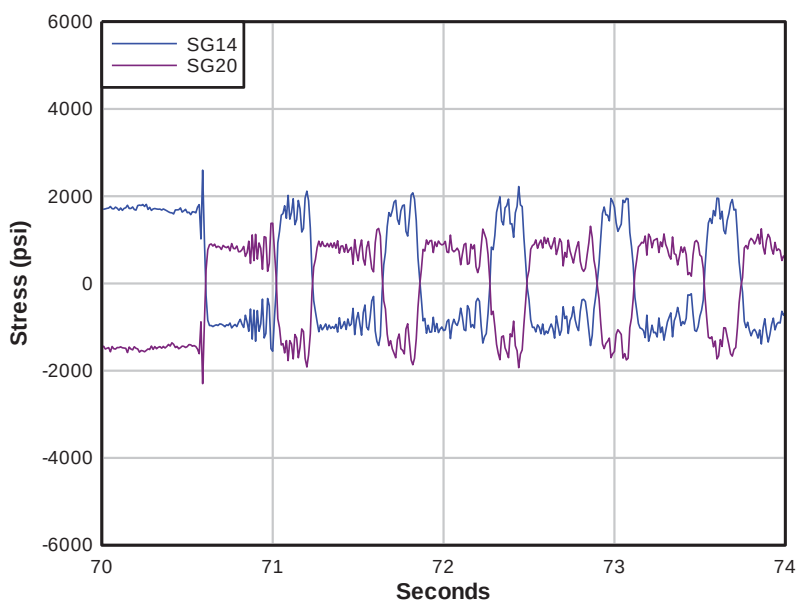

Figure 29. Zoom of stress data at load release for the data shown in Figure 28.

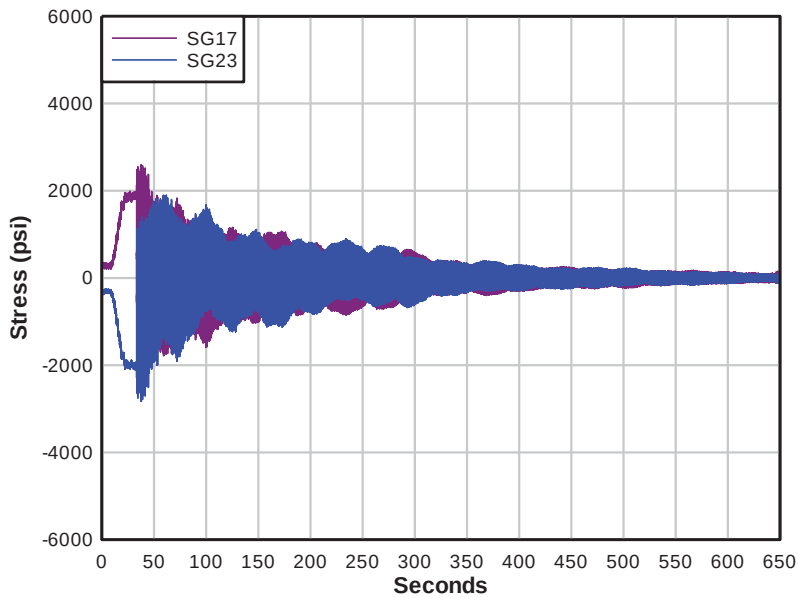

Figure 30. Plot of stress data from selected strain gages in response to the Cable 6R pluck test.

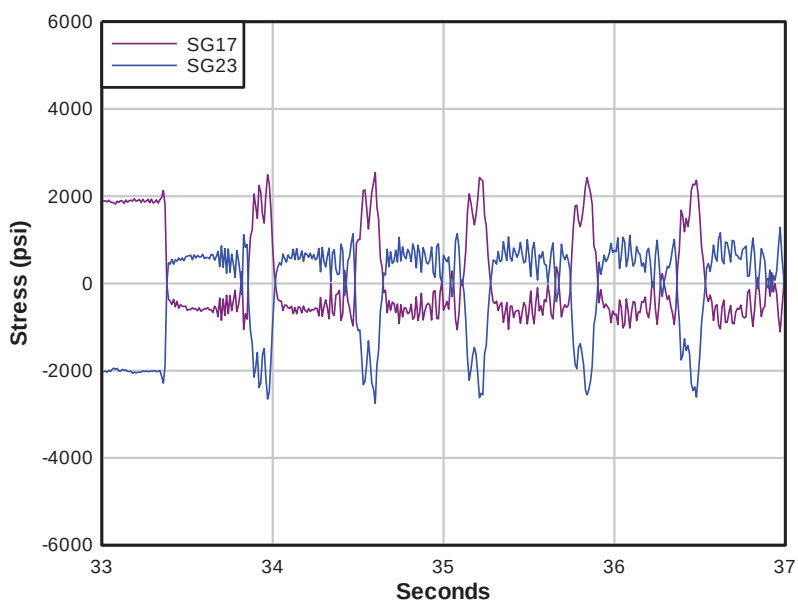

Figure 31. Zoom of stress data at load release for the data shown in Figure 30.

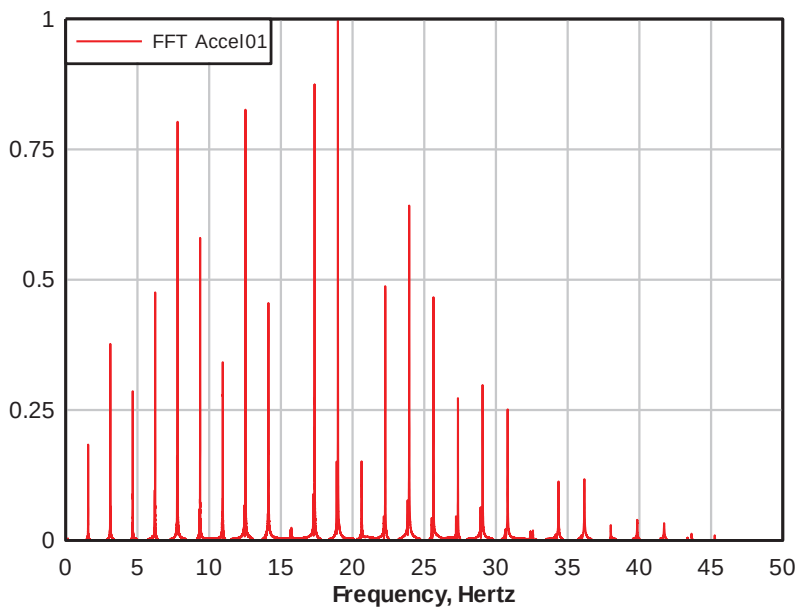

Figure 32. Normalized FFT plot showing multiple modes of vibration during response to the Cable 7L pluck test.

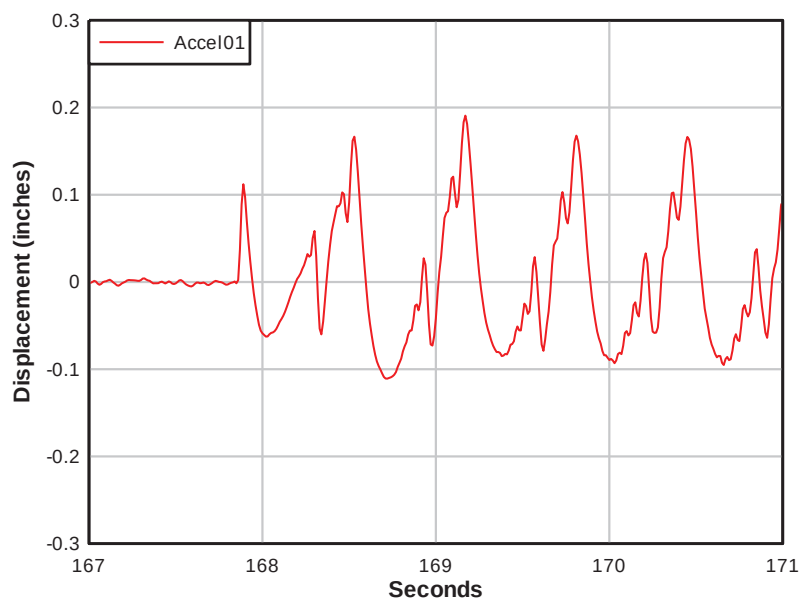

Figure 33. Approximate displacement data generated by double-integration of acceleration data from Accelerometer Accel01 at load release during the pluck test for Cable 7L.

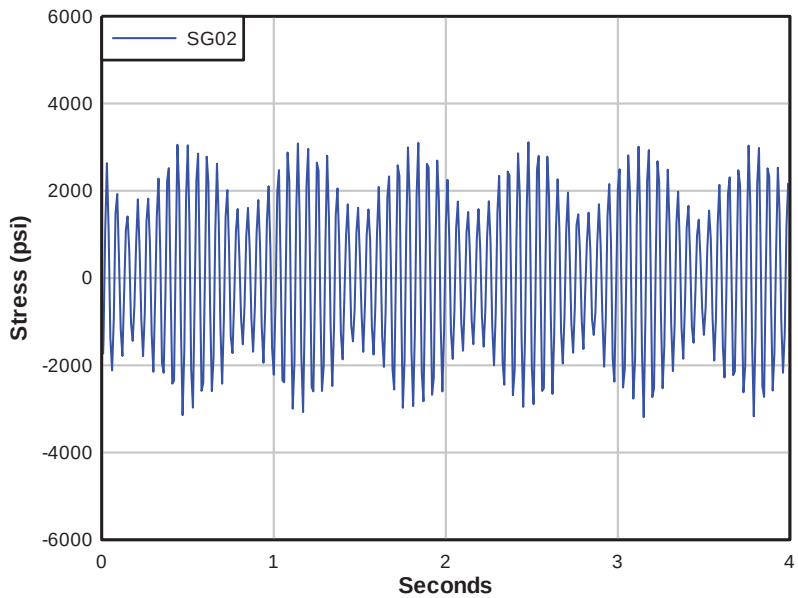

Figure 34. Plot of stress responses from Strain Gage SG02 during Event 007.

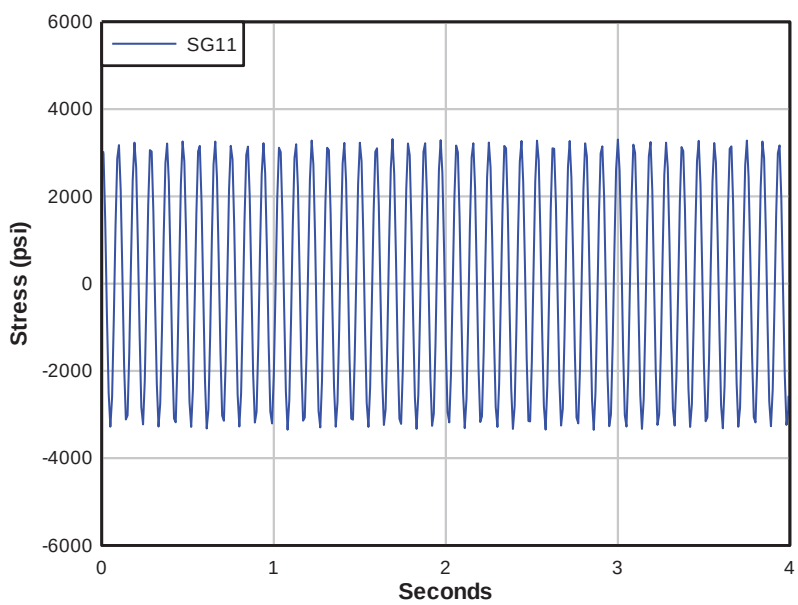

Figure 35. Plot of stress responses for Strain Gage SG11 during Event 225.

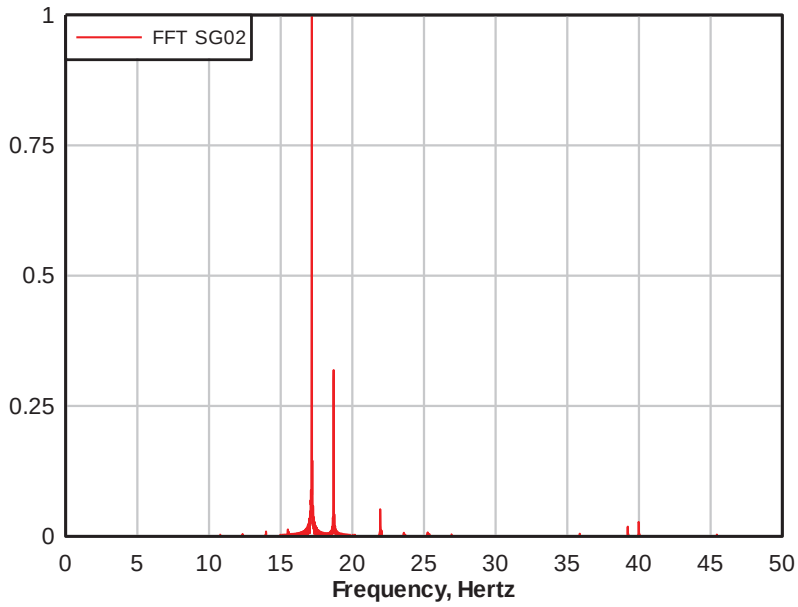

Figure 36. Normalized FFT plot of the stress data from Strain Gage SG02 during Event 007 showing the dominance of cable modes 11, 12 and 14. Note that the approximate first mode of cable vibration is 1.53 Hz.

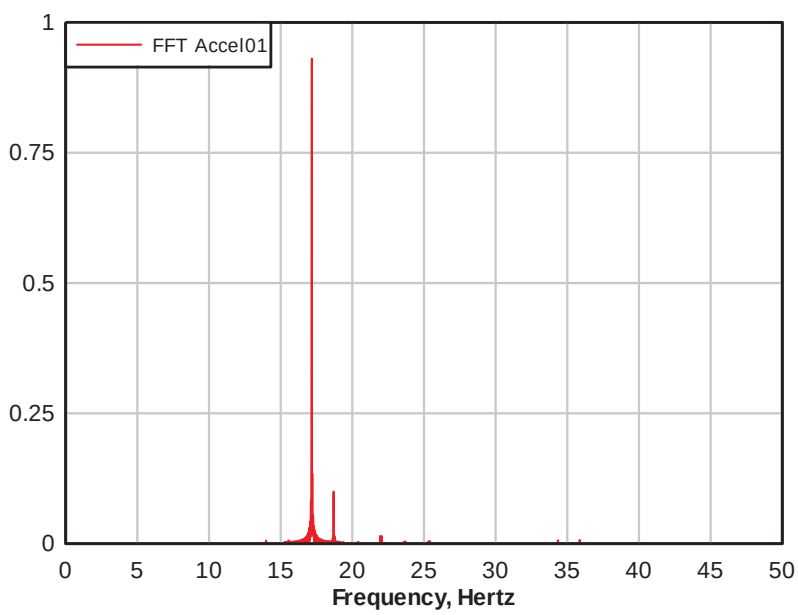

Figure 37. Normalized FFT plot of the acceleration data from Accelerometer Accel01 mounted on Cable 7L during Event 007.

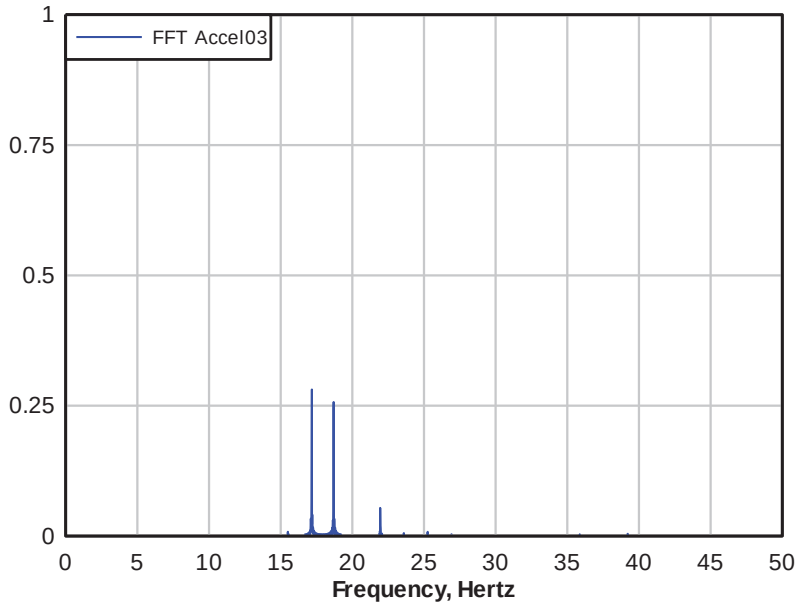

Figure 38. Normalized FFT plot of the acceleration data from Accelerometer Accel03 mounted on Cable 7R during Event 007.

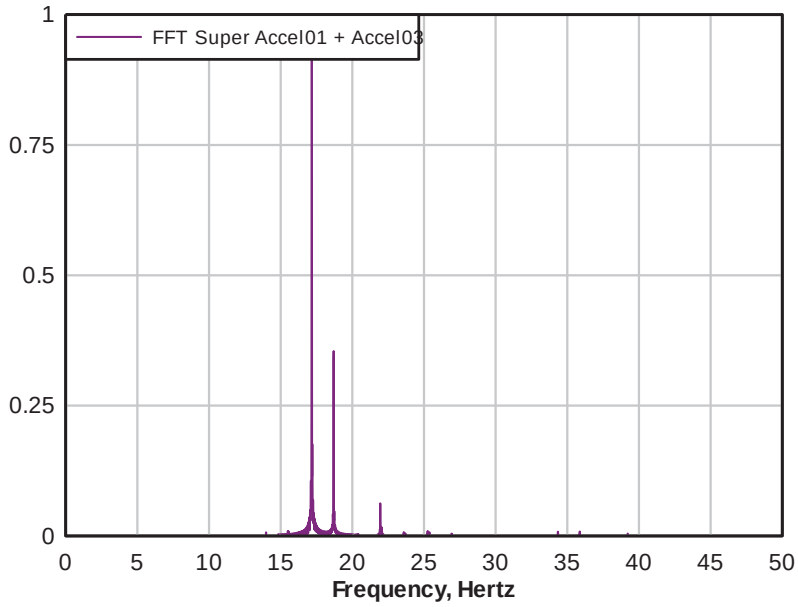

Figure 39. Superposition of normalized FFT plot for the acceleration data from Accelerometers Accel01 and Accel03, mounted on Cables 7L and 7R during Event 007. Similar to plot shown in Figure 36.

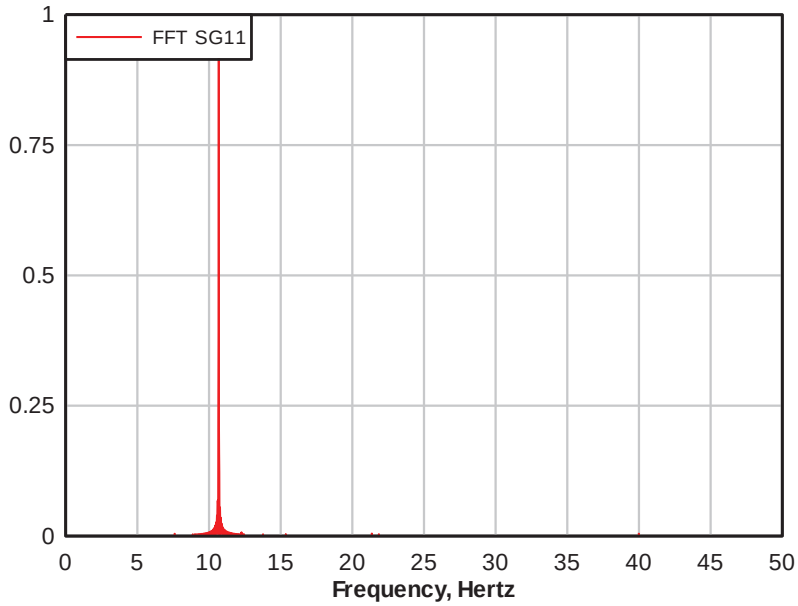

Figure 40. Normalized FFT plot of the stress data from Strain Gage SG11 during Event 225 showing the dominance of cable mode 7. Note that the approximate first mode of cable vibration is 1.53 Hz.

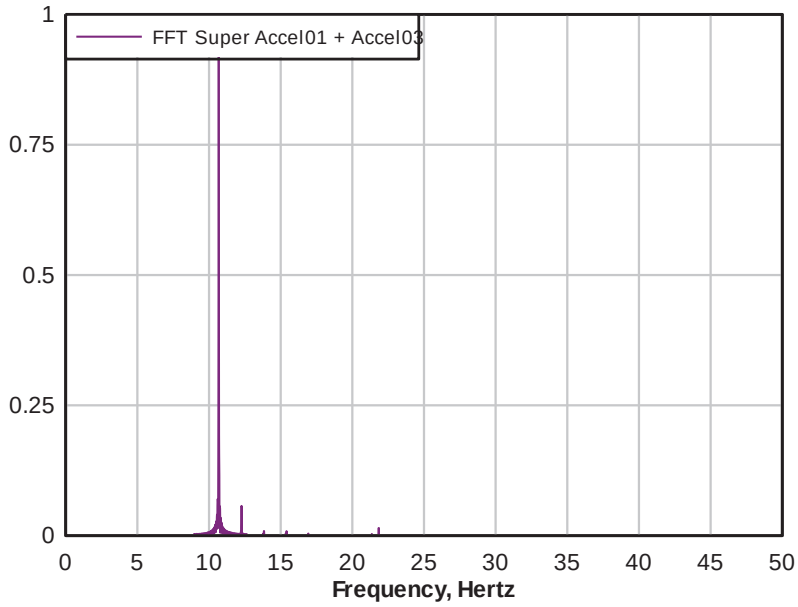

Figure 41. Superposition of normalized FFT plot for the acceleration data from Accelerometers Accel01 and Accel03, mounted on Cables 7L and 7R during Event 225. Similar to plot shown in Figure 40.

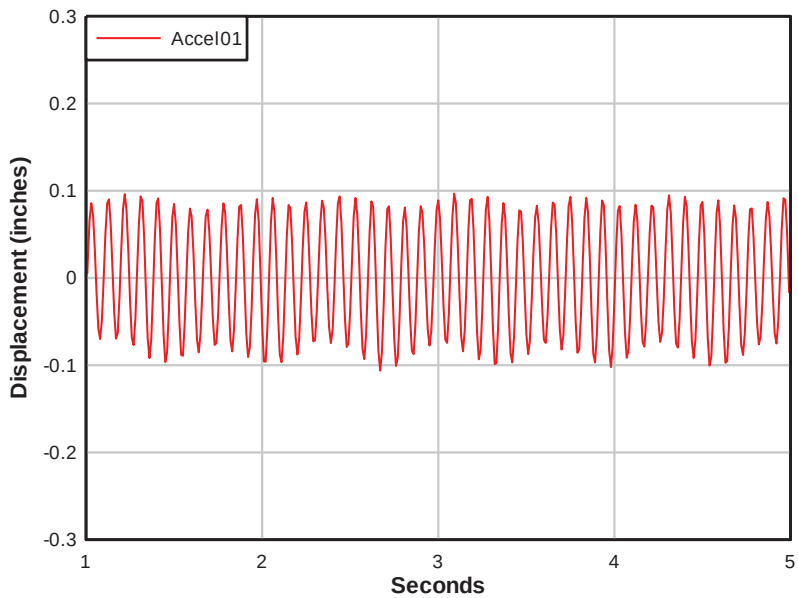

Figure 42. Approximate displacement data generated by double-integration of acceleration data from Accelerometer Accel01 during Event 225.

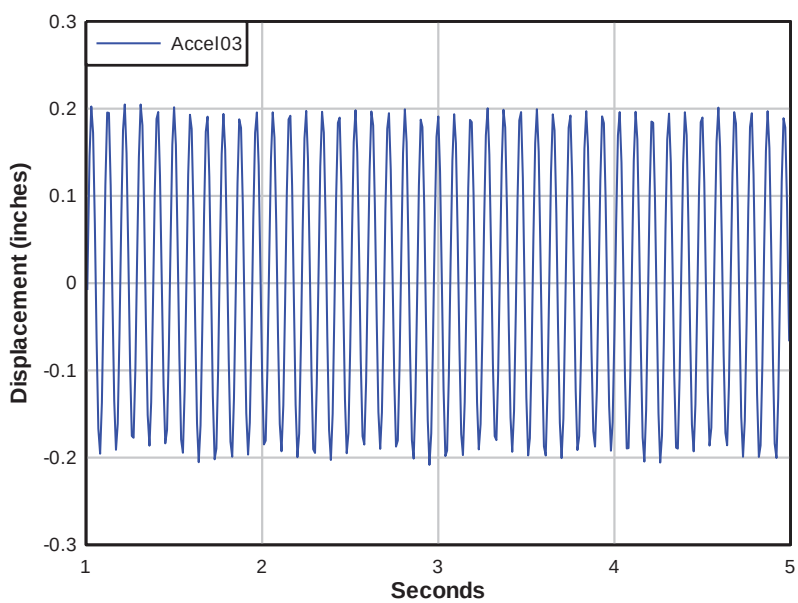

Figure 43. Approximate displacement data generated by double-integration of acceleration data from Accelerometer Accel03 during Event 225.

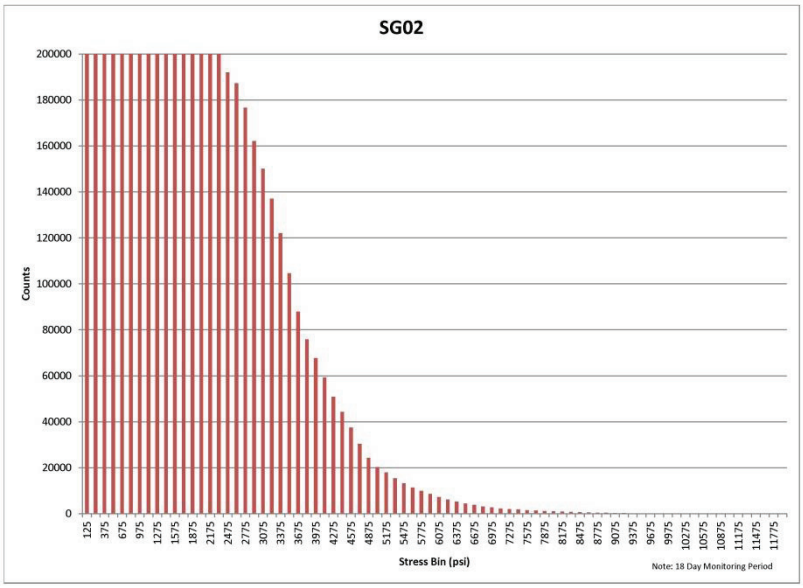

Figure 44. Stress range histogram for Strain Gage SG02. The calculated effective stress range for this gage over the 18 day monitoring period is 3.7 ksi.

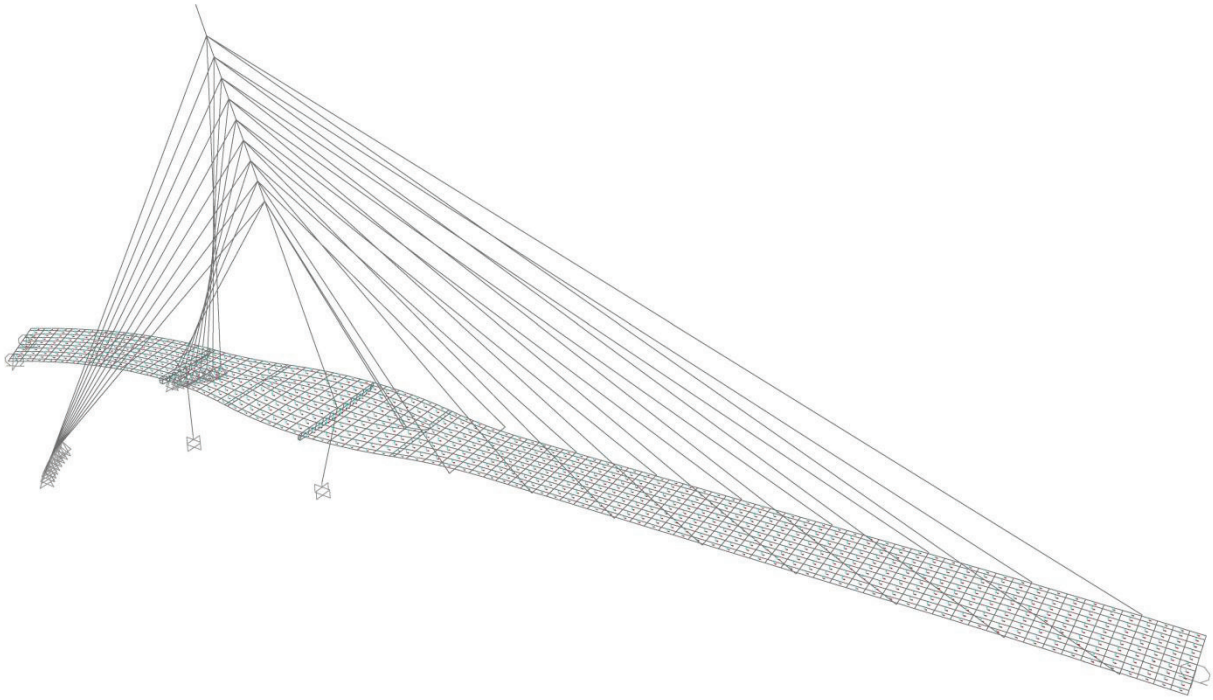

Figure 45. View of finite element model of Spans 1 through 3 created using SAP2000.

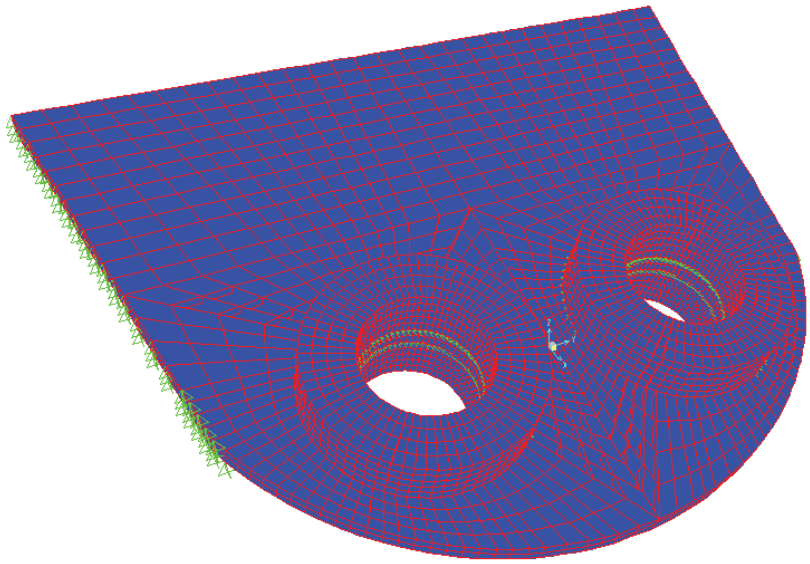

Figure 46. Finite element model of cable diaphragm plate.

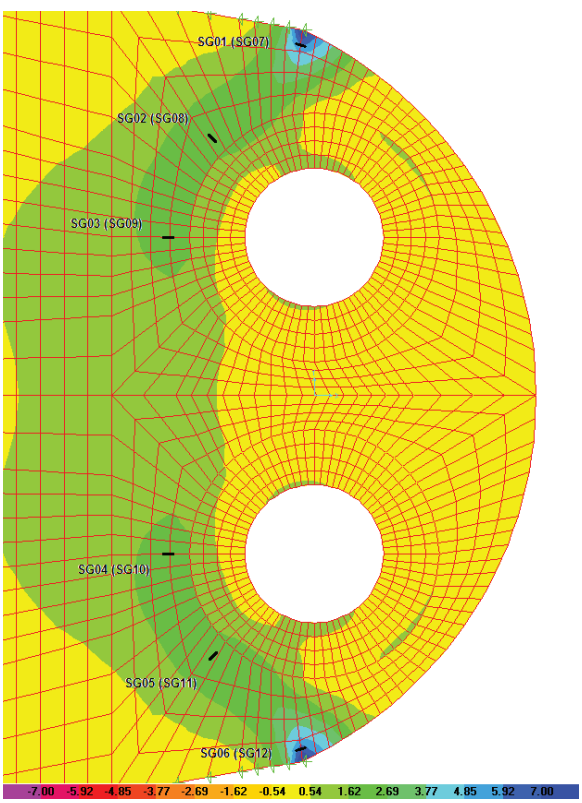

Figure 47. Maximum bending stresses at diaphragm plate surface due to simulated wind-induced vibration.

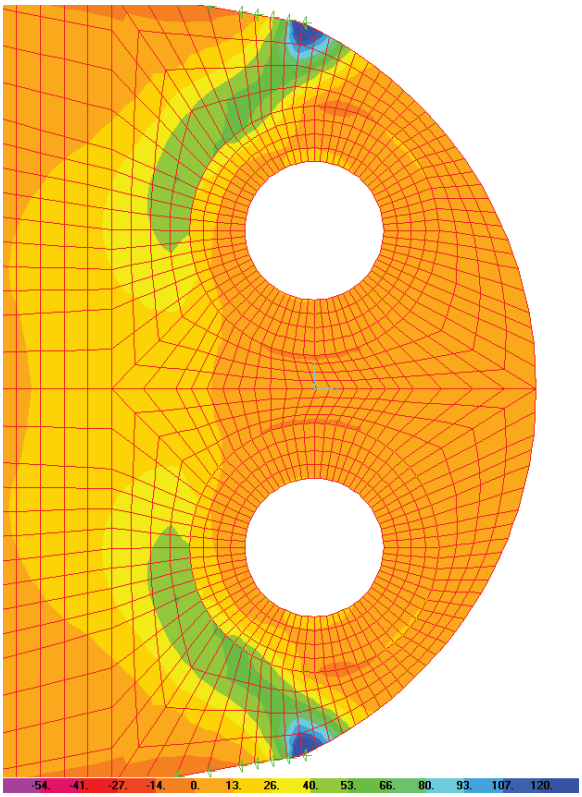

Figure 48. Bending stresses at diaphragm plate surface due to 4.5° misalignment.

WJE ENGINEERS ARCHITECTS MATERIALS SCIENTISTS

Appendix A

John W. Fisher Report

Report on the cracking that developed in the Cable Stay diaphragm plates of the Martin Olav Sabo Pedestrian Bridge Minneapolis, Minnesota

By
John W. Fisher and Eric J. Kaufmann
5-24-12

1. Introduction

a) Cable Diaphragm Plate 9

The discovery of a fractured diaphragm plate for Cables 9L and 9R occurred when the severed diaphragm and attached cables dislodged from their pylon connection. Figure 1 shows the crack surface of the failed plate end with the ring plates welded to the diaphragm plate surfaces. The entire cross section is cracked. Fatigue cracks had formed at four distinct locations: Two at each end of the diaphragm-flange weld terminations and the other two forming at the weld toes of the ring plates on the top surface of the diaphragm plate. These fatigue cracks coalesced into two distinct conditions, as evident from the corrosion covered surfaces, until the final fracture which developed at the two clean looking segments occurred.

Although the transverse distance across the diaphragm plate at the ends of the flange welds is 23½in., the total crack path was longer at about 25in, as it followed the principal stress toward the ring plates from the end welds and around the ring plate weld toes as can be seen in Figure 2 of the diaphragm plate segment that remained in the pylon. The edge crack on the north (left) side (right side of Figure 2) is clearly visible and has propagated following the principal stress behind the primary crack and shielded that end of the primary crack from the north ring plate weld toes.

The weld toe terminations seen at each end of the diaphragm in Figure 2 of the diaphragm-flange welds are both Category E' fatigue details with a fatigue limit of 2.6ksi(1). Likewise, the weld toes of the ring plates to the diaphragm plates provides a

Category E detail for the axial and bending components of cyclic stress introduced into the diaphragm plate. This detail is at the upper bound margin of diaphragm plate thickness so Category E' may also apply. The stress field across the diaphragm width is not uniform and is influenced by the applied cable forces and shear lag.

The segment of Cable Diaphragm Plate 9 that remained in the pylon was removed along with the weld ends and small segments of the pylon flanges as shown in Figure 3. The figure also shows the section from which mechanical properties (tensile and CVN tests) were obtained. The red lines indicate where crack surface segments would be cut to permit cleaning and fracture surface examination.

b) Cable Diaphragm Plate 8

Cable Diaphragm Plate 8 was also discovered to be cracked and can be seen in Figure 4 after Cables 8L and 8R were removed. It is apparent from the failure that the diaphragm was not as symmetrically stressed across the diaphragm to the degree that Cable Diaphragm Plate 9 was. This resulted in the fatigue crack propagation from the south (right) side weld toe of the diaphragm to flange weld. This edge crack intersected and coalesced with a crack that developed at the adjacent ring plate weld toe, and the combined crack reached an edge crack length of about 7.5in at which time it fractured, following the principal stress as a result of the eccentric load acting on the diaphragm plate. Although a similar shorter crack formed at the north (left) flange weld end as seen in Figure 4, it was not through the diaphragm plate thickness. The eccentricity caused by the fracture plastically deformed the north pylon flange out of its plane, as is apparent in Figure 4.

The two diaphragm segments were removed from the pylon along with small pieces of the pylon flanges and can be seen in Figure 5. Both segments of the crack surface were heavily corroded. Segments of the diaphragm plate marked in red were removed for mechanical property tests. The diaphragm-flange segment on the left side of the plate was also removed so that the crack surface could be exposed.

2. Examination of the Crack Surface Segments

a) Cable Diaphragm Plate 9

Cable Diaphragm Plate 9 with attached flange pieces was cut into segments as shown in Figure 6. The segments are identified as Segments 9A through 9F from left to right (north to south). These segments were all cleaned in an ultrasonic bath, first using acetone to remove the petroleum jelly that had been applied to the crack surface. After that it was cleaned with Alconox to remove corrosion product without damaging the crack surface so that micro features could be examined in the Scanning Electron Microscope (SEM).

Figure 7 shows the cleaned crack surface of Segment 9D (the middle segment). Near the middle is where the cleaned semi-elliptical crack extending from the left of the surface in the figure intersects with the inner fracture segment. The beach marks on both the left and right ends of the surface in the figure show semi-elliptical fatigue cracks that originate from the top surface of the diaphragm plate. The adjacent smaller segment which shows the crack surface at the south (right) ring plate welds can be seen in Figure 8. The surface shows extensive corrosion product that could not be removed. Similar corrosion product is shown in Figure 7. Beach marks are visible on the right side of Figure 8 and multiple initiation surface cracks at the weld toe are apparent in the crack offsets seen in Figure 8.

The adjacent crack surface of Segment 9F at the flange weld can be seen in Figure 9. This edge crack from the south (right) flange weld is more heavily corroded than the other crack segments. The linkage of these crack segments provides a total edge crack length of the coalesced fatigue crack that is 11.25in long up to the middle of the diaphragm plate where it intersects with the clean fracture surface. This can be easily seen in the right side mating crack surface shown in Figure 10.

At the north (left) side of the diaphragm plate, cleaned Segment 9C at the left ring plates is seen in Figure 11. This shows beach marks and evidence of multiple crack initiation

sites at the surface of the diaphragm ring plate weld toe that have coalesced into a common crack.

Figure 12 shows a view of the crack in Segment 9B which is adjacent to Segment 9C shown in Figure 11. This marks the boundary of the fatigue crack that originated at the north (left) ring plates. An overview of the left side mating surface is provided in Figure 13. This shows the through thickness crack bounded on each side by fractured segments.

Finally the north (left) edge crack from the diaphragm-flange weld end, as seen in Figures 2 and 6, was exposed to examine the Segment 9A crack surface. Figures 14 and 15 show the mating crack surfaces of this crack that extended behind the primary failure surface. Crack initiation is from the end of the weld as expected. This crack extended across the diaphragm plate more quickly from the top surface which is more apparent at the end of the surface where the segment was fractured to separate the surfaces.

b) Cable Diaphragm Plate 8

Figure 16 shows the segments cut from Cable Diaphragm Plate 8 (see Figure 5 for the components removed from the pylon). One segment was removed from the north (left) side of the plate and is indicated as Segment 8L. Four segments were removed from the south (right) side of the plate and are indicated as Segments 8R1, 8R2, 8R3, and 8R4 from back to front. Note that Segment 8R4 is the mating piece to Segment 8R3. The edge crack initiated from the south (right) diaphragm-flange connection in Segment 8R3 as shown in Figure 17. The mating crack surfaces provide the same characteristics and show that the fatigue crack initiated at the weld end and progressed toward the south (right) ring plates with the top surface advancing faster than the bottom surface of the crack. This edge crack coalesced with the weld toe cracking at the ring plate as seen in Figure 18. A brittle fracture was triggered as a result of an eccentric load from the two cables that completely separated the diaphragm plate as evident in Figure 19.

At the North (left) diaphragm-flange weld end a crack had formed at the top diaphragm plate surface in Segment 8L as seen in Figures 4 and 5. This segment was removed and the fracture surfaces exposed by breaking it open at a reduced temperature and the separated pieces are shown in Figure 20. The bottom surface of the diaphragm plate can be seen in Figure 21. This shows that an independent fatigue crack had initiated in the bottom surface of the diaphragm plate about 1/2in from the larger primary crack whose exposed surfaces are shown in Figures 22 and 23. The segment shown in Figure 23 was cleaned in an ultrasonic bath and the cleaned surface is shown in Figure 24. Fatigue crack beach marks show that the crack was advancing as a semi-elliptical surface crack toward the North (left) ring plate weld. The crack in the bottom surface was also extending parallel to the top surface crack. The bottom of the top surface crack appears to be rubbed and abraised from contact indicating some compression likely from bending.

No evidence of weld toe cracking was observed at the North (left) ring plate weld toe. It seems likely that much of the crack growth seen at Segment 8L occurred after the fracture of the diaphragm plate. The behavior at Cable Diaphragm Plate 8 suggests that the two cable loads were not the same when introducing cyclic forces into the diaphragm. Crack development was significantly different than observed at Cable Diaphragm Plate 9 where nearly equal behavior was seen in the crack development at both sides of the plate.

A segment of the North (left) ring plate and diaphragm plate was saw cut and removed from the connection so that the fillet weld toes on the diaphragm plate could be polished and etched and further examined for the possibility of weld toe cracks. The region removed can be seen in Figure 25.

3. Material Properties

Material properties of Cable Diaphragm Plates 8 and 9 were evaluated to determine their chemical composition, tensile properties and CVN properties. Tensile and CVN specimens were oriented in both the longitudinal direction of the plates (loading direction) and the transverse direction. Test specimens were located in areas of the plates where no evidence of plastic deformation had occurred during fracture.

The test specimen locations are shown in Figures 3 and 5. Since the fracture path in Cable Diaphragm Plate 8 bisected the plate, test specimens were extracted from two separate areas of the plate. Sketches of the test specimen layout are shown in Figures 26 and 27. One 0.505 in. dia. tensile specimen was fabricated in each plate orientation. Twelve standard size CVN specimens were fabricated in each plate orientation positioned at the plate quarter thickness. The CVN specimens were tested in triplicate over a range of test temperatures to define the transition behavior of the steel. Results of the chemical composition, tensile, and CVN testing are provided in the laboratory test report in Appendix A.

Results of the chemical composition analyses of Cable Diaphragm Plates 8 and 9 showing the primary constituents are reproduced in Table 1 with ASTM A572 Gr. 50 requirements for comparison.

Table 1

Diaphragm Plate	Wt%											
	C	**Mn**	**P**	**S**	**Si**	**Ni**	**Cr**	**Mo**	**V**	**Nb**	**Cu**	**Al**
8	0.16	1.11	0.02	0.01	0.31	0.19	0.48	0.016	0.029	0.002	0.23	0.021
9	0.15	1.12	0.02	0.01	0.32	0.19	0.48	0.015	0.029	0.002	0.23	0.022
ASTM A572 Gr. 50	0.23 Max.	1.35 Max.	0.04 Max.	0.05 Max.	0.40 Max.				0.01-0.15 Max.		0.20 Min.*	

*When specified

Both plates conformed to ASTM A572 Gr. 50 steel, which is the steel specified for the diaphragm plates. The close similarity in composition of the two plates strongly suggests they were fabricated from the same heat of steel. It is also noted that the plates also

conform to ASTM A588 steel. The residual alloy elements included in the full analyses (Sn, W,Zn, Zr) were found to be at normal residual levels that would have no measurable effect on the material properties.

Results of tensile tests of the diaphragm plates are shown in Table 2. Both plates satisfied the tensile requirements of ASTM A572 Gr. 50. The tensile properties of the plates were identical, consistent with the chemical composition analyses indicating they were fabricated from the same heat of steel. The properties were also nearly identical in both the longitudinal and transverse directions.

Table 2

Diaphragm Plate	Orientation	Yld. Strength (0.2% Offset) (ksi)	Tensile Strength (ksi)	Elong. (2") (%)	R.A. (%)
8	Long.	61.0	88.0	27	71
	Trans.	60.0	88.5	27	72
9	Long.	60.5	88.5	26	65
	Trans.	59.5	89.0	26	68
ASTM A572 Gr. 50		50 min.	65 min.	21 min.	

The CVN tests were conducted in both the longitudinal and transverse orientation of the diaphragm plates. Tests were performed in triplicate at temperatures selected to encompass the transition temperature range of the steel. Tests were performed at room temperature (70 F), +10 F, corresponding to the AASHTO Zone 3 test temperature for Gr. 50 steel, 40 F, and -30 F. Results of the tests are provided in Appendix A and shown plotted in Figure 28.

The results of the CVN tests show that both plates have similar CVN properties and both satisfy the AASHTO Zone 3 CVN requirement for Gr. 50 steel for both non-fracture critical and fracture-critical members (15 ft-lbs @ 10F and 25 ft-lbs @ 10 F, respectively)

in both orientations tested. The difference in CVN energy in both orientations is small, consistent with the small difference in tensile properties measured in the two orientations. The measured CVN toughness is very high in both plates and explains the large fatigue crack sizes that were observed prior to brittle fracture of the plates.

4. Fractographic Assessment and Crack Growth

a) Segment 8L

The crack surface seen in Figure 29 shows beach marks of fatigue crack growth over much of its width as the fatigue crack initiated from the end of the weld toe at the diaphragm-flange connection. The crack extended across the top of diaphragm plate toward the adjacent ring plate as a semi-elliptical surface crack. The striations seen in Figure 30 were located about 3mm (1/8in) below the top surface of the diaphragm plate.

Figure 30 shows the fatigue crack growth striations that were found at location x at a magnification of 4000X. These represent individual crack growth increments and are seen to be at a very high growth rate of 2μm (7.874×10^{-5}in/cycle) to 5μm (19.6×10^{-5} in/cycle). These high levels of crack growth are in Region III and cannot be used to estimate ΔK levels from the usual Region II relationship $da/dN = 3.6 \times 10^{-10} \Delta K^3$.

It seems logical to assume that these high levels of crack growth occurred after the fatigue crack that developed at the right side of the plate coalesced with the fatigue crack from the adjacent bushing weld toe and fractured the diaphragm plate. Hence, only the remaining section was resisting the forces from the two cables. The stress cycles were stress reversals and may have exceeded the yield point of the diaphragm plate as the paint in the vicinity of the 8L crack showed evidence of yielding with cracked and missing paint.

Figures 31 and 32 show SEM views of the weld toe fatigue crack growth origin in Segment 8L at 11X and 300X. These photos show the existence of corrosion product at the crack origin and no evidence of weld toe defects.

b) Segment 9C

Figure 33 shows the location on the fracture surface of Segment 9C where possible striation or beach mark features were detected at a magnification of 1000X as seen in

Figure 34. The location shows visually obvious beach marks as the crack extended out of the ring plate weld toe region. The spacing of 5μm to 10μm is well into Region III of fatigue crack growth.

The ΔK value is well above the 60ksi√in level of crack growth for ferrite-pearlite steels shown in Figure 9.12 of Barsom & Rolfe for Region II crack growth (2). The through thickness crack at the left side of Cable Diaphragm Plate 9 is about 9in. long (see Figure 13) between the two fracture segments on each side of the crack that developed at the bushing weld toe which is a low fatigue strength Category E detail. The crack development involves both tensile axial stress and bending in the weak axis of the 3/4in. diaphragm plate. Near the ends of this through thickness crack, a crude estimate of ΔK is

$$\Delta K = Sr \sqrt{\pi a}\, F(a/b)$$

Where $a \approx 4.5$in , $F(a/b) \approx 1.5$ and a probable stress range of 10-15ksi or higher results in $\Delta K \approx 85$ksi√in which is compatible with the rapid growth of the large crack implied by the features in Figure 34. Unfortunately, the crack surfaces at the weld toes of the north (left) ring plates is severely corroded as illustrated in Figures 35, 36, and 37. The fatigue crack growth features are not apparent in beach marks nor micro level characteristics in Figure 35. However Figures 36 and 37 show end of life features of beach marks.

5. Fatigue Resistance

The two basic welded details used at the diaphragm cable connection are both very low fatigue resistant details (1). The fillet welded connections between the diaphragm plate and the pylon flanges are both long attachments that are classified as Category E' fatigue details. Shear lag also influences crack growth from these details as the cracks follow the principal tensile as the crack is initiated and propagates from the weld toe termination. The lower bound fatigue limit for Category E' details, is 2.6ksi and occurs at about 20 million cycles.

The second fatigue critical detail is the weld toe of the ring plate to diaphragm plate connections. These details are on the margin between Category E and E' as the diaphragm plate thickness of ¾in is at the limit for Category E. Its fatigue limit is slightly higher at 4.5ksi and occurs at about 10 million cycles.

The applied loads from the cables do not provide a uniform stress field across the diaphragm width. There is a shear lag influence that elevates the principal stress at the end welds and at the ring plate weld toes near the end welds. This is reflected in the crack development at the diaphragm-flange end weld and at the adjacent ring plate weld toe.

Limited measurements by WJE on April 20, 2012 on Cable Diaphragm Plate 7 show that the end of the diaphragm plate is deformed up and down by equal amounts from vibration of the cable at low wind speeds of 5-8mph. The resulting stress cycles are repeatable narrow band cycles for this wind speed at a frequency of 11Hz. The stress range at the end welds (the gage was slightly offset and 0.3in from the weld toe) was a narrow band with a maximum stress range of 2.8ksi on the top and bottom diaphragm plate surfaces as illustrated by the response at Gage SG01 seen in Figure 38. This cyclic stress is always in tension as a result of the axial force in the cables. At the weld toe this cyclic stress is likely greater. Since the variable stress range spectrum exceeds the fatigue limit by more than 0.01%, stress cycles above 0.5 x Fatigue Limit will contribute to fatigue damage at Cable Diaphragm Plate 7.

Strain gages were also installed at 0.3in from the ring plate weld toe at half the distance between the line of action of the cable and the diaphragm plate to pylon flange weld, where fatigue crack growth was dominate in both Cable Diaphragm Plates 8 and 9. The narrow band maximum stress range was 6.3ksi which also exceeds the fatigue limit of Category E by more than 0.01% as is visually apparent in Figure 39 as the stress cycles above 0.5 x Fatigue Limit will all contribute to fatigue damage at the top and bottom ring plate weld toes at Cable Diaphragm Plate 7.

There is every reason to expect that the response of Cable Diaphragm Plates 8 and 9 will have experienced cyclic stresses that are greater than those measured at Cable No 7. Fatigue crack growth and eventual failure would be expected at the stress ranges that developed at the end welds and adjacent ring plates. At 11Hz, 1million stress range cycles would accumulate in about 28hrs of comparable wind conditions. Higher wind speeds are likely to result in higher stress cycles at higher modes and frequency.

From the extensive corrosion on the crack surfaces, portions of these fatigue cracks likely reached full diaphragm plate thickness several years ago. Cable vibration is the cause of high frequency stress cycles and it is clear that these cycles exceed the fatigue limit at both welded details. At Cable Diaphragm Plate 9, the crack development is nearly symmetrical leading to crack growth at all 4 locations. At the south (right) side of Cable Diaphragm Plate 9 the two cracks joined providing an 11.25in edge crack at the final failure. At the north (left) side of Cable Diaphragm Plate 9 the two cracks were offset so that the ring plate weld toe crack extended to a through thickness crack about 9in long. The left side edge crack extended over 6in behind the through thickness crack which shielded the larger ring plate crack at that end.

The gross section capacity at Cable Diaphragm Plate 9, based on yield strength of the diaphragm plate, is about 203kips, as the remaining section was about 3.4in^2 prior to fracture. The reported total dead service load cable force at Cable Diaphragm Plate 9 is about 162kips. Hence, the observed brittle fracture is consistent with the high toughness

of the diaphragm material that allowed such large fatigue cracks to form at Cable Diaphragm Plate 9.

At Cable Diaphragm Plate 8, the fatigue crack growth was not symmetrical as no detectable cracking was found at the left ring plate and much of the cracking that developed at the left end weld may have occurred after the failure originating at the right side of the plate. This edge crack fracture suggests that the cable loading was not symmetric at Cable Diaphragm Plate 8. The critical edge crack length at fracture was about 7.5in. The high frequency vibration observed at Cable Diaphragm Plate 7 provides a loading rate much higher than that associated with the 1 second loading rate used for bridge structures subjected to truck traffic. This is an order of magnitude greater which contributes to the brittle fracture in the lower fracture toughness direction provided by TL CVN tests.

6. Metallography

Weld macro-cross-sections were prepared from the segment removed from the north (left) ring plate of Cable Diaphragm Plate 8 (see Figure 25) to determine if crack development had occurred at the fillet weld toe. Figure 40 shows the etched surfaces of the segment. No weld toe cracking was detected in either of the cross-sections.

A weld cross-section was also prepared from the diaphragm-flange weld at the right side of Cable Diaphragm Plate 9 to characterize the weld geometry. The cross-section was located near the weld termination. Figure 41 shows the etched cross-section. The weld joint consists of two multi-pass fillet welds. No weld defects were observed in the cross-section.

7. Summary and Conclusions

1. Fatigue crack growth developed at Cable Diaphragm Plates 8 and 9 as a result of low fatigue strength weld details at four locations.

2. The cyclic stress range driving the crack development and growth was due to the vibrations of the stay cables from wind. The high frequency response resulted in large numbers of stress cycles in only a few years of service that exceeded 0.5 of the Fatigue Limit. This was verified by strain gage measurements on Cable Diaphragm Plate 7.

3. Since the cable tension forces were always present, all stress cycles were in tension at high R ratios at the top and bottom surfaces of the diaphragm plates.

4. Both Cable Diaphragm Plates 8 and 9 showed evidence of crack development mainly from the top surface of the diaphragm plates. This indicates that the applied cable forces created some initial bending in the diaphragm plates due to the plate geometry.

5. At the end welds that were wrapped around the diaphragm plate some embedded slag and porosity existed. These did not influence the weld toe cracks that formed in the diaphragm plate. As observed at left side of Cable Diaphragm Plate 8 these toe cracks could form in more than one plane.

6. Although corrosion damage prevented detection of crack growth striations near the weld toes on the micro level, fatigue beach marks and the crack surface characteristics verified that stable fatigue crack propagation existed over most of the crack surface at Cable Diaphragm Plate 9 and at the north (left) side of Cable Diaphragm Plate 8 up to the left ring plate.

7. The plate material used for the diaphragms had tensile properties that were in compliance with the Specifications. The CVN test results showed that the material exceeded the toughness required for Zone 3.

8. The brittle fracture that occurred at Cable Diaphragm Plate 8 suggests that an eccentric load contributed to fatigue crack growth and initiated a brittle fracture in the lower toughness direction.

9. The high frequency of the fatigue loading is a significant order of magnitude greater than normally considered for bridge structures. This has reduced the fracture resistance of the diaphragm material.

8. References

1) AASHTO LRFD Bridge Design Specifications, Section 6.6, Table 6.6.1.2.3-1 section 7, 2009 (see also the AISC Specifications, Appendix 3 Fatigue Design, 2005)

2) Barsom, J.M. and Rolfe, S.T., Fracture and Fatigue Control in Structures, 3rd Edition, ASTM, West Conshohocken, PA 1999

Figure 1: View of fracture surface of Cable Diaphragm Plate 9 showing crack growth from weld toes of ring plates and end welds

Figure 2: View of cracked Cable Diaphragm Plate 9 before removal from pylon

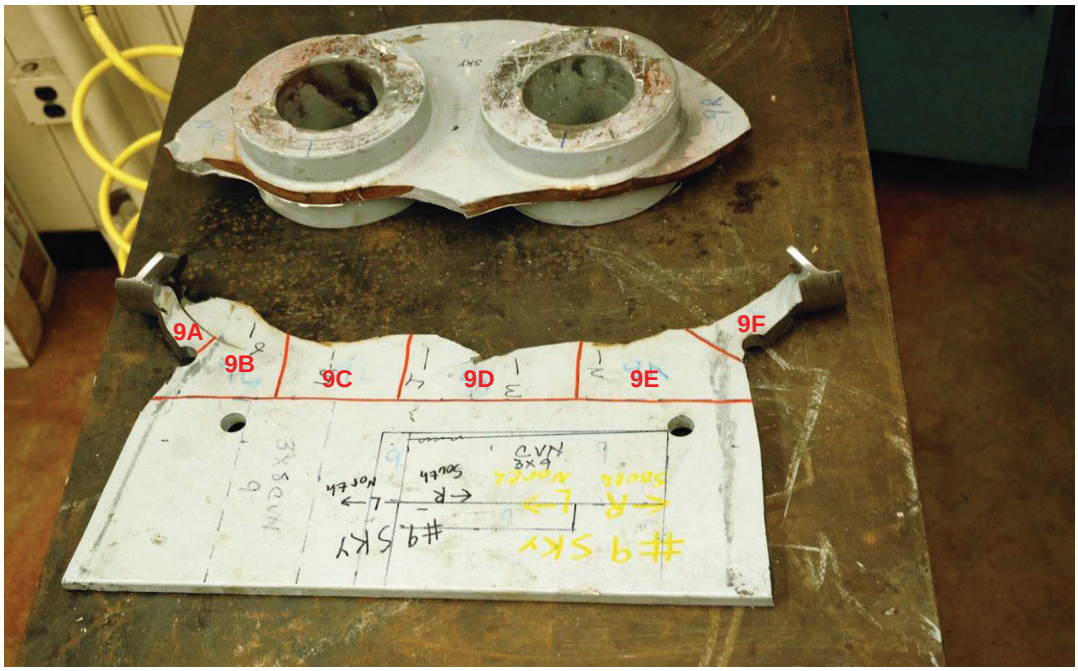

Figure 3: View of Cable Diaphragm Plate 9 segments with ring plates. Note markings for mechanical test samples (black marks) and fractographic samples (red marks). Fractographic sample segments are indicated 9A through 9F from left to right.

Figure 4: View of Cable Diaphragm Plate 8 after cables were removed showing fracture, crack, and flange plastic distortion

Figure 5: View of Cable Diaphragm Plate 8 after removal from pylon. Note markings for mechanical and fractographic test samples. Fractographic test sample segments are indicated as 8L, 8R1, 8R2, 8R3, and 8R4.

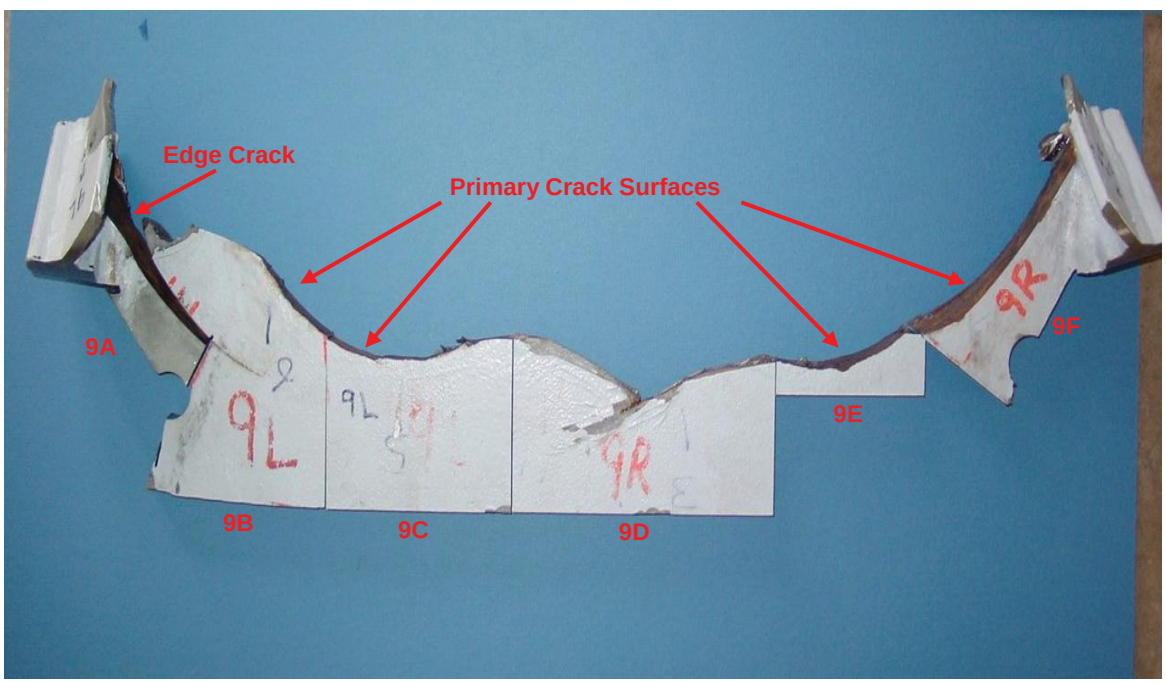

Figure 6: View of segments of Cable Diaphragm Plate 9 looking at the top surface

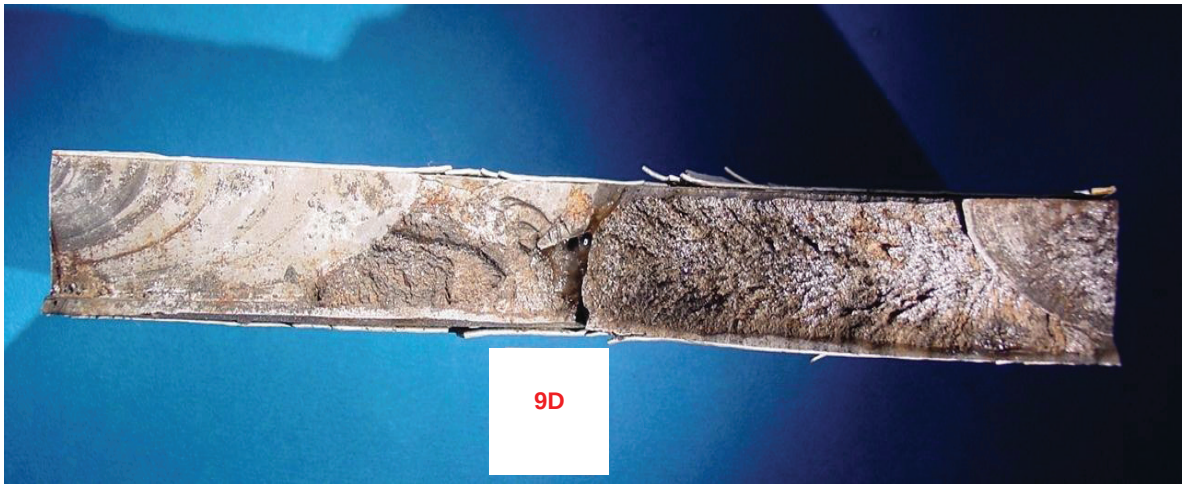

Figure 7: Cleaned crack surface of Segment 9D (middle segment) with the top surface corresponding to the top surface in Figure 6.

Figure 8: Cleaned crack surface Segment 9E (the smaller segment at the ring plate weld toe adjacent to the surface seen in Figure 7).

Figure 9: View of crack surface of Segment 9F propagating from the end weld of diaphragm-flange weld

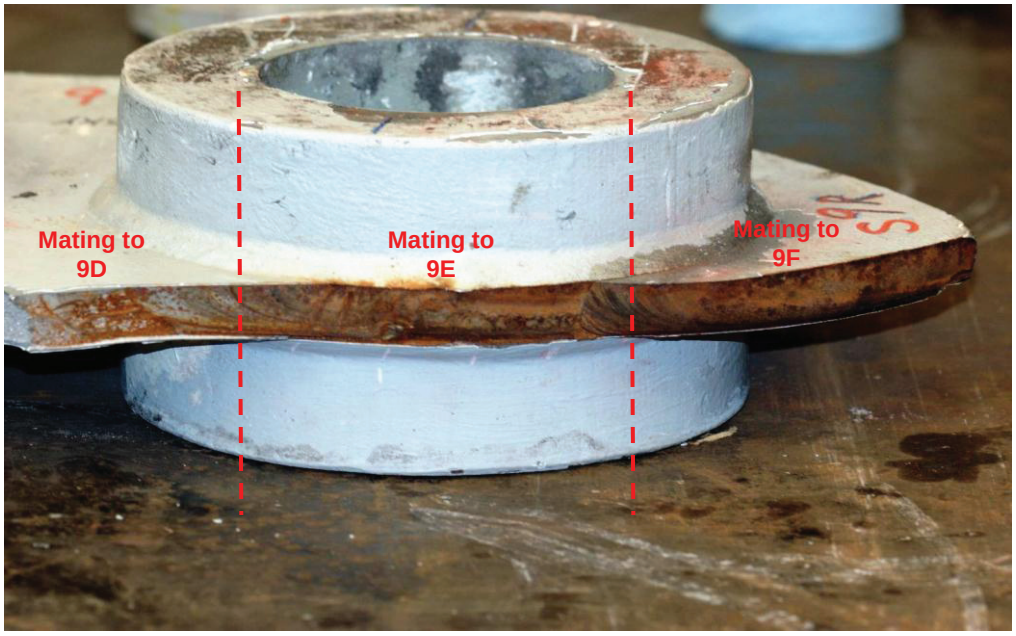

Figure 10: Mating crack surface of right side of Cable Diaphragm Plate 9 showing coalesced edge crack. The approximate mating surfaces of Segments 9D, 9E, and 9F are indicated.

Figure 11: View of cleaned surface of Segment 9C at the left ring plate weld toe showing multiple initiation sites and coalescence of the cracks

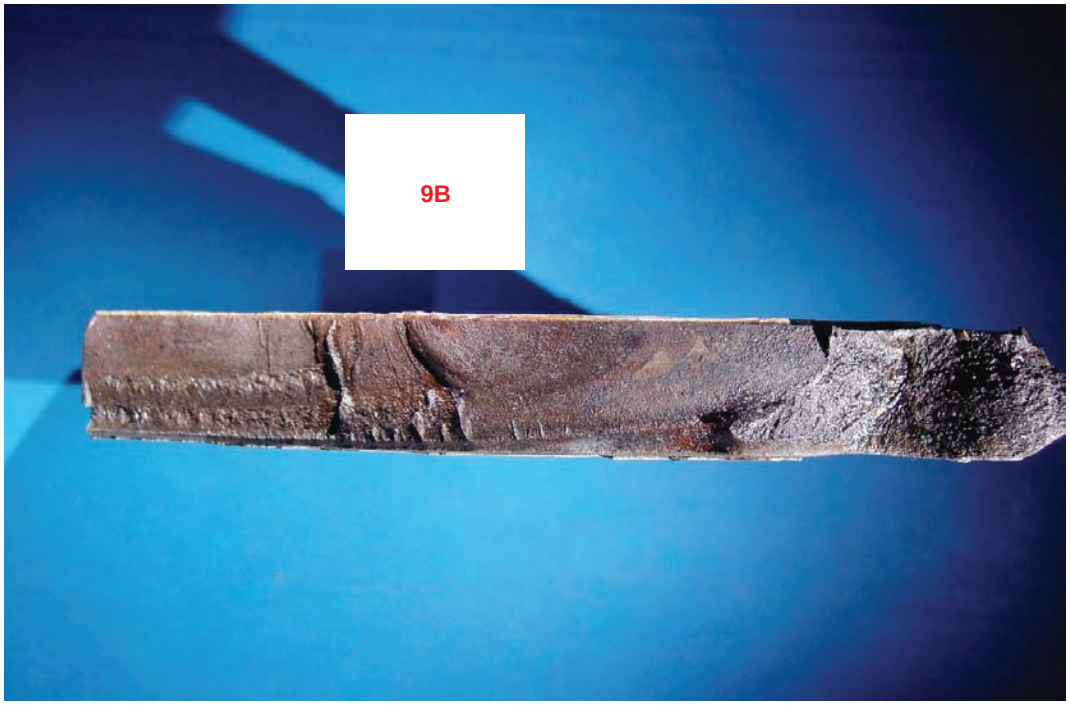

Figure 12: View of primary crack surface in Segment 9B on the left side of Cable Diaphragm Plate 9 in front of edge crack

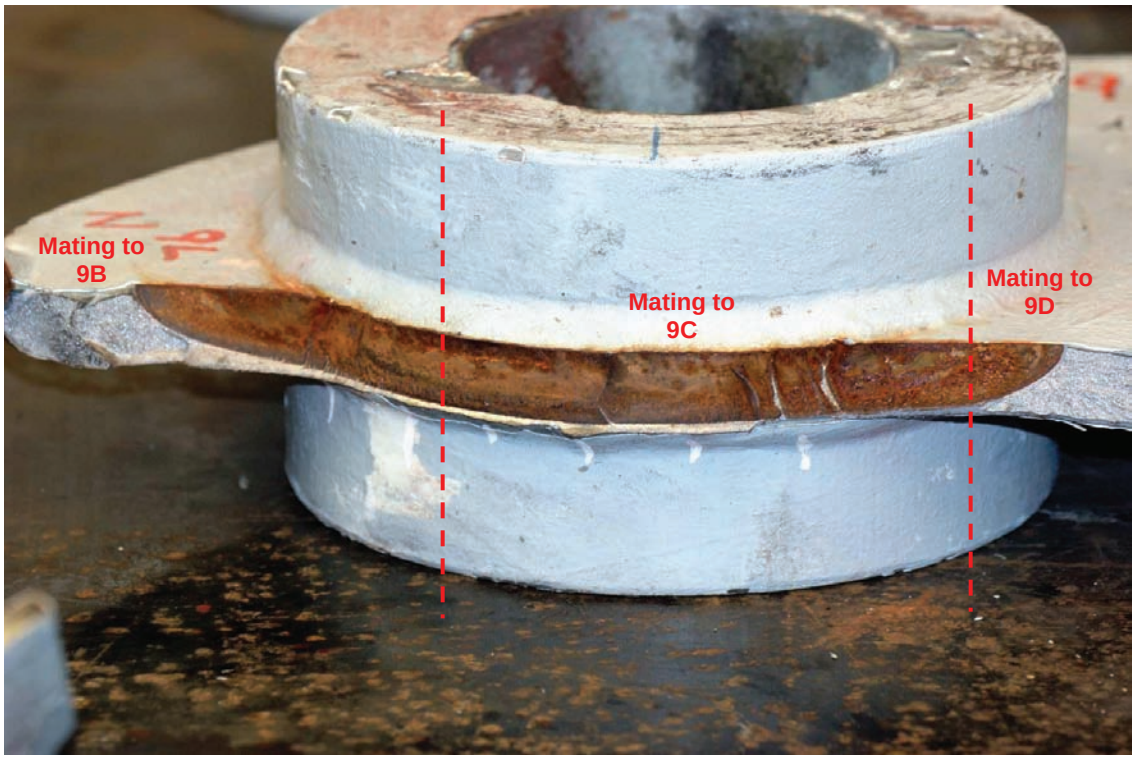

Figure 13: Overview of mating crack surface at left ring plates for Cable Diaphragm Plate 9 showing fracture segments on each side of the primary crack. The approximate limits of the mating surfaces for Segments 9B, 9C, and 9D are indicated.

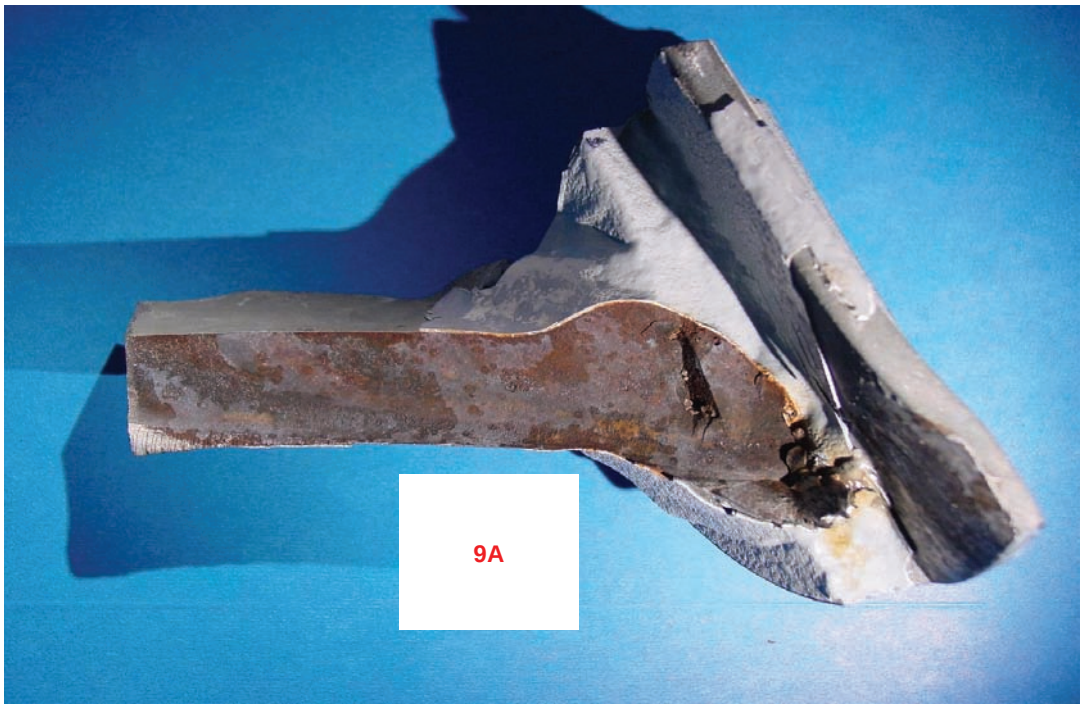

Figure 14: Exposed and cleaned crack surface of edge crack in Segment 9A behind the primary crack showing corrosion product on surface and crack growth from the weld toe

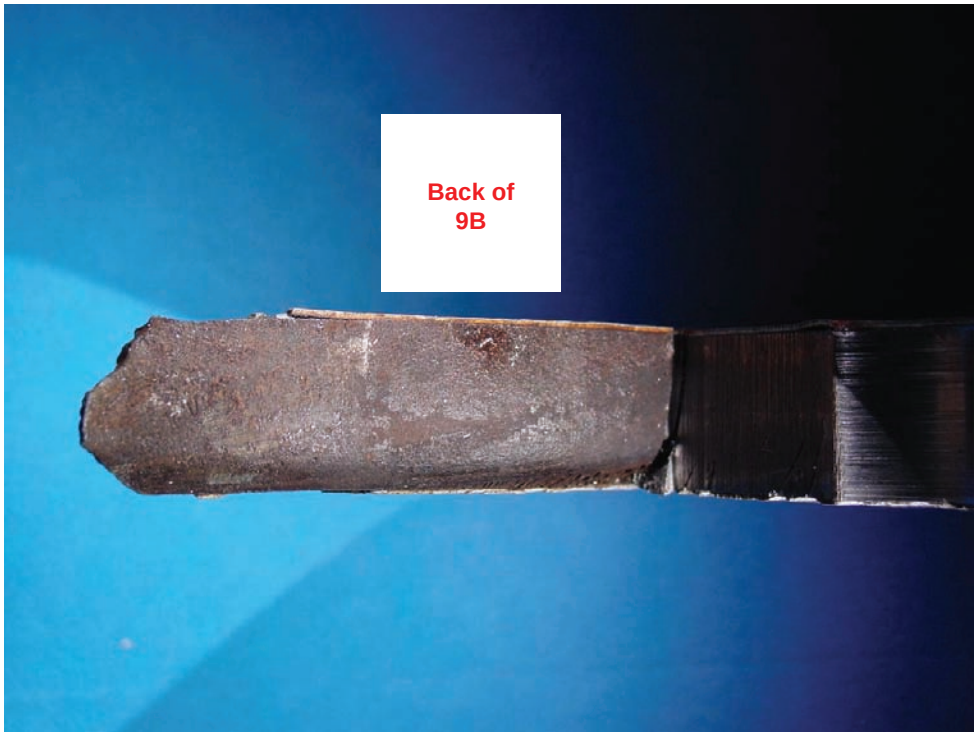

Figure 15: Mating crack surface to Segment 9A of the edge crack in Segment 9B behind the primary crack.

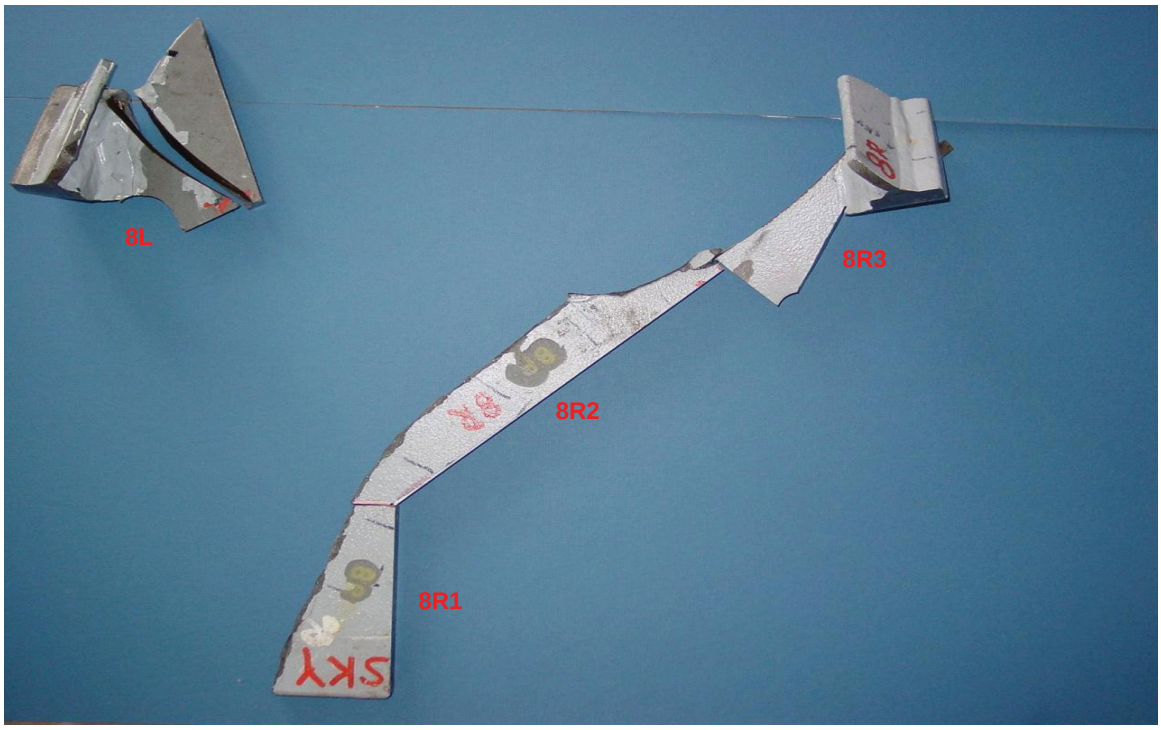

Figure 16: View of segments cut from Cable Diaphragm Plate 8

Figure 17: View of cleaned crack surface of diaphragm to flange edge crack in Segment 8R3 and the mating crack face (Segment 8R4) showing the end weld at the flange

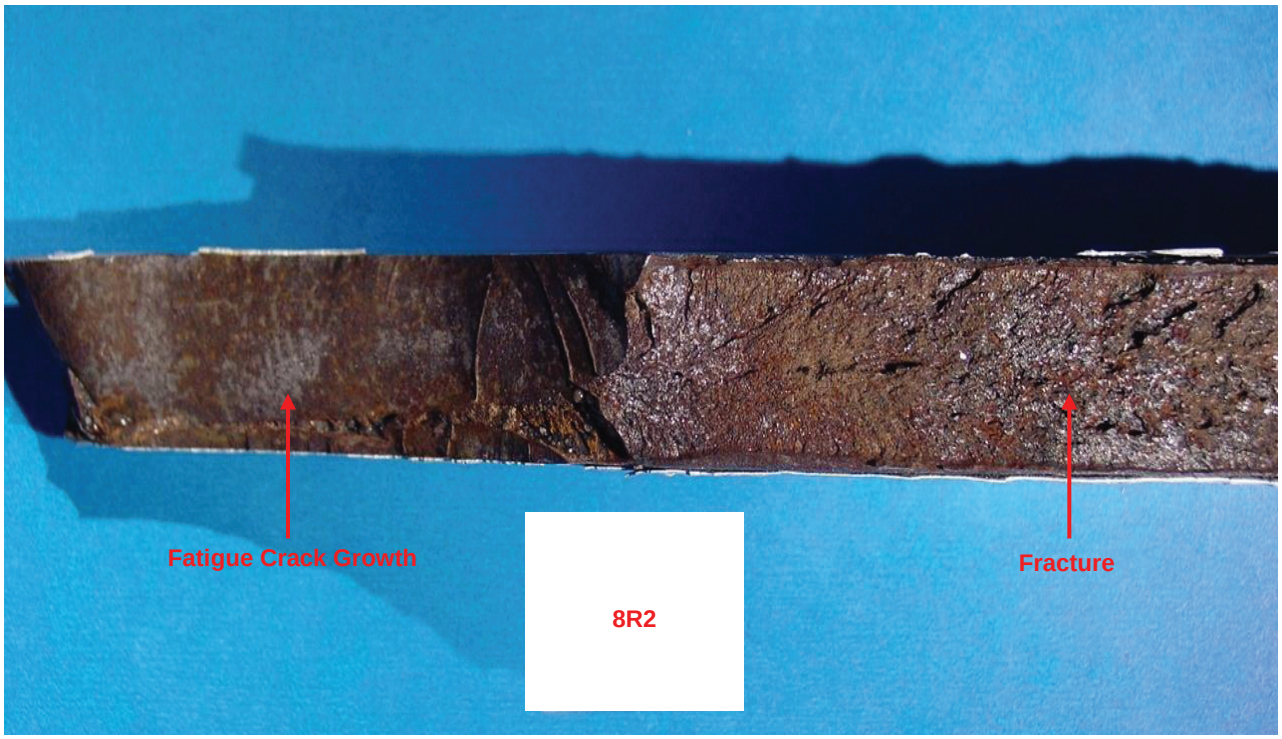

Figure 18: Cleaned fatigue crack surface of Segment 8R2 at the south (left) ring plate and adjacent fracture

Figure 19: Overview of the unstable fracture that broke the diaphragm plate in Segment 8R2

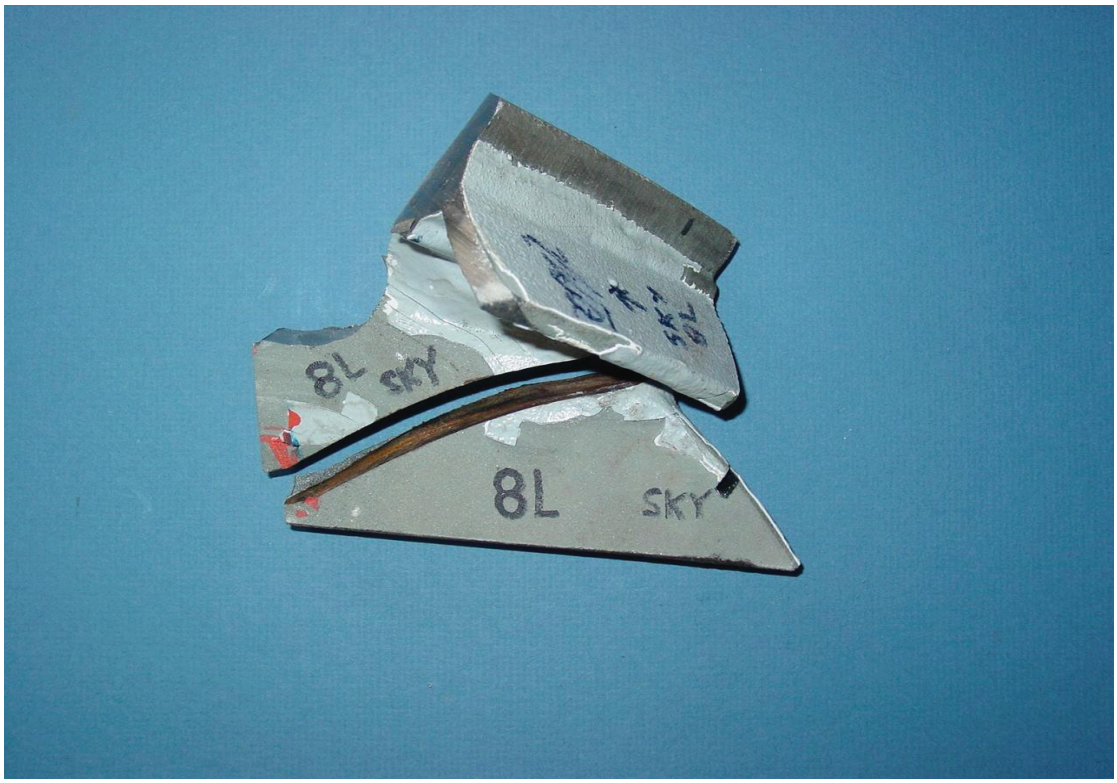

Figure 20: Primary crack surfaces of Segment 8L separated at reduced temperature

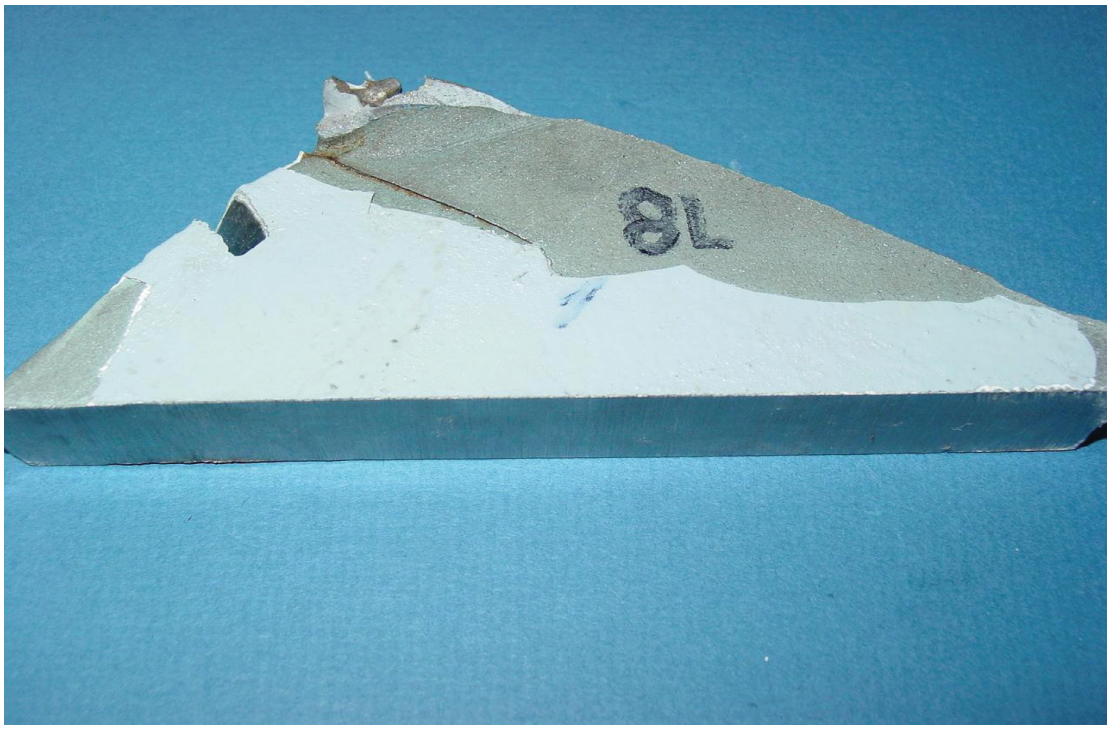

Figure 21: Secondary crack on bottom surface of Segment 8L parallel to the primary crack surface. Note this is a view of the bottom side of the lower piece in Figure 20.

Figure 22: View of primary exposed fatigue crack surface of Segment 8L originating at the weld toe and propagating as a elliptical surface crack from the top surface

Figure 23: View of matching crack surface of Segment 8L; secondary crack seen in Figure 21 lies behind the primary crack surface and propagates from the bottom surface

Figure 24: Cleaned crack surface of Segment 8L showing fatigue beach marks and rubbing near bottom of crack

Figure 25: showing where segments were cut from the left side of Cable Diaphragm Plate 8 at the ring plates and crack face from the right side of the plate

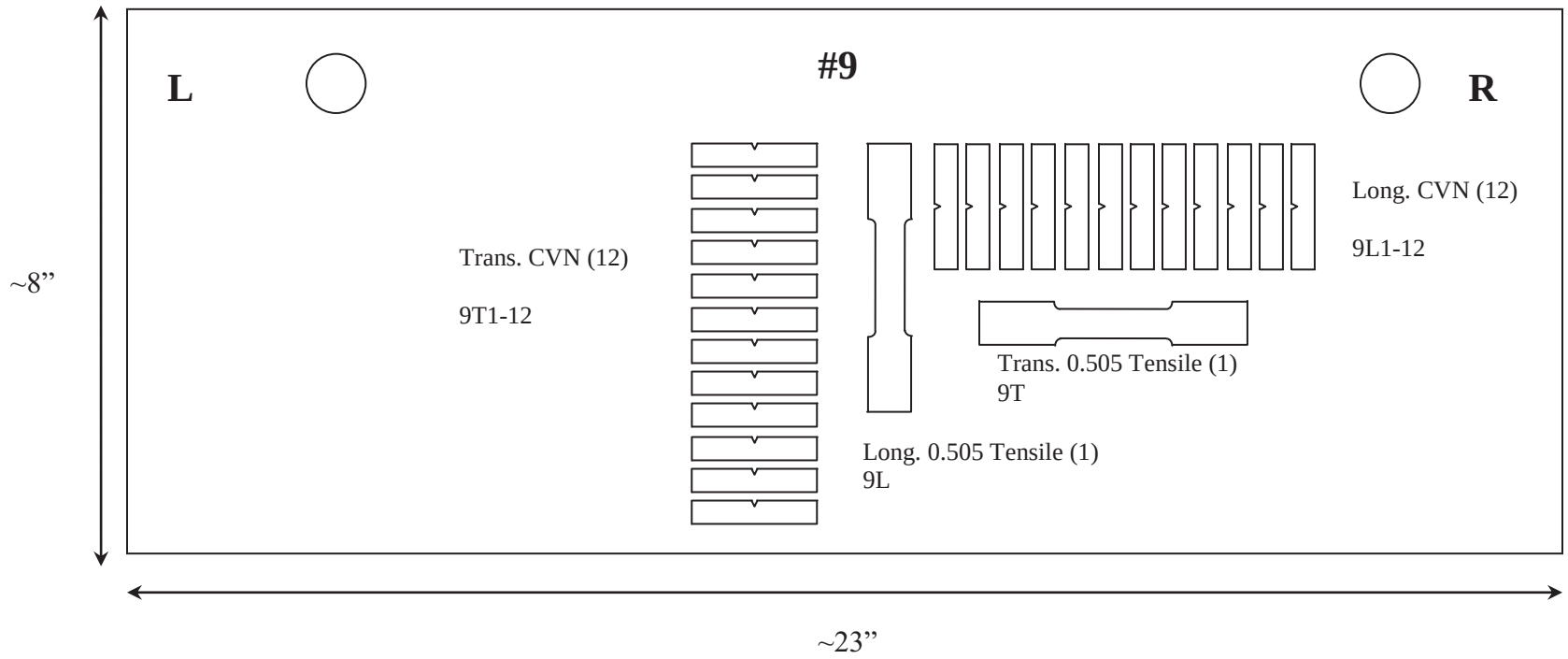

Figure 26: Test Specimen Layout for Diaphragm Plate 9.

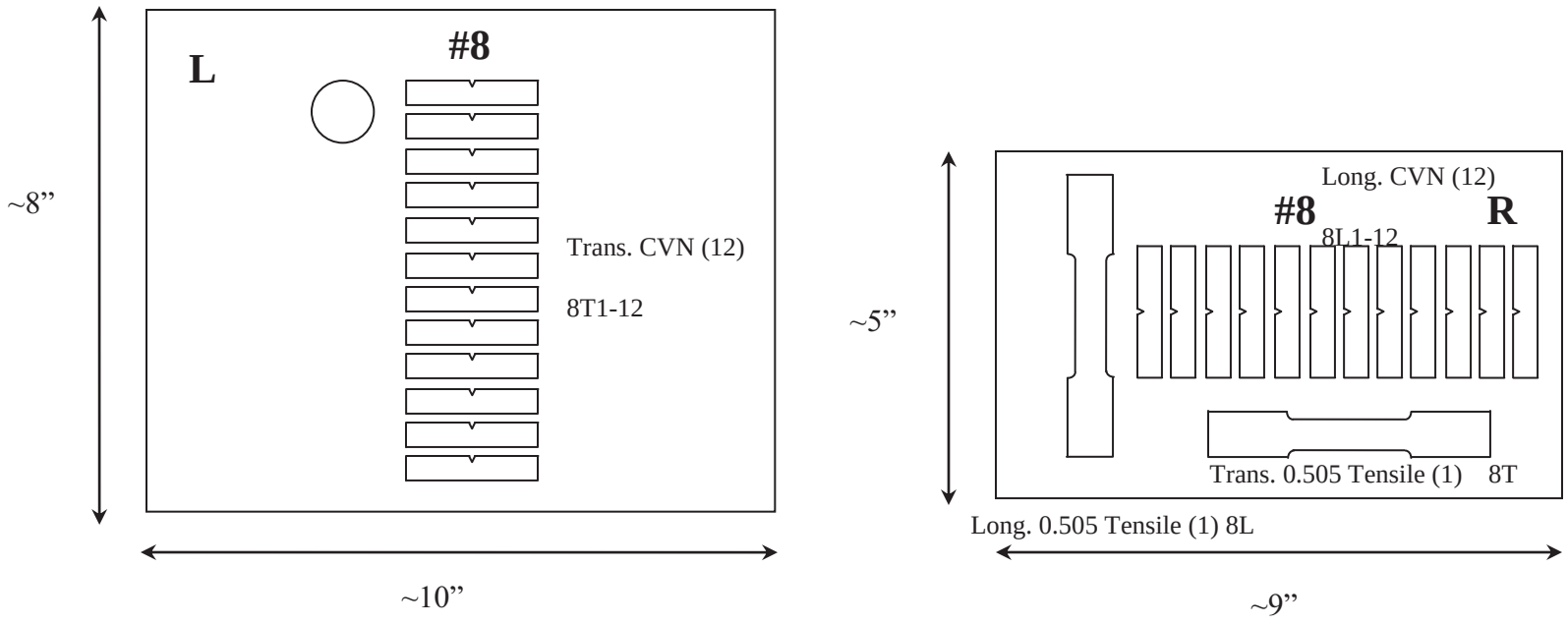

Figure 27: Test Specimen Layout for Diaphragm Plate 8.

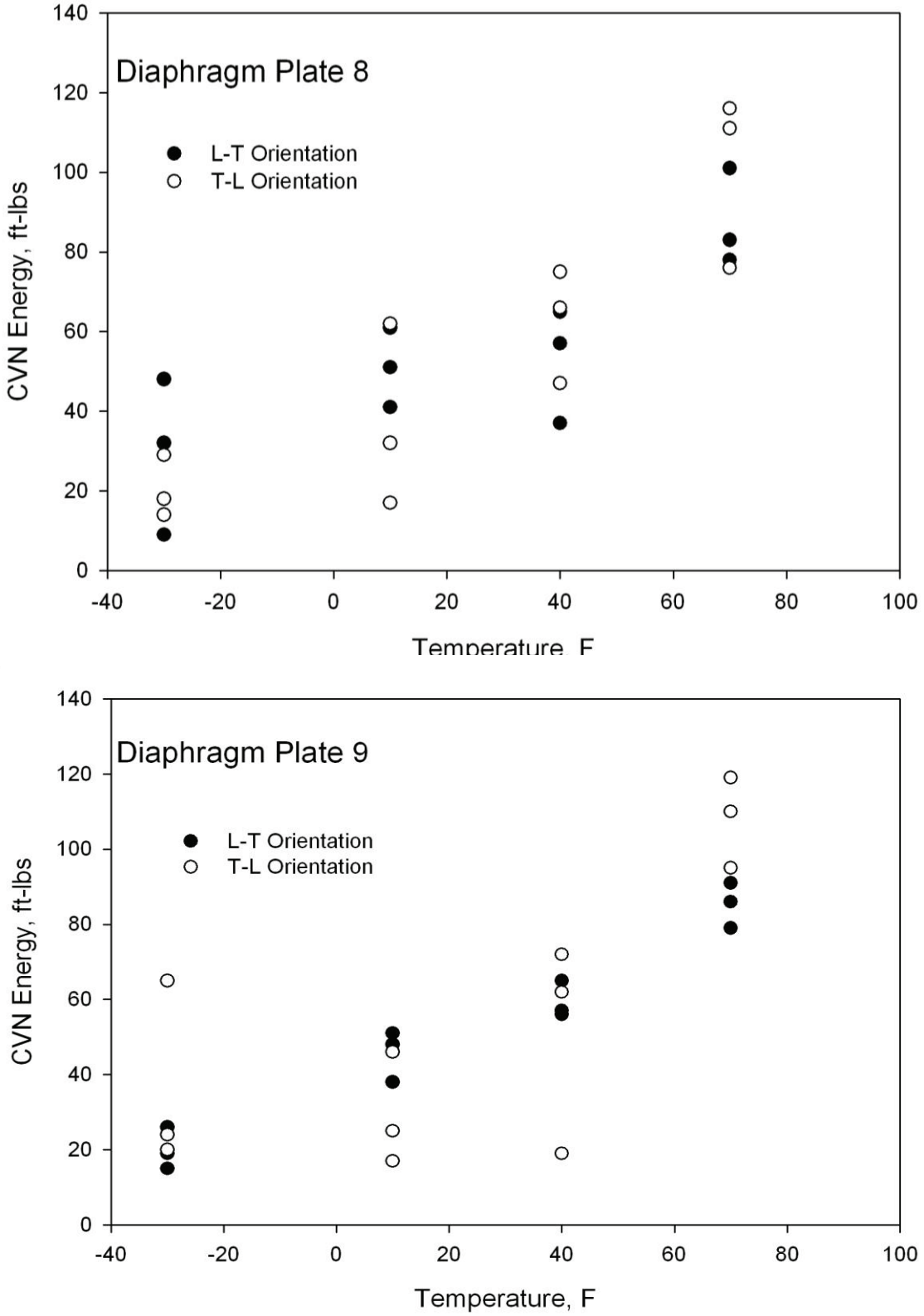

Figure 28: Diaphragm Plate CVN Test Results.

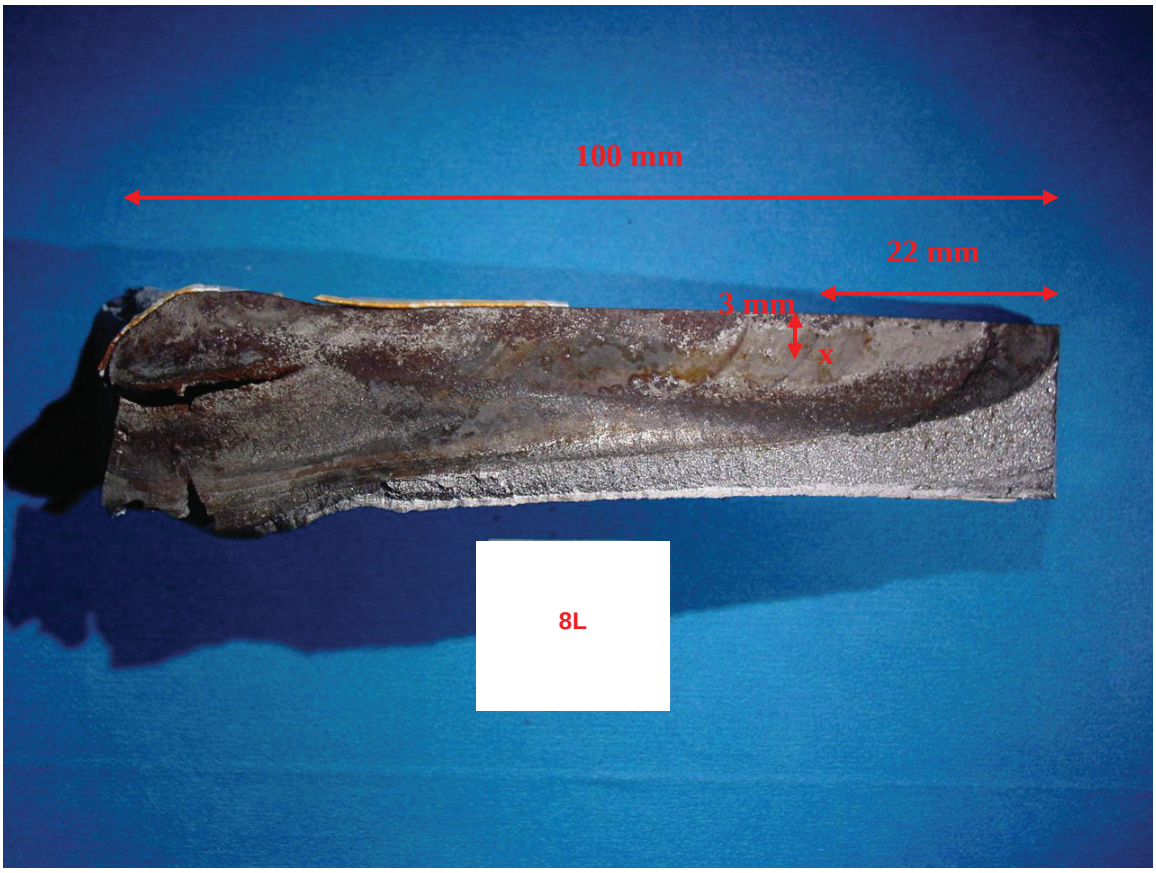

Figure 29: Cleaned crack surface of Segment 8L with location of region where fatigue striations were detected is identified with an “x”

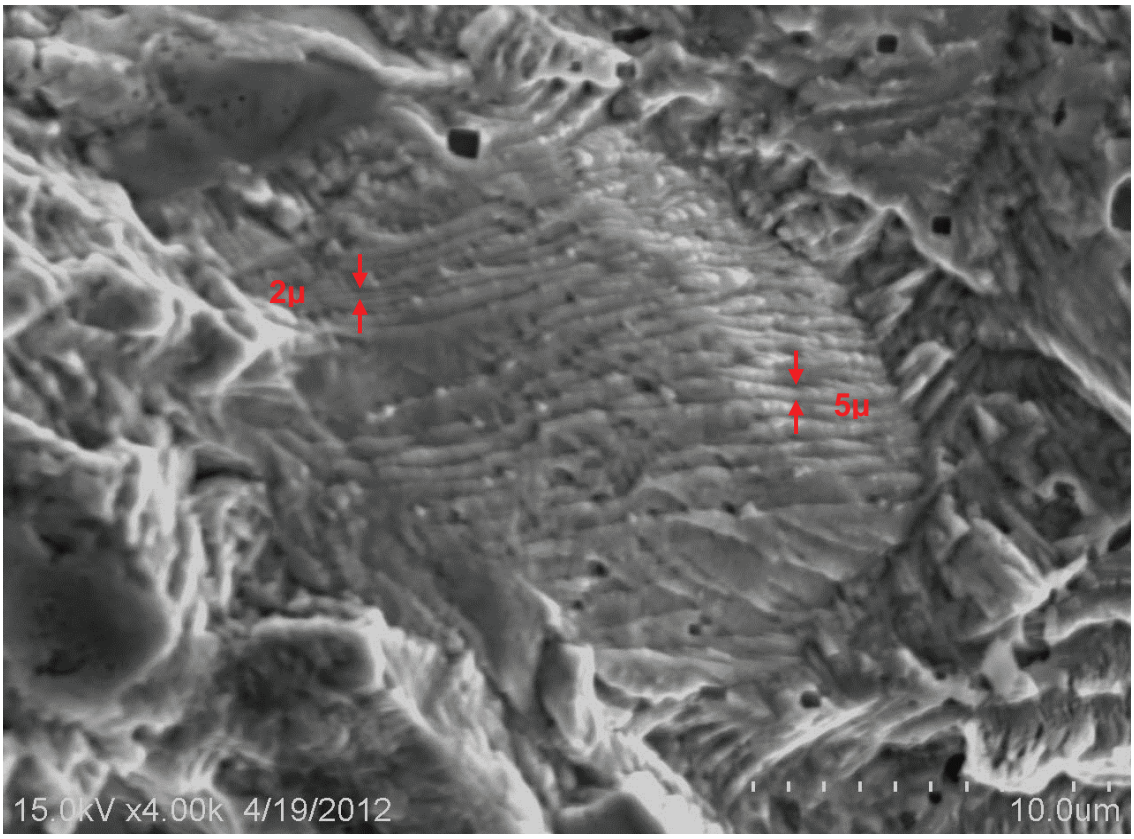

Figure 30: SEM view of the fatigue crack surface of the Segment 8L crack at the location shown in Figure 29. Magnification 4000X

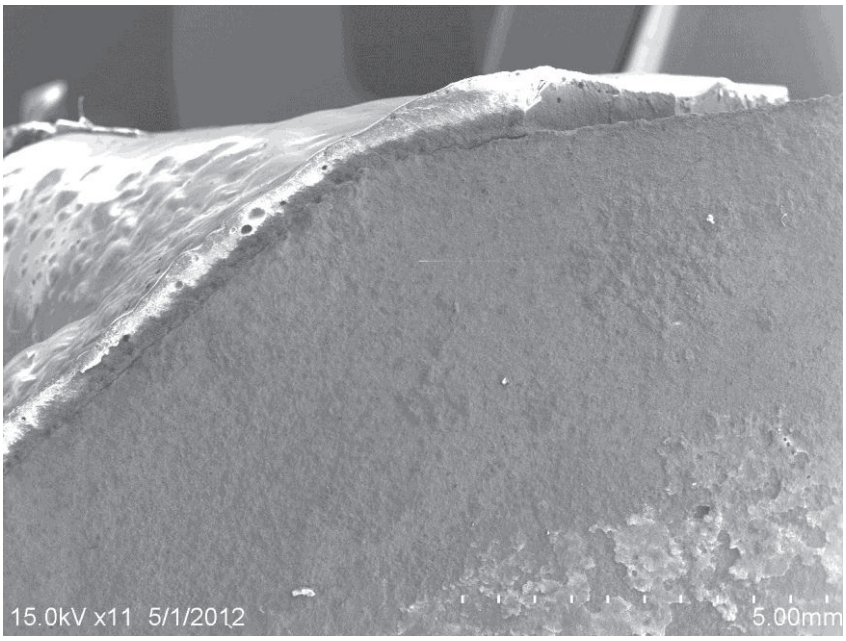

Figure 31: SEM view of Segment 8L at weld toe crack origin @11X

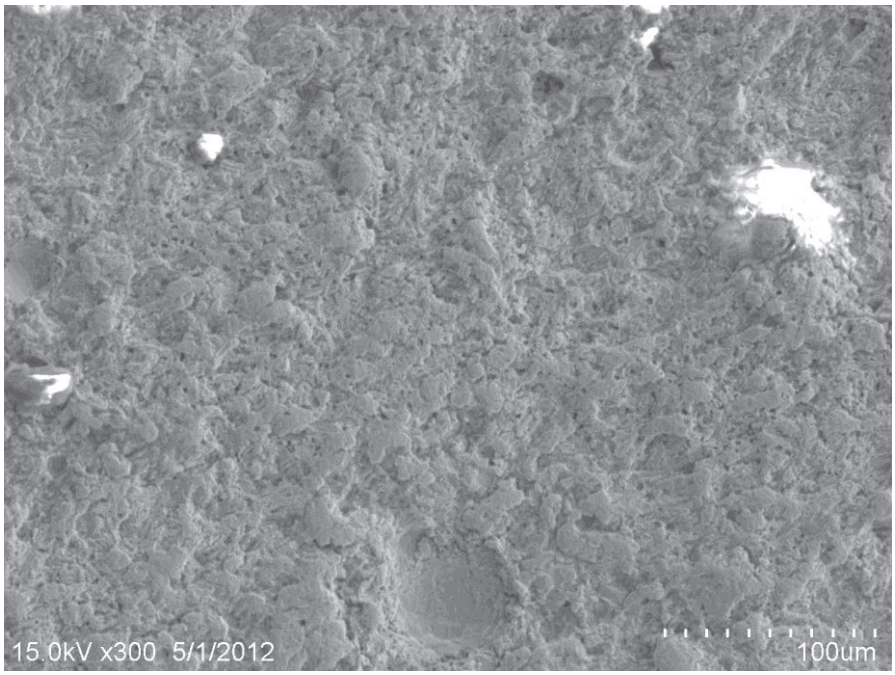

Figure 32: Enlarged view of Figure 31 showing corrosion product on crack surface 8L @300X

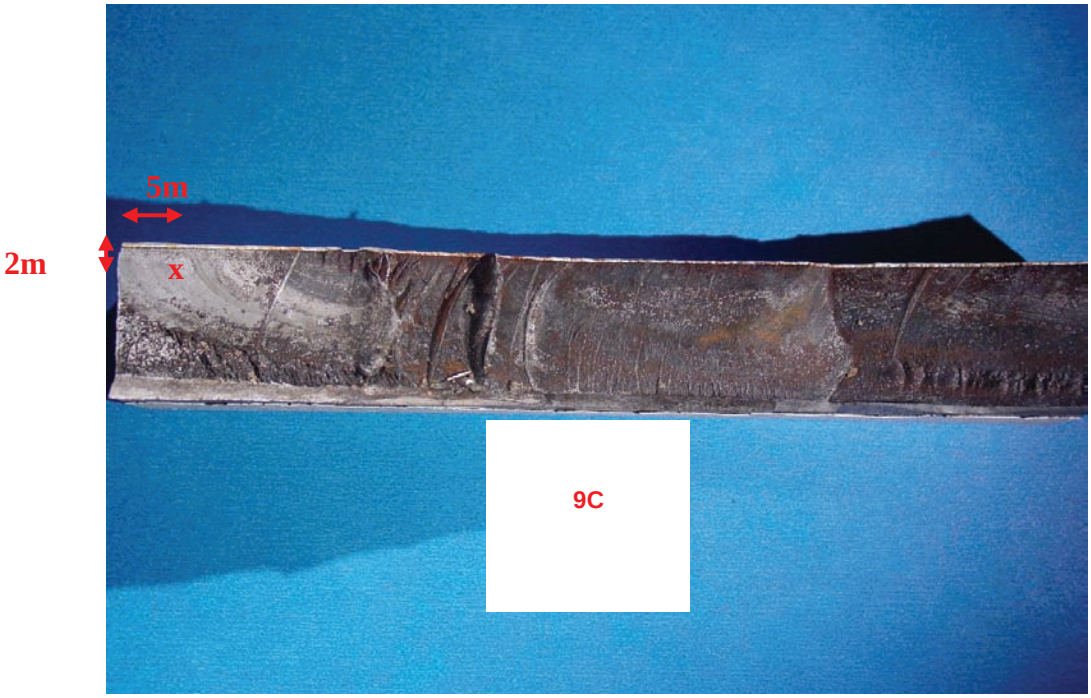

Figure 33: View of crack surface of Segment 9C at ring plate weld showing beach marks and multiple initiation sites from weld toe on top surface

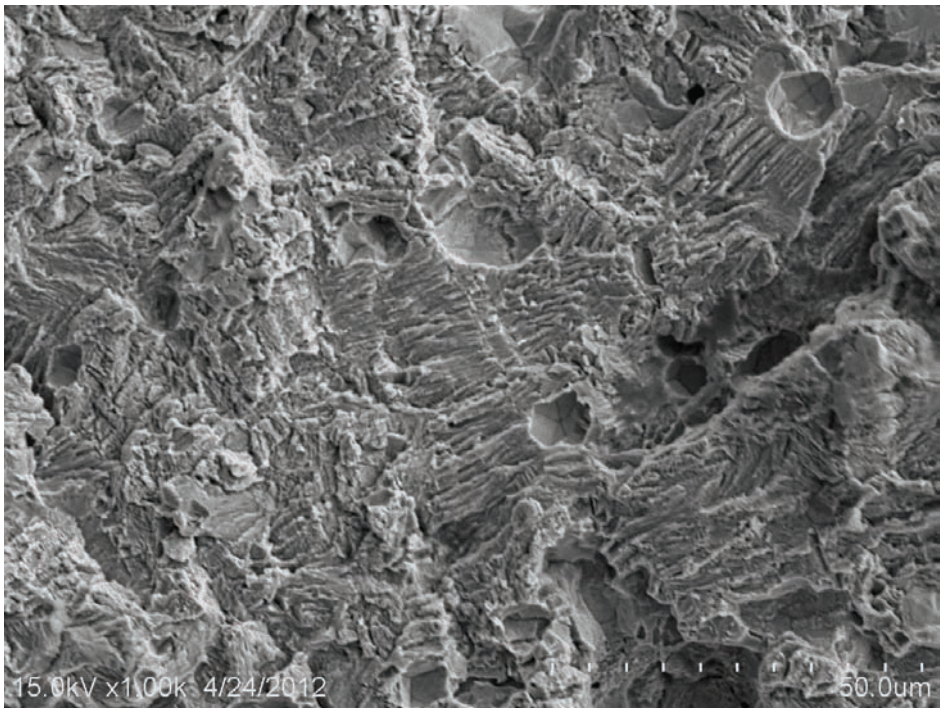

Figure 34: SEM (1000X) of crack surface of Segment 9C at point “x” in Figure 33

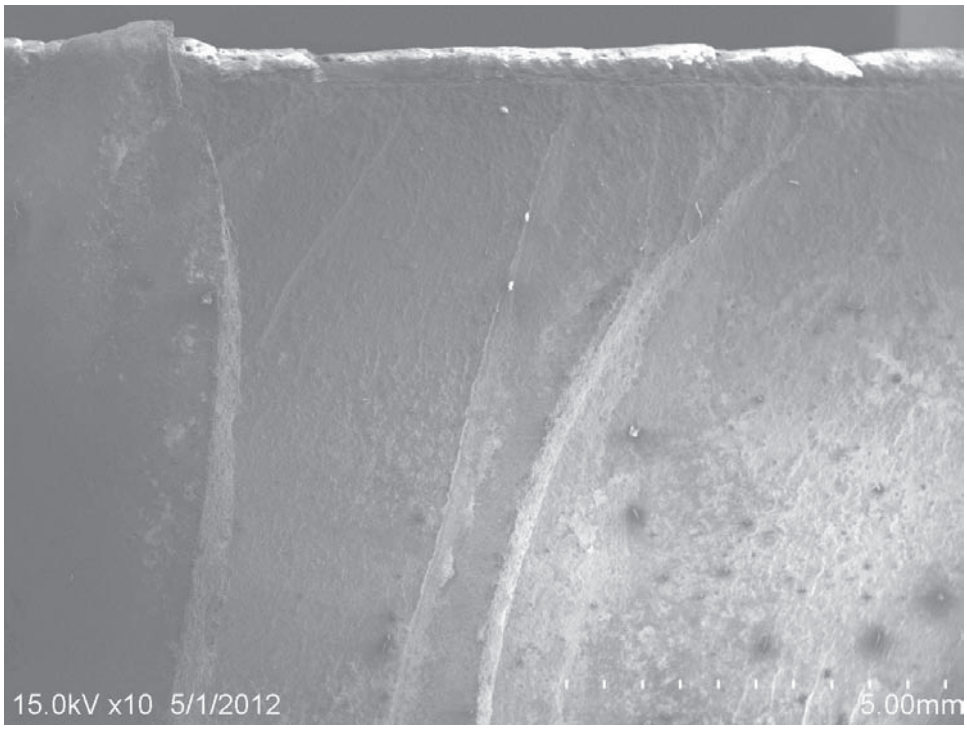

Figure35: SEM view of weld toe region @10X of Segment 9C showing multiple initiation sites of fatigue crack growth

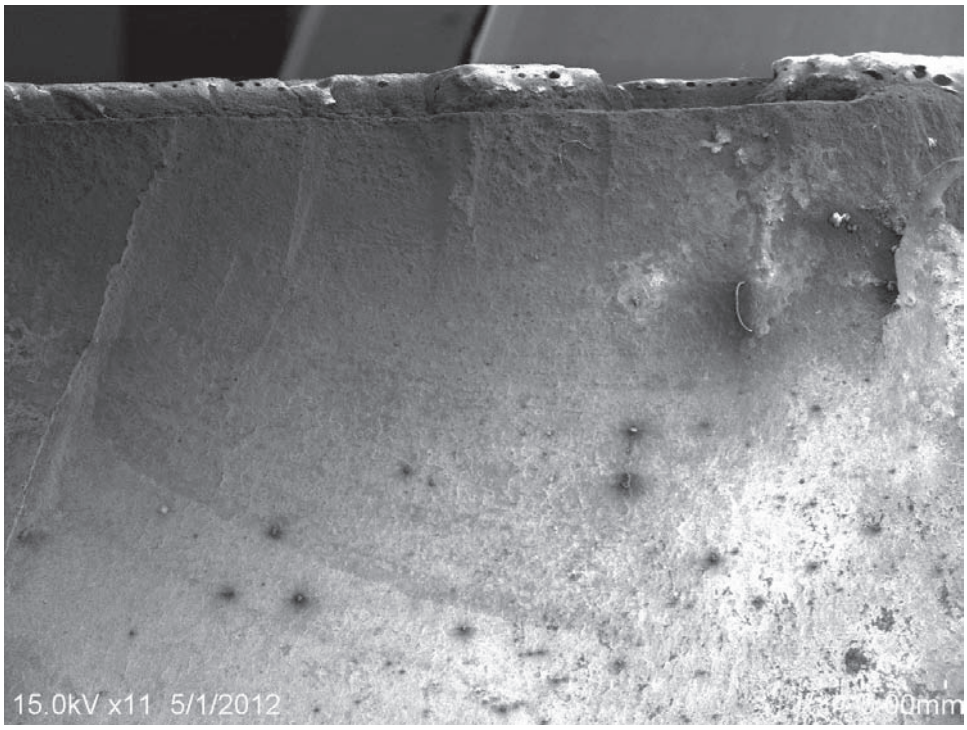

Figure 36: SEM view of crack initiation from the weld toe and beach marks at Segment 9C @ 11X

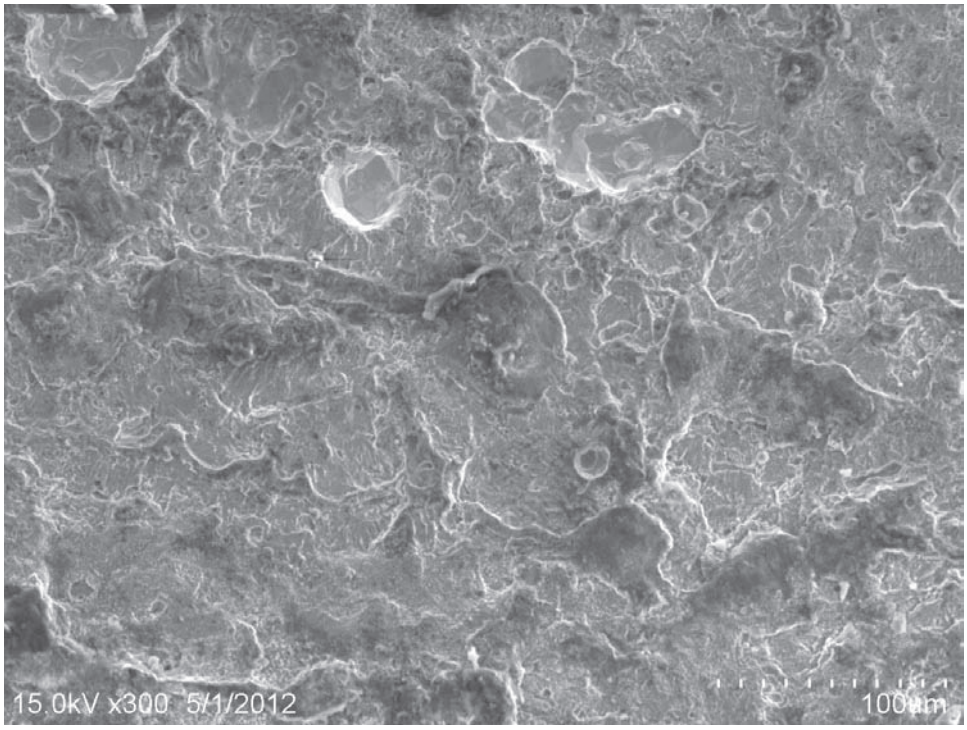

Figure 37: SEM view of crack surface in Figure 36 showing fatigue fracture surface @300X

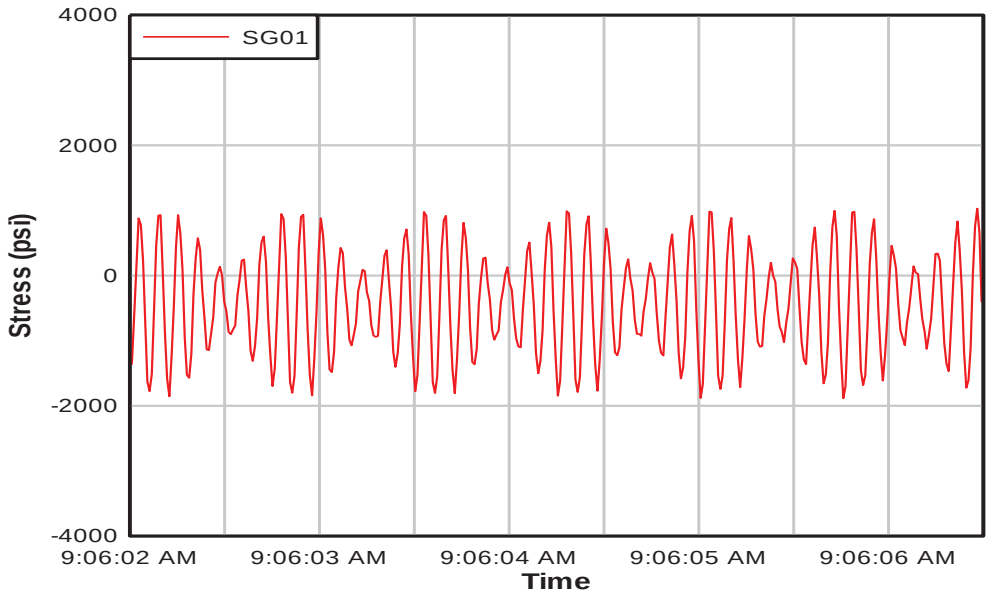

Figure 38: Stress response from strain gage SG01 located adjacent to the left end diaphragm plate to pylon flange weld toe at Cable Diaphragm Plate 7 for a wind speed of 5 mph to 8 mph at a direction of about 20 degrees. Note 0 degrees is taken as perpendicular left of the structure with increasing increments clockwise looking down.

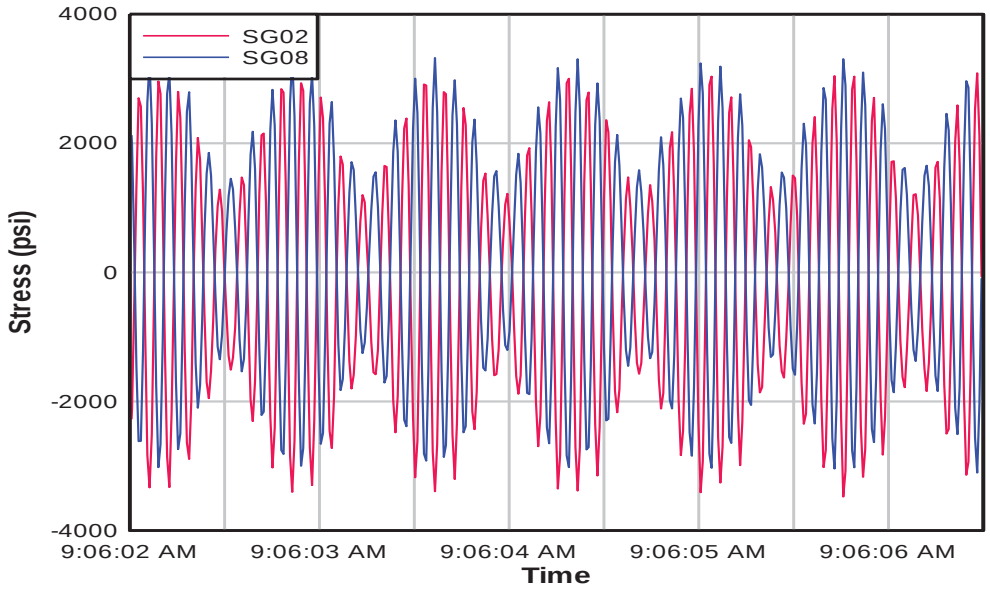

Figure 39: Stress response from strain gages SG02 and SG08 for the wind event shown above. SG02 is positioned on top of Cable Diaphragm Plate 7 normal to the ring plate weld toe at the midpoint between the line of action of the cable and the diaphragm plate to pylon flange weld termination. SG08 is positioned on the bottom of the plate opposite SG02.

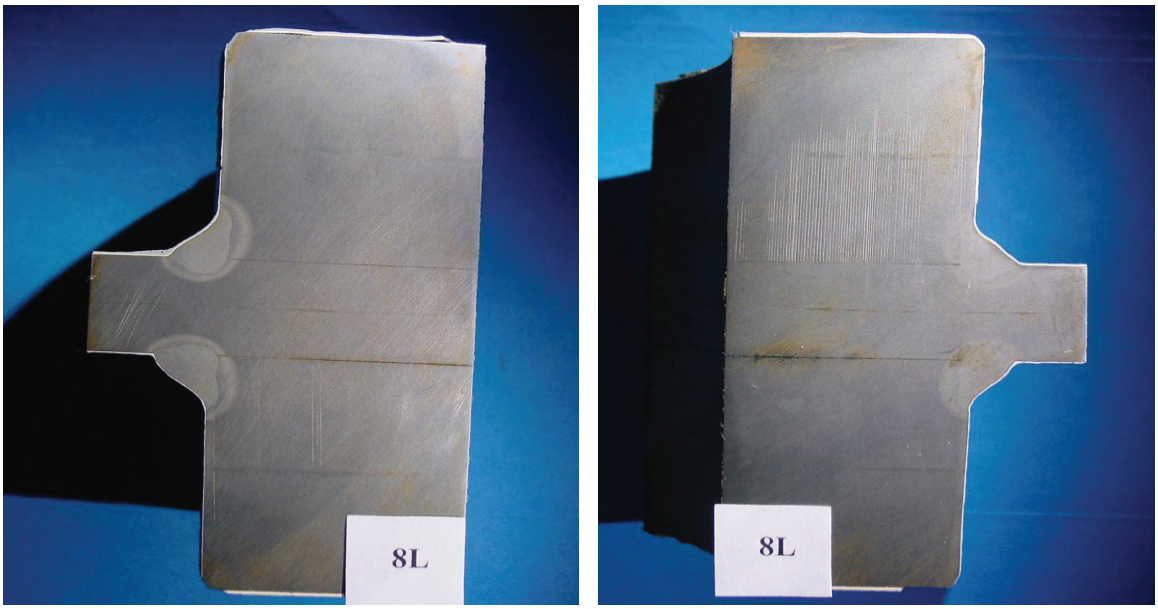

Figure 40: Polished and etched sections of the diaphragm plate and ring plate weld toes

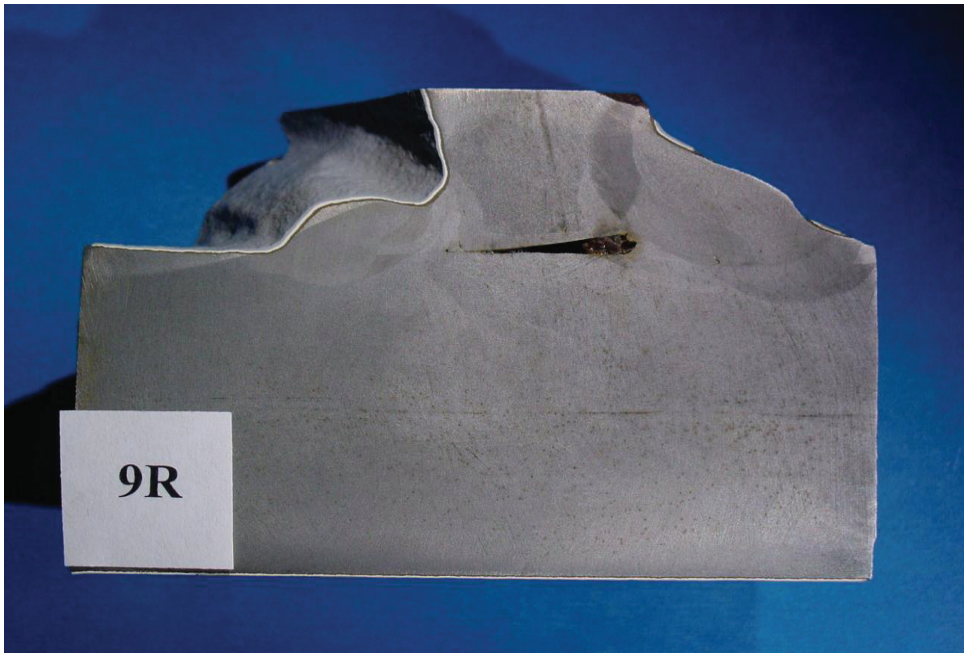

Figure 41: Cross section of the diaphragm-flange welds at the right side of Cable Diaphragm Plate 9 (Segment 9F) showing weld profile

APPENDIX A

LABORATORY TESTING INC.

2331 Topaz Drive, Hatfield, PA 19440
TEL: 800-219-9095 • FAX: 800-219-9096

Certified Test Report

EJK001-12-04-12626-1

Accredited Nadcap
Materials Testing Laboratory
Nondestructive Testing

SOLD TO
Eric J. Kaufmann
117 Atlss Drive
Bethlehem, PA 18015

SHIP TO
Eric J. Kaufmann
117 Atlss Drive
Bethlehem, PA 18015
ATTN: Eric Kaufmann

CUSTOMER P.O.	CERTIFICATION DATE	SHIP VIA
CREDIT-CARD	4/9/2012	EMAIL & LTI DELIVERY

DESCRIPTION

Quantity:	2	**Quantity:**	1
Plate No.:	8	**Plate No.:**	9
Size:	3/4" Thick x (1 pc. 8" x 10" and 1 pc. 5" x 9")	**Size:**	3/4" Thick x 8" x 24"
Material:	ASTM A572, Grade 50	**Material:**	ASTM A572, Grade 50
Description:	Plate	**Description:**	Plate
Project:	Sabo Bridge	**Project:**	Sabo Bridge

AMENDED CERTIFICATION (4/24/12)

Two pieces of the referenced samples were submitted to chemical content evaluation and (2) pieces were found to be in conformance to ASTM A572-07, Grade 50 with the following results:

	REQUIREMENTS		PLATE NO.	
ELEMENT	MIN	MAX	8	9
Al			0.021%	0.022%
B			0.0007%	0.0007%
C		0.23	0.16%	0.15%
Cb			0.002%	0.002%
Cb+V			0.031%	0.031%
Co			0.009%	0.009%
Cr			0.48%	0.48%
Cu			0.23%	0.23%
Mn		1.35	1.11%	1.12%
Mn:C	2:1		7:1	7:1
Mo			0.016%	0.015%
N			0.005%	0.005%
Ni			0.19%	0.19%
P		0.04	0.02%	0.02%
S		0.05	0.01%	0.01%
Si		0.40	0.31%	0.32%
Sn			0.010%	0.010%
Ti			0.002%	0.002%
V			0.029%	0.029%
W			0.016%	0.018%
Zn			0.005%	0.004%
Zr			0.002%	0.003%

Procedures/Methods: 86-SCA-0, Rev. 11, Direct Reading Atom Emissions Spectroscopy

LABORATORY TESTING INC.
2331 Topaz Drive, Hatfield, PA 19440
TEL: 800-219-9095 • FAX: 800-219-9096

Certified Test Report

EJK001-12-04-12626-1

Accredited Nadcap
Materials Testing Laboratory
Nondestructive Testing

AMENDED CERTIFICATION (4/24/12)

CHARPY V-NOTCH IMPACT TESTING:
SPECIMEN TYPE: Notched, Longitudinal, 1/4 Thickness
APPLICABLE SPECIFICATIONS: Customer's requirements
KEY: C - Conforms NC - Non-Conformance R-Report for Information

PLATE NO.	(°F) TEMP	(FT-LBS.) ENERGY	(INCHES) LAT. EXP.	(%) SHEAR	SPECIMEN SIZE	KEY C/NC/R
8						
Required	+70					
1		78	0.057	60	Full Size 10mm x 10mm	R
2		101	0.067	70	Full Size 10mm x 10mm	R
3		93	0.064	60	Full Size 10mm x 10mm	R
AVERAGE		91	0.063			R
8						
Required	+10					
1		61	0.046	50	Full Size 10mm x 10mm	R
2		51	0.040	40	Full Size 10mm x 10mm	R
3		41	0.032	30	Full Size 10mm x 10mm	R
AVERAGE		51	0.039			R
8						
Required	+40					
1		57	0.048	30	Full Size 10mm x 10mm	R
2		37	0.033	25	Full Size 10mm x 10mm	R
3		65	0.054	30	Full Size 10mm x 10mm	R
AVERAGE		53				R
8						
Required	-30					
1		9	0.008	5	Full Size 10mm x 10mm	R
2		48	0.038	40	Full Size 10mm x 10mm	R
3		32	0.028	30	Full Size 10mm x 10mm	R
AVERAGE		30				R

LABORATORY TESTING INC.
2331 Topaz Drive, Hatfield, PA 19440
TEL: 800-219-9095 • FAX: 800-219-9096

Certified Test Report
EJK001-12-04-12626-1

Accredited Nadcap
Materials Testing Laboratory
Nondestructive Testing

AMENDED CERTIFICATION (4/24/12)

CHARPY V-NOTCH IMPACT TESTING:
SPECIMEN TYPE: Notched, Transverse, 1/4 Thickness
APPLICABLE SPECIFICATIONS: Customer's requirements
KEY: C - Conforms NC - Non-Conformance R-Report for Information

PLATE NO.	(°F) TEMP	(FT-LBS.) ENERGY	(INCHES) LAT. EXP.	(%) SHEAR	SPECIMEN SIZE	KEY C/NC/R
8						
Required	+70					
1		116	0.074	70	Full Size 10mm x 10mm	R
2		76	0.056	60	Full Size 10mm x 10mm	R
3		111	0.072	70	Full Size 10mm x 10mm	R
AVERAGE		101	0.067			R
8						
Required	+10					
1		32	0.025	30	Full Size 10mm x 10mm	R
2		17	0.016	20	Full Size 10mm x 10mm	R
3		62	0.048	50	Full Size 10mm x 10mm	R
AVERAGE		37	0.030			R
8						
Required	+40					
1		66	0.052	40	Full Size 10mm x 10mm	R
2		75	0.059	45	Full Size 10mm x 10mm	R
3		47	0.040	35	Full Size 10mm x 10mm	R
AVERAGE		63				R
8						
Required	-30					
1		18	0.017	15	Full Size 10mm x 10mm	R
2		14	0.012	10	Full Size 10mm x 10mm	R
3		29	0.024	20	Full Size 10mm x 10mm	R
AVERAGE		20				R

LABORATORY TESTING INC.
2331 Topaz Drive, Hatfield, PA 19440
TEL: 800-219-9095 • FAX: 800-219-9096

Certified Test Report

EJK001-12-04-12626-1

Accredited Nadcap
Materials Testing Laboratory
Nondestructive Testing

AMENDED CERTIFICATION (4/24/12)

CHARPY V-NOTCH IMPACT TESTING:
SPECIMEN TYPE: Notched, Longitudinal, 1/4 Thickness
APPLICABLE SPECIFICATIONS: Customer's requirements
KEY: C - Conforms NC - Non-Conformance R-Report for Information

PLATE NO.	(°F) TEMP	(FT-LBS.) ENERGY	(INCHES) LAT. EXP.	(%) SHEAR	SPECIMEN SIZE	KEY C/NC/R
9						
Required	+70					
1		91	0.065	70	Full Size 10mm x 10mm	R
2		79	0.056	60	Full Size 10mm x 10mm	R
3		86	0.063	60	Full Size 10mm x 10mm	R
AVERAGE		85	0.061			R
9						
Required	+10					
1		51	0.038	40	Full Size 10mm x 10mm	R
2		48	0.037	40	Full Size 10mm x 10mm	R
3		38	0.029	30	Full Size 10mm x 10mm	R
AVERAGE		46	0.035			R
9						
Required	+40					
1		65	0.050	45	Full Size 10mm x 10mm	R
2		57	0.048	40	Full Size 10mm x 10mm	R
3		56	0.046	40	Full Size 10mm x 10mm	R
AVERAGE		59				R
9						
Required	-30					
1		26	0.022	20	Full Size 10mm x 10mm	R
2		15	0.014	15	Full Size 10mm x 10mm	R
3		19	0.017	15	Full Size 10mm x 10mm	R
AVERAGE		20				R

LABORATORY TESTING INC.
2331 Topaz Drive, Hatfield, PA 19440
TEL: 800-219-9095 • FAX: 800-219-9096

Certified Test Report
EJK001-12-04-12626-1

Accredited Nadcap
Materials Testing Laboratory
Nondestructive Testing

AMENDED CERTIFICATION (4/24/12)

CHARPY V-NOTCH IMPACT TESTING:
SPECIMEN TYPE: Notched, Transverse, 1/4 Thickness
APPLICABLE SPECIFICATIONS: Customer's requirements
KEY: C - Conforms NC - Non-Conformance R-Report for Information

PLATE NO.	(°F) TEMP	(FT-LBS.) ENERGY	(INCHES) LAT. EXP.	(%) SHEAR	SPECIMEN SIZE	KEY C/NC/R
9						
Required	+70					
1		119	0.081	80	Full Size 10mm x 10mm	R
2		95	0.062	60	Full Size 10mm x 10mm	R
3		110	0.070	70	Full Size 10mm x 10mm	R
AVERAGE		108	0.071			R
9						
Required	+10					
1		17	0.014	15	Full Size 10mm x 10mm	R
2		46	0.034	30	Full Size 10mm x 10mm	R
3		25	0.023	20	Full Size 10mm x 10mm	R
AVERAGE		29	0.024			R
9						
Required	+40					
1		19	0.019	20	Full Size 10mm x 10mm	R
2		62	0.048	30	Full Size 10mm x 10mm	R
3		72	0.052	35	Full Size 10mm x 10mm	R
AVERAGE		51				R
9						
Required	-30					
1		24	0.021	20	Full Size 10mm x 10mm	R
2		20	0.020	20	Full Size 10mm x 10mm	R
3		65	0.052	35	Full Size 10mm x 10mm	R
AVERAGE		36				R

LABORATORY TESTING INC.
2331 Topaz Drive, Hatfield, PA 19440
TEL: 800-219-9095 • FAX: 800-219-9096

Certified Test Report

EJK001-12-04-12626-1

Accredited Nadcap
Materials Testing Laboratory
Nondestructive Testing

AMENDED CERTIFICATION (4/24/12)

TENSILE TEST:
APPLICABLE SPECIFICATIONS: ASTM A370 and Customer's instructions
KEY: C - Conforms NC - Non-Conformance R-Report for Information

PLATE NO.	(KSI) TENSILE STRENGTH	(KSI) YIELD (.2%) STRENGTH	(%) ELONGATION (IN 2")	(%) REDUCTION OF AREA	KEY C/NC/R
8 Longitudinal	88.0	61.0	27	71	R
8 Transverse	88.5	60.0	27	72	R
9 Longitudinal	88.5	60.5	26	65	R
9 Transverse	89.0	59.5	26	68	R

The services performed above were done in accordance with LTI's Quality System Program Manual Revision 19 dated 11/11/11 and ISO/IEC 17025. These results relate only to the items tested and this report shall not be reproduced, except in full, without the written approval of Laboratory Testing, Inc. L.T.I. is accredited by PRI to ISO17025 and by Nadcap for NDT and Materials Testing for the test methods and specific services as listed in the Scopes of Accreditation available at www.labtesting.com and www.eAuditNet.com. The results reported on this test report represent the actual attributes of the material tested and indicate full compliance with all applicable specification and contract requirements.

MERCURY CONTAMINATION: During the testing and inspection, the product did not come in direct contact with mercury or any of its compounds nor with any mercury containing devices employing a single boundary of containment.

NOTE: The recording of false, fictitious or fraudulent statements or entries on this document may be punishable as a felony under Federal Statutes.

Sherri L. Scheifele
QA Specialist

Sherri L Scheifele

Authorized Signature (ES)

Page 6 of 6

WJE ENGINEERS ARCHITECTS MATERIALS SCIENTISTS

Appendix B

Instrumentation Plan Drawings

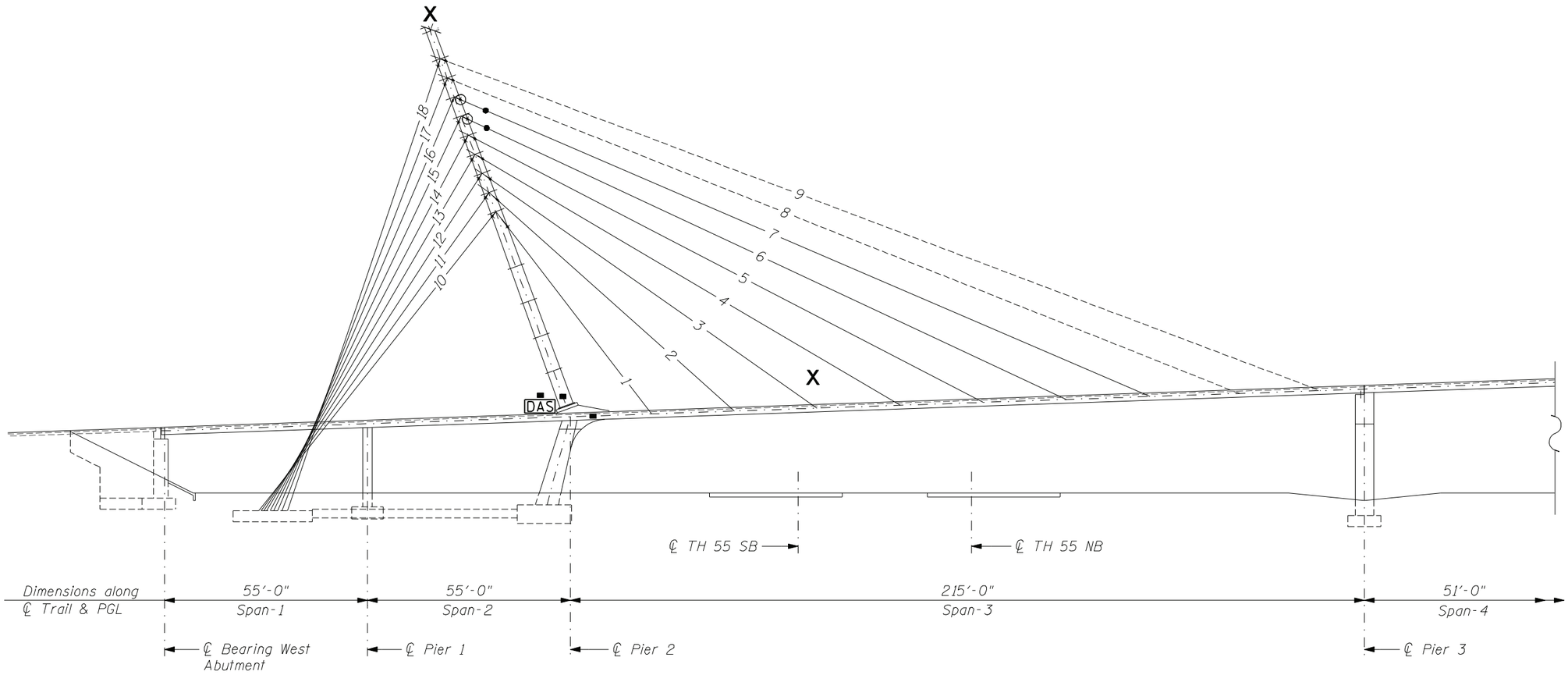

PARTIAL ELEVATION

Legend:

- ○ Instrumented Cable Diaphragm Plate
- ● Accelerometer
- X Anemometer
- ■ Thermocouple

WJE ENGINEERS ARCHITECTS MATERIALS SCIENTISTS

Wiss, Janney, Elstner Associates, Inc.
330 Pfingsten Road
Northbrook, Illinois 60062
847.272.7400 tel | 847.291.9599 fax

Headquarters & Laboratories: Northbrook, Illinois
Atlanta | Austin | Boston | Chicago | Cleveland | Dallas | Denver | Detroit
Honolulu | Houston | Memphis | Minneapolis | New Haven | New York
Princeton | San Francisco | Seattle | Washington, D.C.

Seal

Consultants

Project

Martin Olav Sabo Pedestrian Bridge Over TH 55 and LRT Hennepin County Minneapolis, Minnesota

Owner

City of Minneapolis Department of Public Works

Mark	Date	Description

Project No.	2012.0901
Date	April 11, 2012
Drawn	IMG
Checked	BJS
Scale	NTS

GENERAL ELEVATION

Sheet Title

Sheet No. Si-1

DATE: 6/27/2012
FILENAME: p:\2012\0901-1000\2012.0901 - sabo bridge\drawings\Si-1.dgn

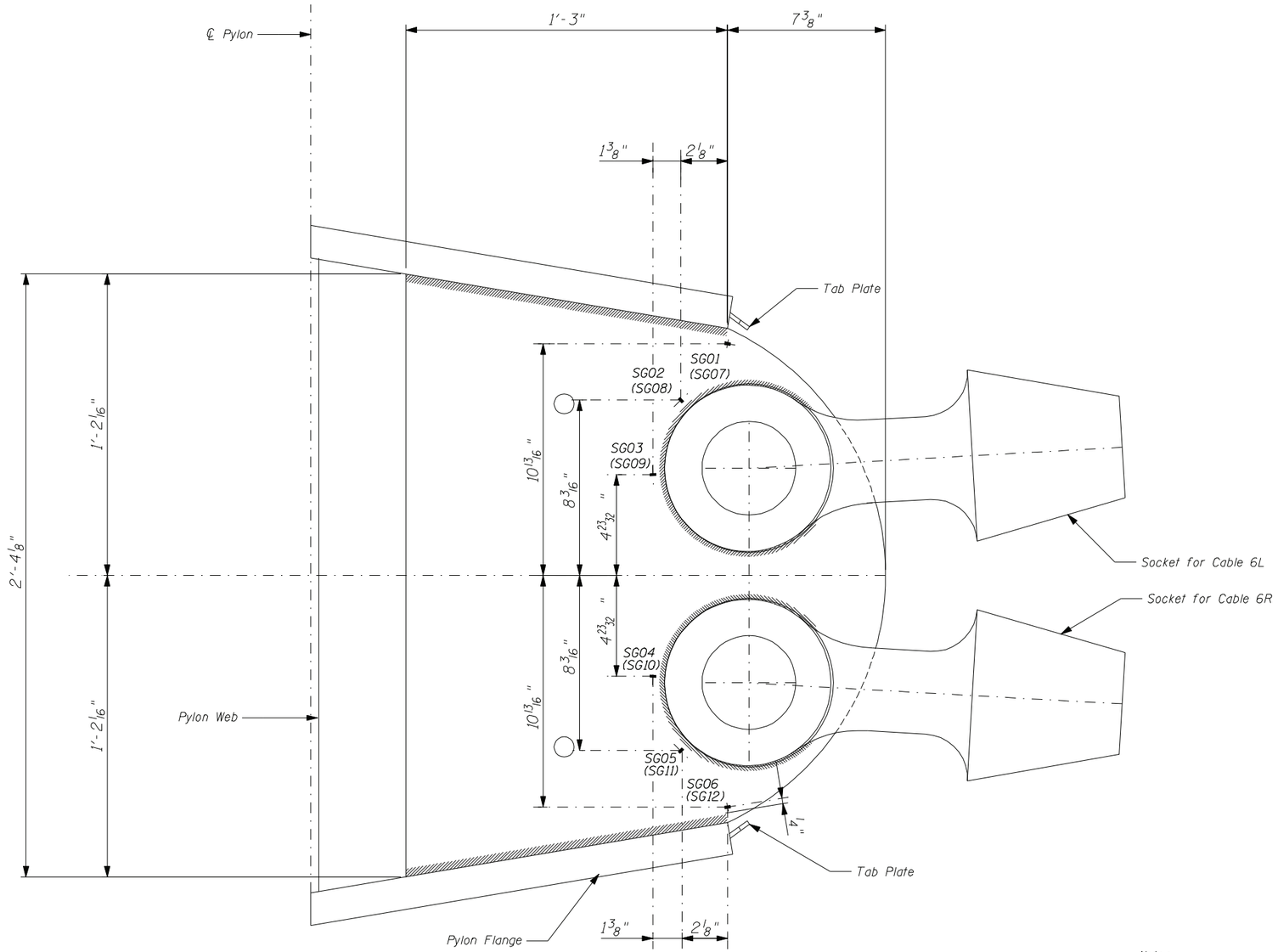

CABLE DIAPHRAGM PLATE 7

Notes:

1. Strain gages installed at top and bottom of cable diaphragm plate at locations shown.
2. Strain gages designated in parenthesis are installed on plate bottom.
3. Strain gages installed 0.3" from weld toe at measurement location.

LEGEND:

▬ Strain gage Micro-Measurements Type CEA-06-125UN-350

WJE ENGINEERS ARCHITECTS MATERIALS SCIENTISTS

Wiss, Janney, Elstner Associates, Inc.
330 Pfingsten Road
Northbrook, Illinois 60062
847.272.7400 tel | 847.291.9599 fax

Headquarters & Laboratories: Northbrook, Illinois
Atlanta | Austin | Boston | Chicago | Cleveland | Dallas | Denver | Detroit
Honolulu | Houston | Memphis | Minneapolis | New Haven | New York
Princeton | San Francisco | Seattle | Washington, D.C.

Seal

Consultants

Project

Martin Olav Sabo Pedestrian Bridge Over TH 55 and LRT Hennepin County Minneapolis, Minnesota

Owner

City of Minneapolis Department of Public Works

Mark	Date	Description

Project No.	2012.0901
Date	April 11, 2012
Drawn	IMG
Checked	BJS
Scale	NTS

Strain Gage Details Cable Diaphragm Plate 7

Sheet Title

Sheet No. Si-2

DATE: 6/27/2012
FILENAME: p:\2012\0901-1000\2012.0901 - sabo bridge\drawings\Si-2.dgn

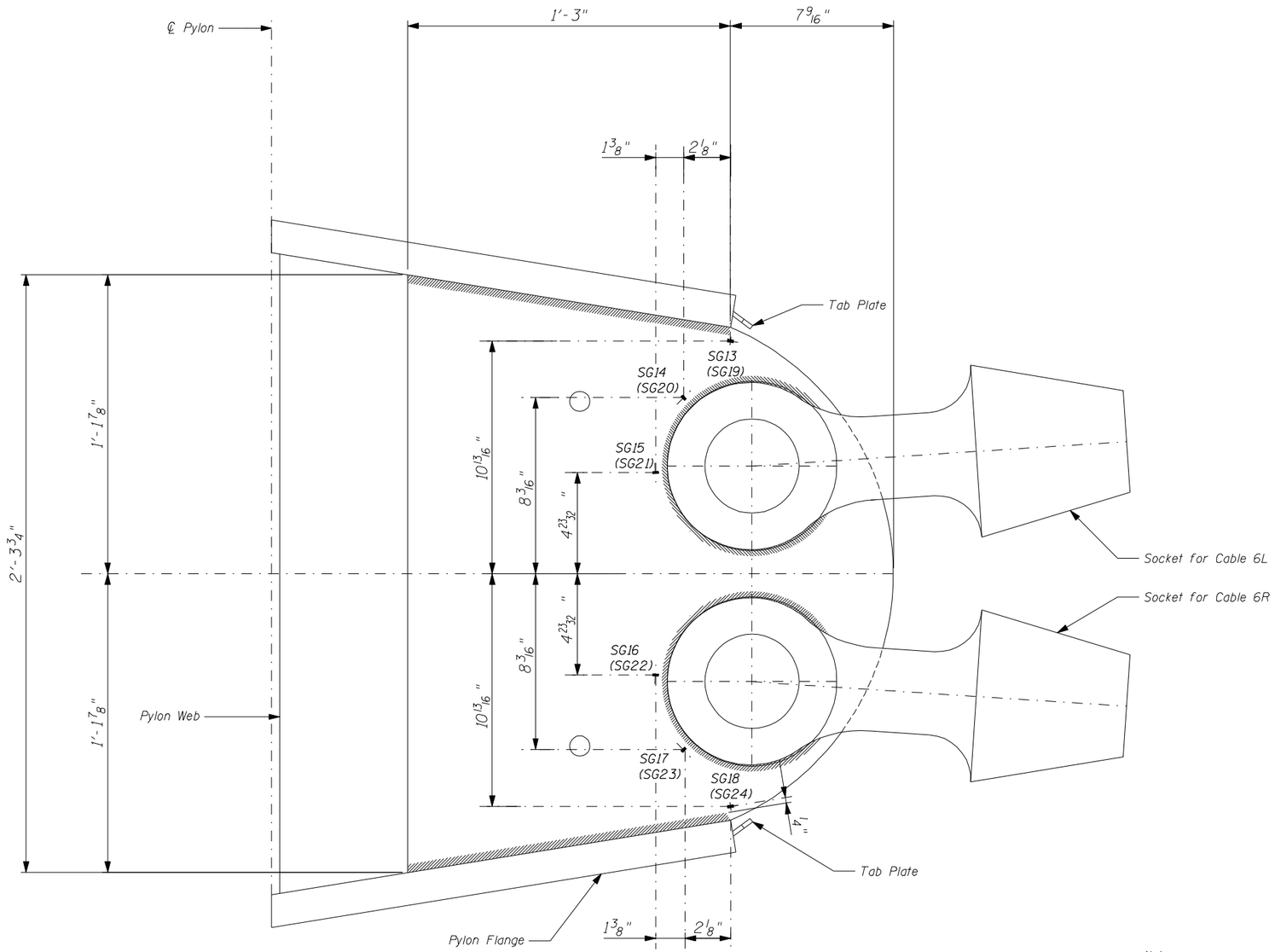

CABLE DIAPHRAGM PLATE 6

Notes:

1. Strain gages installed at top and bottom of cable diaphragm plate at locations shown.
2. Strain gages designated in parenthesis are installed on plate bottom.
3. Strain gages installed 0.3" from weld toe at measurement location.

LEGEND:

▬ Strain gage Micro-Measurements Type CEA-06-125UN-350

WJE ENGINEERS ARCHITECTS MATERIALS SCIENTISTS

Wiss, Janney, Elstner Associates, Inc.
330 Pfingsten Road
Northbrook, Illinois 60062
847.272.7400 tel | 847.291.9599 fax

Headquarters & Laboratories: Northbrook, Illinois
Atlanta | Austin | Boston | Chicago | Cleveland | Dallas | Denver | Detroit
Honolulu | Houston | Memphis | Minneapolis | New Haven | New York
Princeton | San Francisco | Seattle | Washington, D.C.

Seal

Consultants

Project

Martin Olav Sabo
Pedestrian Bridge
Over
TH 55 and LRT
Hennepin County
Minneapolis, Minnesota

Owner

City of Minneapolis
Department of Public Works

Mark	Date	Description

Project No.	2012.0901
Date	April 11, 2012
Drawn	IMG
Checked	BJS
Scale	NTS

Strain Gage Details
Cable Diaphragm
Plate 6

Sheet Title

Sheet No. Si-3

DATE: 6/27/2012
FILENAME: p:\2012\0901-1000\2012.0901 - sabo bridge\drawings\Si-3.dgn

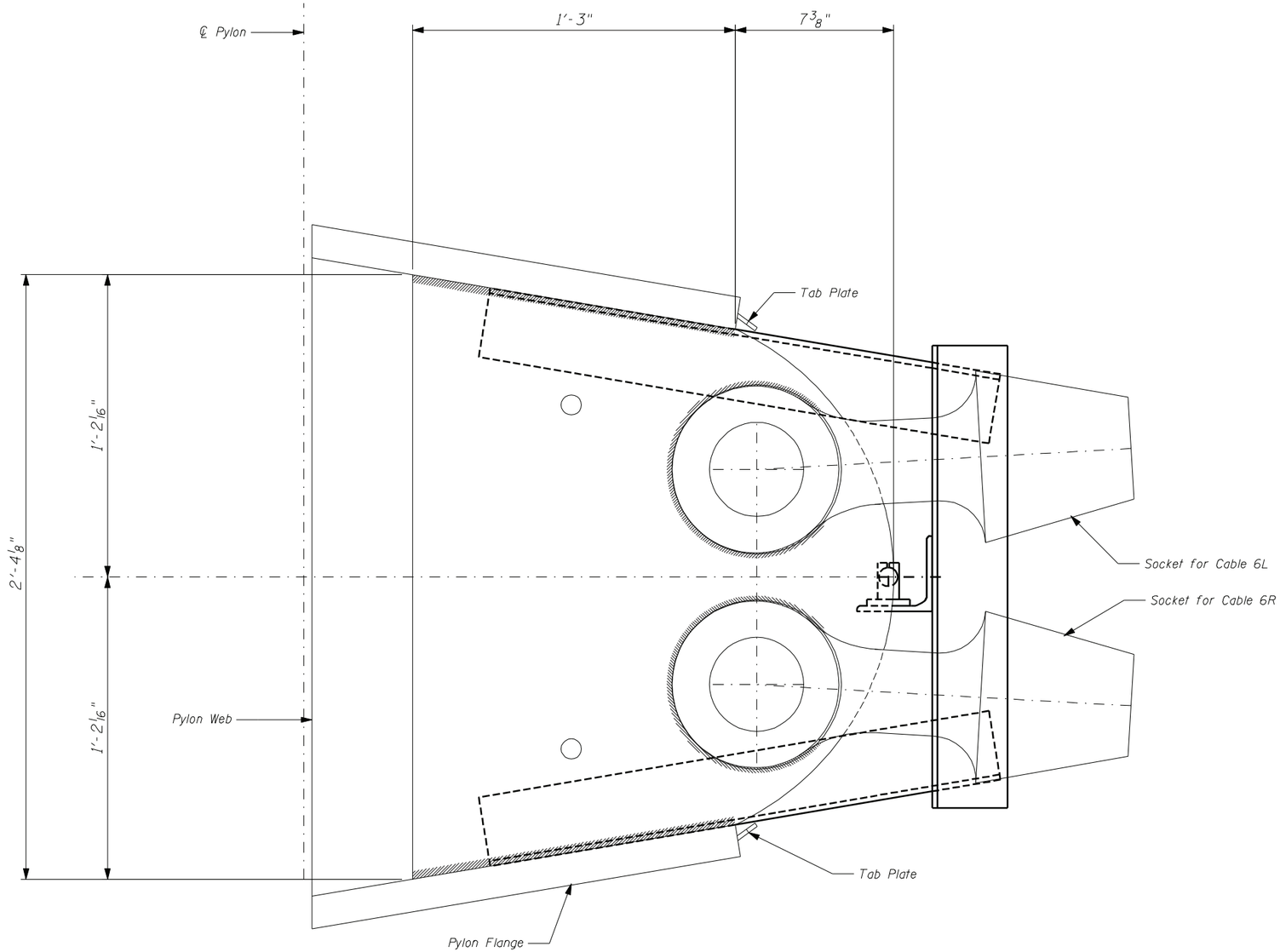

CABLE DIAPHRAGM PLATE 7

DATE: 6/27/2012
FILENAME: p:\2012\0901-1000\2012.0901 - sabo bridge\drawings\Si-4.dgn

WJE ENGINEERS ARCHITECTS MATERIALS SCIENTISTS

Wiss, Janney, Elstner Associates, Inc.
330 Pfingsten Road
Northbrook, Illinois 60062
847.272.7400 tel | 847.291.9599 fax

Headquarters & Laboratories: Northbrook, Illinois
Atlanta | Austin | Boston | Chicago | Cleveland | Dallas | Denver | Detroit
Honolulu | Houston | Memphis | Minneapolis | New Haven | New York
Princeton | San Francisco | Seattle | Washington, D.C.

Seal

Consultants

Project

Martin Olav Sabo
Pedestrian Bridge
Over
TH 55 and LRT
Hennepin County
Minneapolis, Minnesota

Owner

City of Minneapolis
Department of Public Works

Mark	Date	Description

Project No.	2012.0901
Date	April 11, 2012
Drawn	IMG
Checked	BJS
Scale	NTS

Sheet Title

LVDT Details
Cable Diaphragm
Plate 7

Sheet No. Si-4

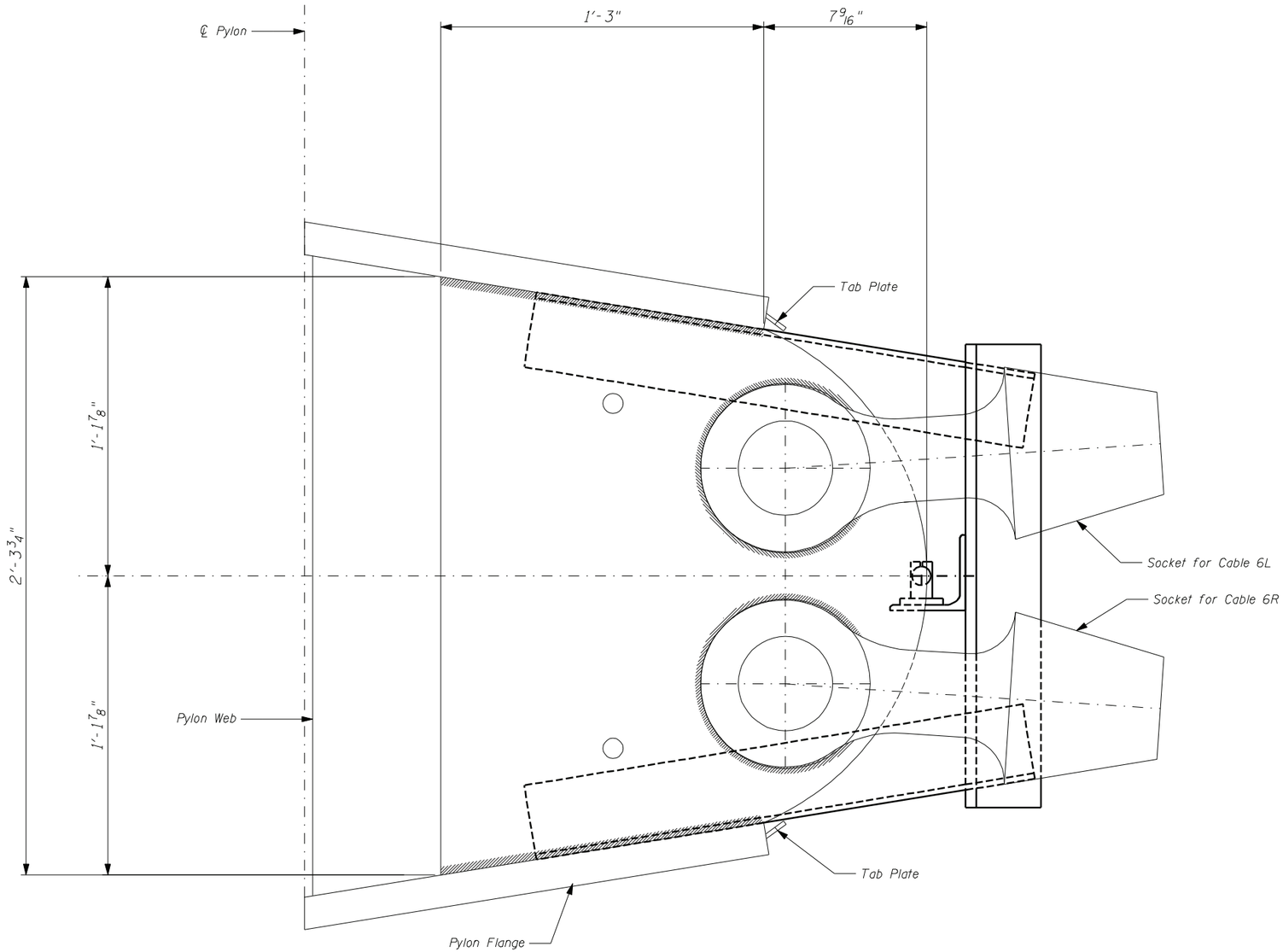

CABLE DIAPHRAGM PLATE 7

WJE ENGINEERS ARCHITECTS MATERIALS SCIENTISTS

Wiss, Janney, Elstner Associates, Inc.
330 Pfingsten Road
Northbrook, Illinois 60062
847.272.7400 tel | 847.291.9599 fax

Headquarters & Laboratories: Northbrook, Illinois
Atlanta | Austin | Boston | Chicago | Cleveland | Dallas | Denver | Detroit
Honolulu | Houston | Memphis | Minneapolis | New Haven | New York
Princeton | San Francisco | Seattle | Washington, D.C.

Seal

Consultants

Project

Martin Olav Sabo Pedestrian Bridge Over TH 55 and LRT Hennepin County Minneapolis, Minnesota

Owner

City of Minneapolis
Department of Public Works

Mark	Date	Description

Project No.	2012.0901
Date	April 11, 2012
Drawn	IMG
Checked	BJS
Scale	NTS

LVDT Details
Cable Diaphragm
Plate 6

Sheet Title

Sheet No. Si-5

DATE: 6/27/2012
FILENAME: P:\2012\0901-1000\2012.0901 - Sabo Bridge\Drawings\Si-5.dgn

Appendix C

Effective Stress Range Histograms

Martin Olav Sabo Pedestrian Bridge
Stress Range Histogram Data

Bin (psi)	SG01	SG02	SG03	SG04	SG05	SG06	SG07	SG08	SG09	SG10	SG11	SG12
125	10879221	10561097	11017861	2487208	5011781	10434023	1496533	1862868	846270	0	864833	0
225	16957203	5593941	3921012	2707615	3605996	3258355	2135496	2575925	1524606	0	1628493	0
375	1538857	1457515	1293846	1097399	1250238	1193037	1119642	1171466	740484	0	808117	0
525	1035787	849274	868486	683149	766490	836739	937415	744065	531266	0	520307	0
675	878703	601253	758811	499993	569604	674244	775013	550897	467547	0	372985	0
825	690680	478765	661781	431348	452993	528986	600540	463148	419582	0	295635	0
975	539842	438561	543004	395594	402514	410101	480999	429150	358394	0	255786	0
1125	453882	405973	448163	357874	376229	331629	429557	397599	297242	0	222577	0
1275	388080	384203	376640	328406	347930	292177	367077	382162	250696	0	205311	0
1425	312993	361844	331966	281334	324742	250921	288511	354685	216486	0	189736	0
1575	231351	333938	289711	243838	295115	196507	206853	326536	199949	0	172335	0
1725	171958	299684	252858	217039	272170	137302	156611	290487	170159	0	158565	0
1875	125472	267264	210135	189764	239988	101257	111777	260560	147463	0	151343	0
2025	83435	243729	171197	176739	211392	68783	71610	240473	120817	0	133751	0
2175	56609	223571	143815	168477	185686	45992	50072	219583	94009	0	114282	0
2325	38805	203514	120975	150375	167431	30781	33818	199198	75558	0	103046	0
2475	26416	192051	94492	140088	154386	19990	22995	191875	63596	0	97997	0
2625	18137	187248	70619	128109	138651	12732	15905	188762	51757	0	90658	0
2775	12032	176701	55207	101846	127783	7674	10554	174953	36973	0	78217	0
2925	8131	162181	43416	81607	125129	4583	6919	158936	28759	0	73027	0
3075	5697	150092	33091	70622	122174	2162	5082	148332	24245	0	77495	0
3225	4098	137042	25158	58581	113735	947	3721	133251	18365	0	75521	0
3375	3062	122108	18071	46460	103478	457	2769	117640	13936	0	70199	0
3525	2215	104594	12917	37568	99073	209	1975	99605	10554	0	62251	0
3675	1659	87900	9195	28875	94663	111	1392	82016	8031	0	59938	0
3825	1088	75792	6669	23972	84913	58	1007	72219	5790	0	57618	0
3975	783	67621	5196	18064	71592	21	599	65239	3651	0	53039	0
4125	483	59302	4025	14193	59858	7	372	55658	2222	0	45617	0
4275	304	50849	3038	10849	52022	3	230	47455	1588	0	38224	0
4425	174	44276	2485	8330	48884	0	97	41210	1037	0	33732	0
4575	82	37423	1975	6361	44538	0	50	33803	737	0	31973	0
4725	46	30400	1521	4161	38213	0	20	26541	477	0	29141	0
4875	10	24284	1232	3392	31858	0	16	21626	368	0	25637	0
5025	6	20278	873	2449	27621	0	5	18638	238	0	21299	0
5175	8	17958	710	1570	23046	0	2	16485	156	0	18603	0
5325	1	15367	519	879	19283	0	0	14178	81	0	15767	0
5475	0	13213	393	492	16944	0	0	11852	60	0	12559	0
5625	0	11351	266	265	15317	0	0	10551	28	0	11154	0
5775	0	9892	169	195	12751	0	0	9023	13	0	10799	0
5925	0	8497	117	133	10509	0	0	7565	7	0	9476	0
6075	0	7177	67	80	9128	0	0	6306	3	0	7504	0
6225	0	6116	39	54	7640	0	0	5434	1	0	6069	0
6375	0	5225	18	31	6600	0	0	4668	1	0	5571	0
6525	0	4422	6	18	5487	0	0	3934	0	0	4359	0
6675	0	3790	5	8	4539	0	0	3221	0	0	3636	0
6825	0	3042	6	4	3642	0	0	2674	0	0	3159	0
6975	0	2677	2	2	3055	0	0	2361	0	0	2447	0
7125	0	2255	0	1	2645	0	0	2102	0	0	1868	0
7275	0	2026	0	0	2153	0	0	1781	0	0	1552	0
7425	0	1831	0	0	1676	0	0	1513	0	0	1453	0
7575	0	1446	0	0	1199	0	0	1308	0	0	1179	0
7725	0	1309	0	0	903	0	0	1178	0	0	819	0
7875	0	1144	0	0	642	0	0	995	0	0	540	0
8025	0	1016	0	0	502	0	0	852	0	0	375	0
8175	0	864	0	0	364	0	0	787	0	0	205	0
8325	0	724	0	0	263	0	0	585	0	0	125	0
8475	0	669	0	0	188	0	0	533	0	0	84	0
8625	0	514	0	0	163	0	0	409	0	0	40	0
8775	0	439	0	0	115	0	0	398	0	0	33	0
8925	0	409	0	0	69	0	0	292	0	0	17	0
9075	0	292	0	0	64	0	0	193	0	0	3	0
9225	0	236	0	0	53	0	0	182	0	0	4	0
9375	0	193	0	0	40	0	0	140	0	0	2	0
9525	0	164	0	0	28	0	0	112	0	0	3	0
9675	0	110	0	0	24	0	0	81	0	0	0	0
9825	0	95	0	0	10	0	0	63	0	0	0	0
9975	0	80	0	0	7	0	0	36	0	0	0	0
10125	0	42	0	0	14	0	0	27	0	0	0	0
10275	0	39	0	0	3	0	0	16	0	0	0	0
10425	0	22	0	0	2	0	0	20	0	0	0	0
10575	0	16	0	0	2	0	0	11	0	0	0	0
10725	0	19	0	0	3	0	0	9	0	0	0	0
10875	0	9	0	0	1	0	0	5	0	0	0	0
11025	0	6	0	0	1	0	0	6	0	0	0	0
11175	0	3	0	0	1	0	0	6	0	0	0	0
11325	0	7	0	0	0	0	0	3	0	0	0	0
11475	0	4	0	0	0	0	0	0	0	0	0	0
11625	0	2	0	0	0	0	0	0	0	0	0	0
11775	0	0	0	0	0	0	0	2	0	0	0	0
11925	0	1	0	0	0	0	0	0	0	0	0	0
12075	0	0	0	0	0	0	0	0	0	0	0	0

Martin Olav Sabo Pedestrian Bridge
Stress Range Histogram Data

Bin (psi)	SG13	SG14	SG15	SG16	SG17	SG18	SG19	SG20	SG21	SG22	SG23	SG24
125	796002	2395682	1751353	1454193	3700324	7472074	1536725	2242135	0	7220388	0	3334555
225	1370457	3012589	2041722	1756740	3458512	3171206	1951819	2732852	0	3106022	0	3166097
375	678138	1014500	838810	690557	970689	802260	829588	944521	0	477319	0	918085
525	270028	599071	571922	437234	550615	466187	561488	583538	0	222792	0	520488
675	137823	436209	430151	318479	389705	354004	422871	428591	0	148117	0	367799
825	77730	349140	315099	273880	290328	289903	338343	349605	0	125138	0	275389
975	42717	294804	209917	231220	237097	253153	245598	285089	0	109876	0	229836
1125	22261	244659	137362	214052	209396	190639	168705	243866	0	108208	0	205196
1275	10434	215209	97825	185233	179852	132400	112639	205613	0	94772	0	177830
1425	4267	181300	74285	143593	166319	93906	83856	163273	0	72985	0	167044
1575	1214	144589	58211	106719	154359	69026	65065	126934	0	50963	0	154981
1725	307	115735	44988	81907	134330	50020	52326	94186	0	35654	0	132816
1875	109	87479	35795	64856	110976	36434	41681	72097	0	26509	0	107734
2025	32	68098	28452	50288	90288	26000	32784	58665	0	19268	0	87797
2175	8	56247	22034	38451	71124	17591	26608	49385	0	13953	0	68834
2325	1	47442	17174	29425	58307	10763	20913	41653	0	10958	0	56855
2475	0	40658	13113	22622	48688	6184	16195	35249	0	8180	0	48253
2625	0	34993	9624	16763	41165	3343	12911	30347	0	5773	0	39712
2775	0	30706	7144	12090	33793	1792	9890	25543	0	3116	0	32864
2925	0	26353	5131	7174	28259	979	7546	21761	0	1421	0	26795
3075	0	22588	3693	4074	23480	528	5569	18113	0	718	0	22462
3225	0	19313	2465	2421	19889	236	4157	15127	0	334	0	18630
3375	0	16588	1708	1376	16471	160	2906	12578	0	192	0	14938
3525	0	13969	1019	853	13282	62	2115	10340	0	102	0	11770
3675	0	11810	555	531	10856	47	1354	8770	0	52	0	9463
3825	0	9984	293	278	8301	37	868	7334	0	16	0	6902
3975	0	8569	175	171	6225	10	476	5890	0	13	0	4808
4125	0	7190	105	100	4719	9	297	4948	0	2	0	3502
4275	0	6099	57	49	3683	1	154	3945	0	2	0	2439
4425	0	5085	50	38	2657	1	108	3127	0	2	0	1744
4575	0	4187	23	38	1902	0	61	2458	0	0	0	1122
4725	0	3463	18	11	1413	0	45	1970	0	0	0	817
4875	0	2803	4	8	960	0	34	1476	0	0	0	596
5025	0	2221	4	4	666	0	18	1114	0	0	0	377
5175	0	1802	3	2	514	0	12	796	0	0	0	258
5325	0	1472	1	0	335	0	6	536	0	0	0	169
5475	0	1104	0	0	233	0	2	376	0	0	0	124
5625	0	817	0	0	165	0	4	265	0	0	0	82
5775	0	609	0	0	95	0	1	157	0	0	0	52
5925	0	377	0	0	88	0	0	116	0	0	0	33
6075	0	311	0	0	46	0	0	82	0	0	0	33
6225	0	206	0	0	40	0	0	63	0	0	0	15
6375	0	136	0	0	29	0	0	47	0	0	0	29
6525	0	101	0	0	19	0	0	31	0	0	0	6
6675	0	76	0	0	22	0	0	25	0	0	0	10
6825	0	59	0	0	19	0	0	21	0	0	0	5
6975	0	42	0	0	8	0	0	14	0	0	0	4
7125	0	28	0	0	3	0	0	10	0	0	0	1
7275	0	27	0	0	4	0	0	9	0	0	0	1
7425	0	24	0	0	5	0	0	1	0	0	0	0
7575	0	12	0	0	0	0	0	3	0	0	0	0
7725	0	14	0	0	1	0	0	3	0	0	0	0
7875	0	8	0	0	0	0	0	1	0	0	0	0
8025	0	5	0	0	0	0	0	1	0	0	0	0
8175	0	1	0	0	0	0	0	0	0	0	0	0
8325	0	3	0	0	0	0	0	0	0	0	0	0
8475	0	3	0	0	0	0	0	0	0	0	0	0
8625	0	1	0	0	0	0	0	0	0	0	0	0
8775	0	1	0	0	0	0	0	0	0	0	0	0
8925	0	0	0	0	0	0	0	0	0	0	0	0
9075	0	0	0	0	0	0	0	0	0	0	0	0
9225	0	0	0	0	0	0	0	0	0	0	0	0
9375	0	0	0	0	0	0	0	0	0	0	0	0
9525	0	0	0	0	0	0	0	0	0	0	0	0
9675	0	0	0	0	0	0	0	0	0	0	0	0
9825	0	0	0	0	0	0	0	0	0	0	0	0
9975	0	0	0	0	0	0	0	0	0	0	0	0
10125	0	0	0	0	0	0	0	0	0	0	0	0
10275	0	0	0	0	0	0	0	0	0	0	0	0
10425	0	0	0	0	0	0	0	0	0	0	0	0
10575	0	0	0	0	0	0	0	0	0	0	0	0
10725	0	0	0	0	0	0	0	0	0	0	0	0
10875	0	0	0	0	0	0	0	0	0	0	0	0
11025	0	0	0	0	0	0	0	0	0	0	0	0
11175	0	0	0	0	0	0	0	0	0	0	0	0
11325	0	0	0	0	0	0	0	0	0	0	0	0
11475	0	0	0	0	0	0	0	0	0	0	0	0
11625	0	0	0	0	0	0	0	0	0	0	0	0
11775	0	0	0	0	0	0	0	0	0	0	0	0
11925	0	0	0	0	0	0	0	0	0	0	0	0
12075	0	0	0	0	0	0	0	0	0	0	0	0

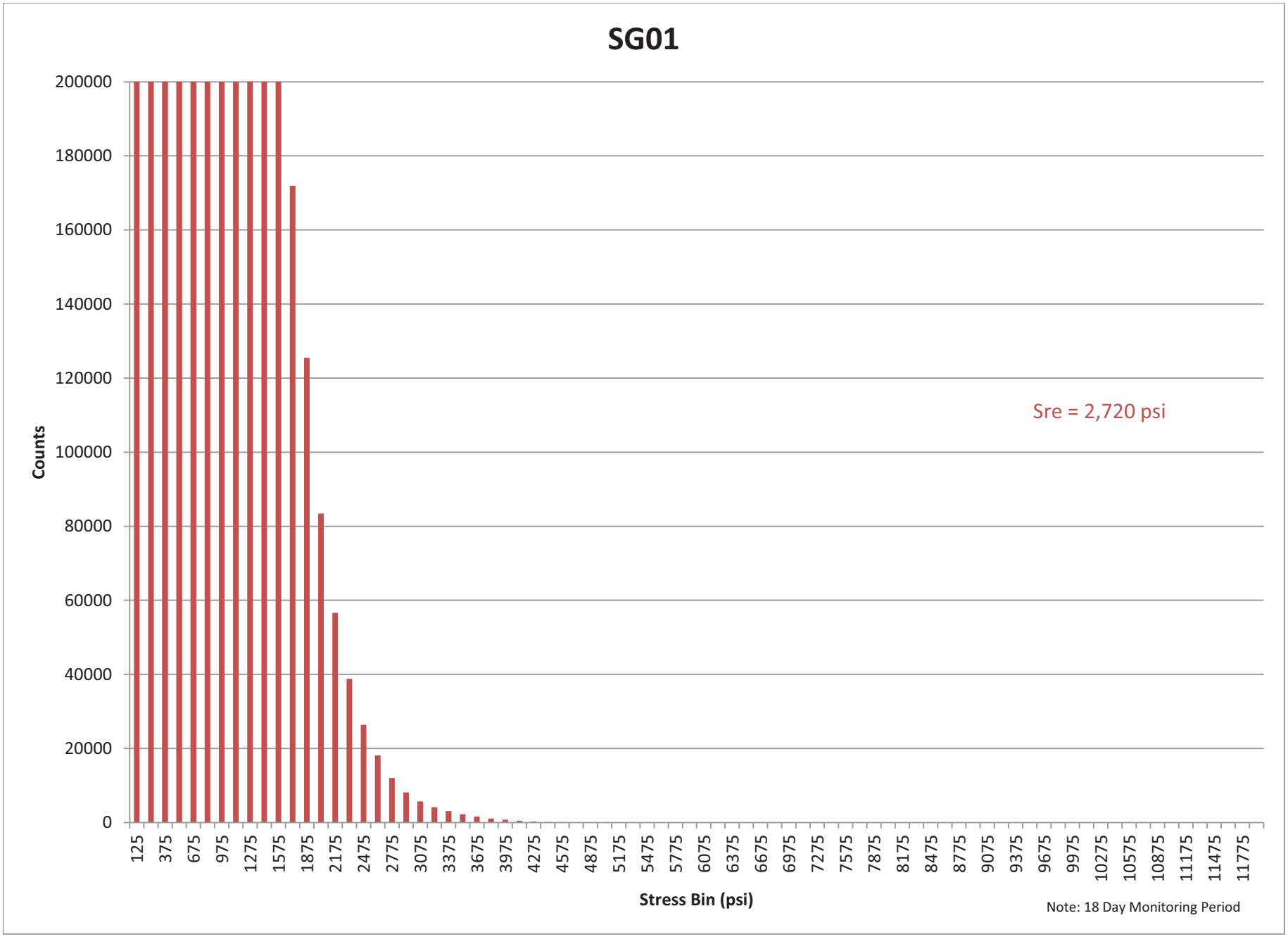
SG01
Counts
200000
180000
160000
140000
120000
100000
80000
60000
40000
20000
0
Sre = 2,720 psi
125
375
675
975
1275
1575
1875
2175
2475
2775
3075
3375
3675
3975
4275
4575
4875
5175
5475
5775
6075
6375
6675
6975
7275
7575
7875
8175
8475
8775
9075
9375
9675
9975
10275
10575
10875
11175
11475
11775
Stress Bin (psi)
Note: 18 Day Monitoring Period

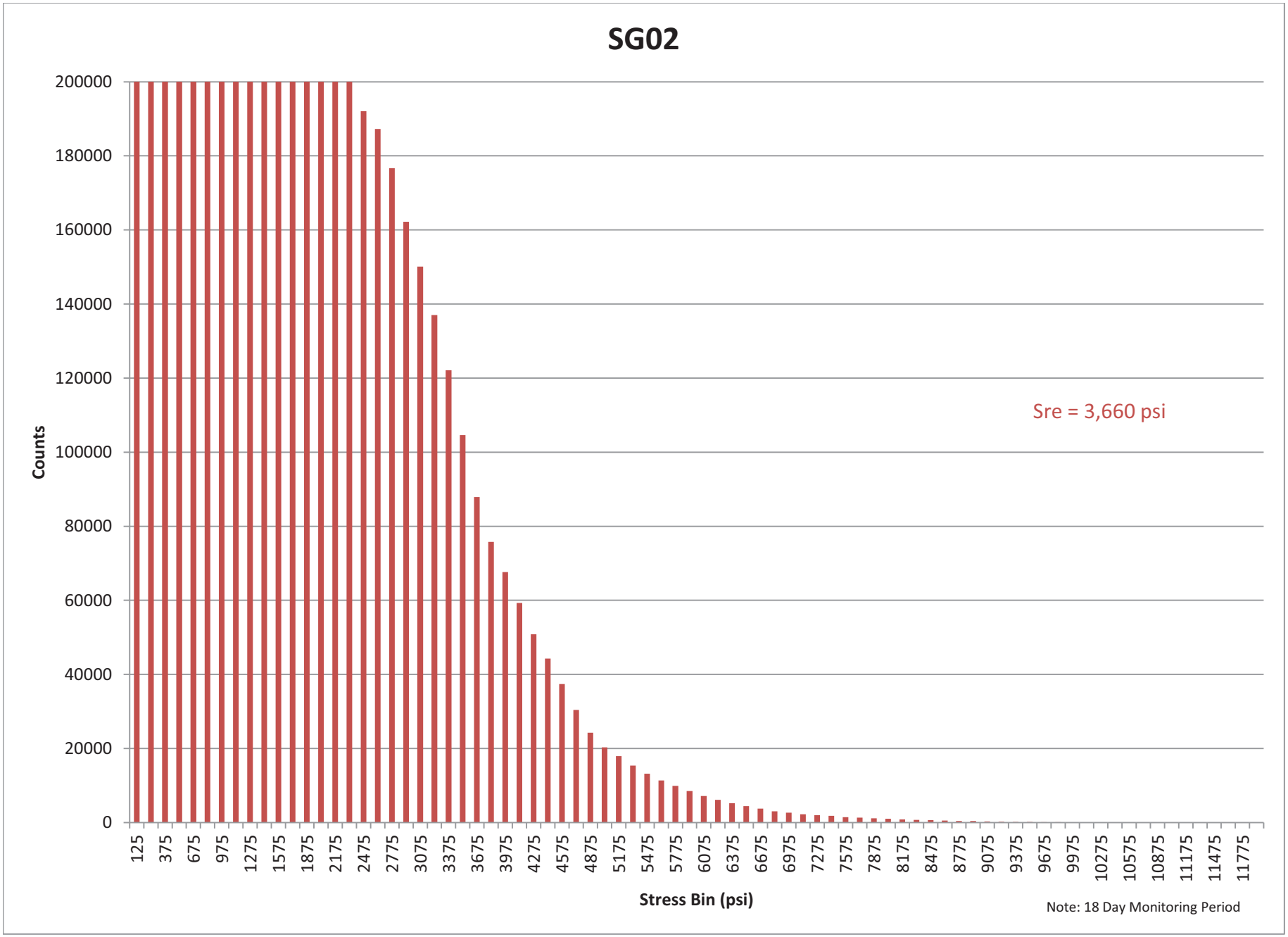
SG02
Counts
200000
180000
160000
140000
120000
100000
80000
60000
40000
20000
0
Sre = 3,660 psi
125
375
675
975
1275
1575
1875
2175
2475
2775
3075
3375
3675
3975
4275
4575
4875
5175
5475
5775
6075
6375
6675
6975
7275
7575
7875
8175
8475
8775
9075
9375
9675
9975
10275
10575
10875
11175
11475
11775
Stress Bin (psi)
Note: 18 Day Monitoring Period

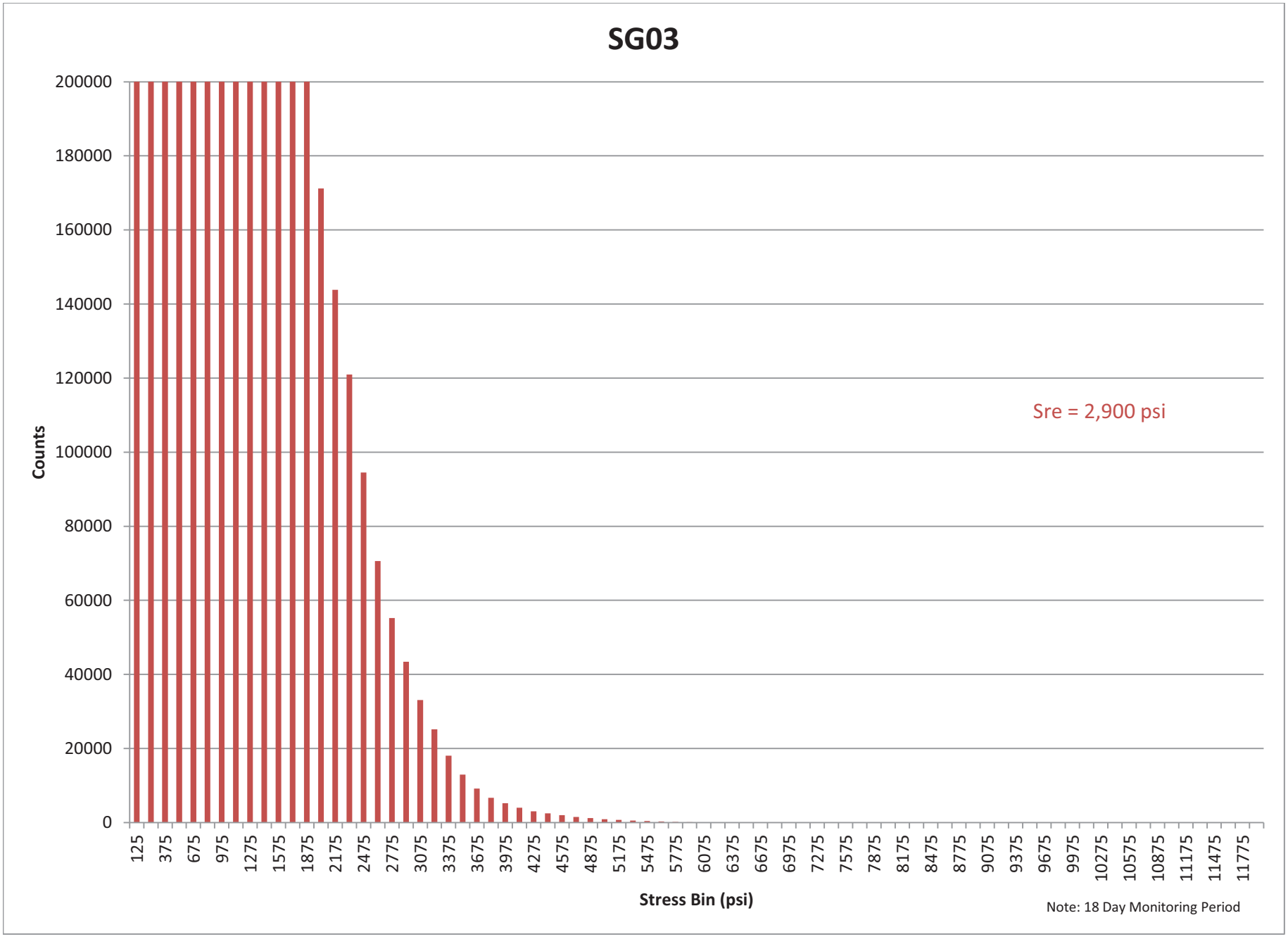
SG03
Counts
200000
180000
160000
140000
120000
100000
80000
60000
40000
20000
0
Sre = 2,900 psi
125
375
675
975
1275
1575
1875
2175
2475
2775
3075
3375
3675
3975
4275
4575
4875
5175
5475
5775
6075
6375
6675
6975
7275
7575
7875
8175
8475
8775
9075
9375
9675
9975
10275
10575
10875
11175
11475
11775
Stress Bin (psi)
Note: 18 Day Monitoring Period

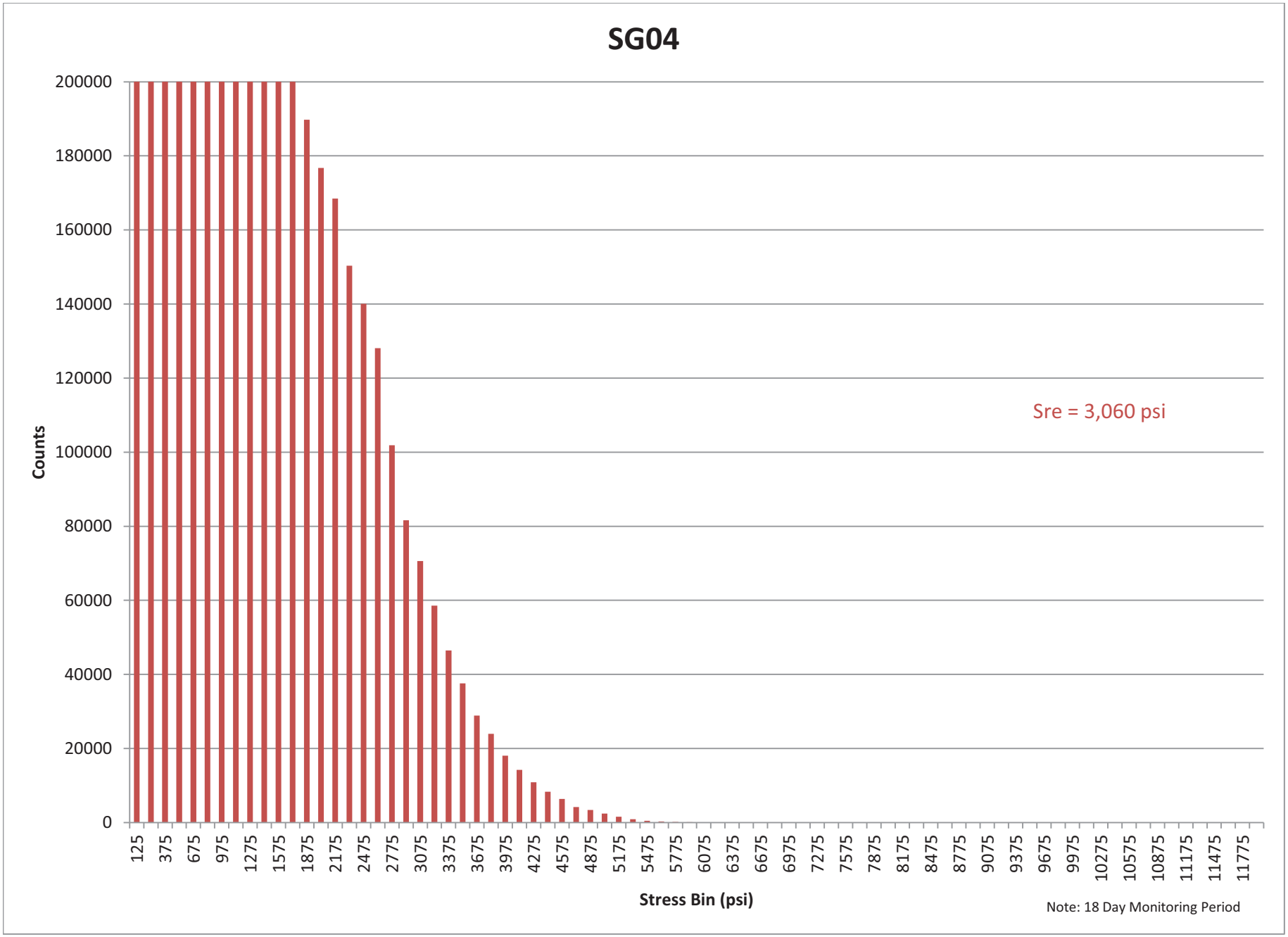
SG04
Counts
200000
180000
160000
140000
120000
100000
80000
60000
40000
20000
0
Sre = 3,060 psi
125
375
675
975
1275
1575
1875
2175
2475
2775
3075
3375
3675
3975
4275
4575
4875
5175
5475
5775
6075
6375
6675
6975
7275
7575
7875
8175
8475
8775
9075
9375
9675
9975
10275
10575
10875
11175
11475
11775
Stress Bin (psi)
Note: 18 Day Monitoring Period

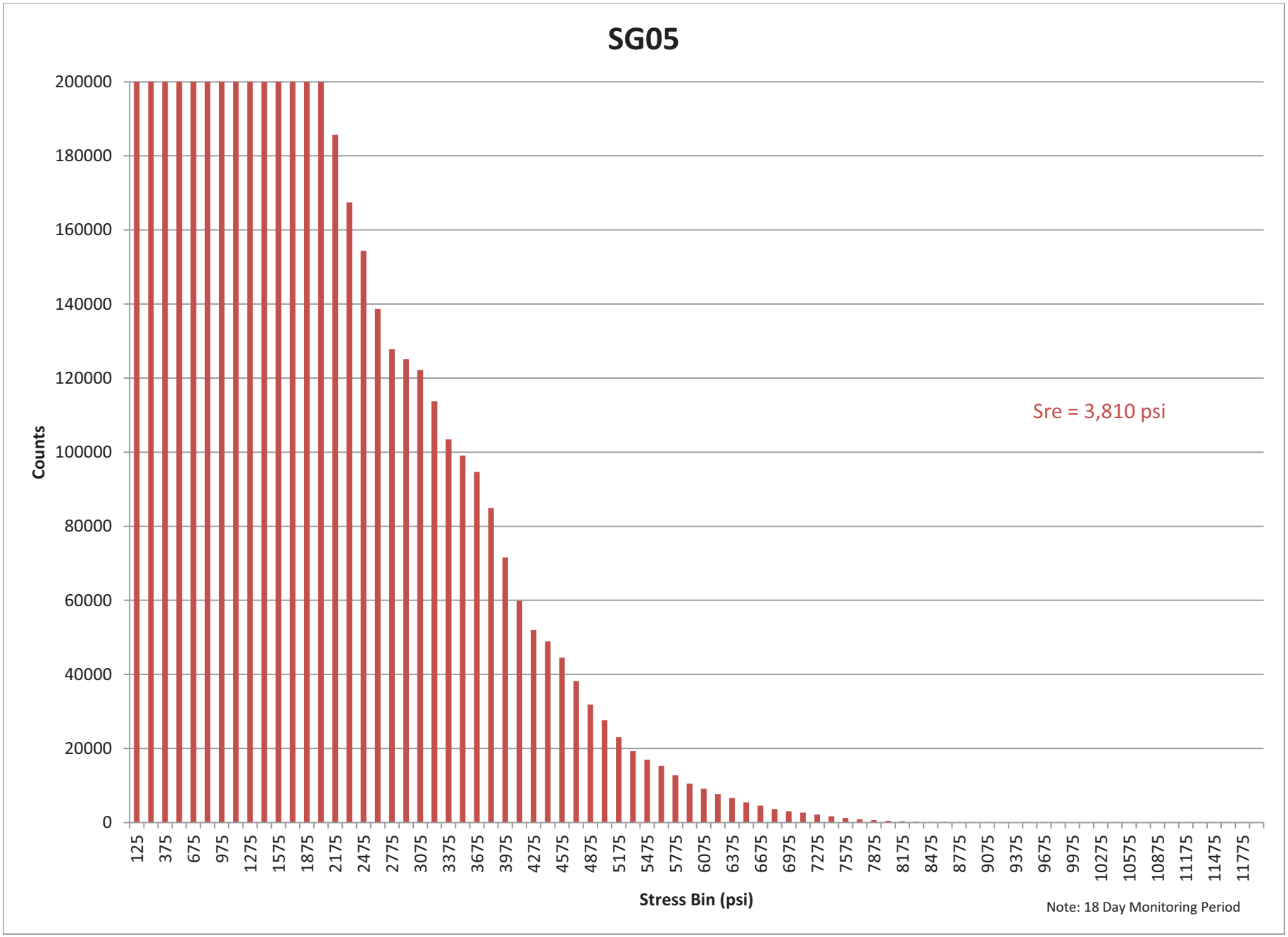
SG05
Counts
200000
180000
160000
140000
120000
100000
80000
60000
40000
20000
0
Sre = 3,810 psi
125
375
675
975
1275
1575
1875
2175
2475
2775
3075
3375
3675
3975
4275
4575
4875
5175
5475
5775
6075
6375
6675
6975
7275
7575
7875
8175
8475
8775
9075
9375
9675
9975
10275
10575
10875
11175
11475
11775
Stress Bin (psi)
Note: 18 Day Monitoring Period

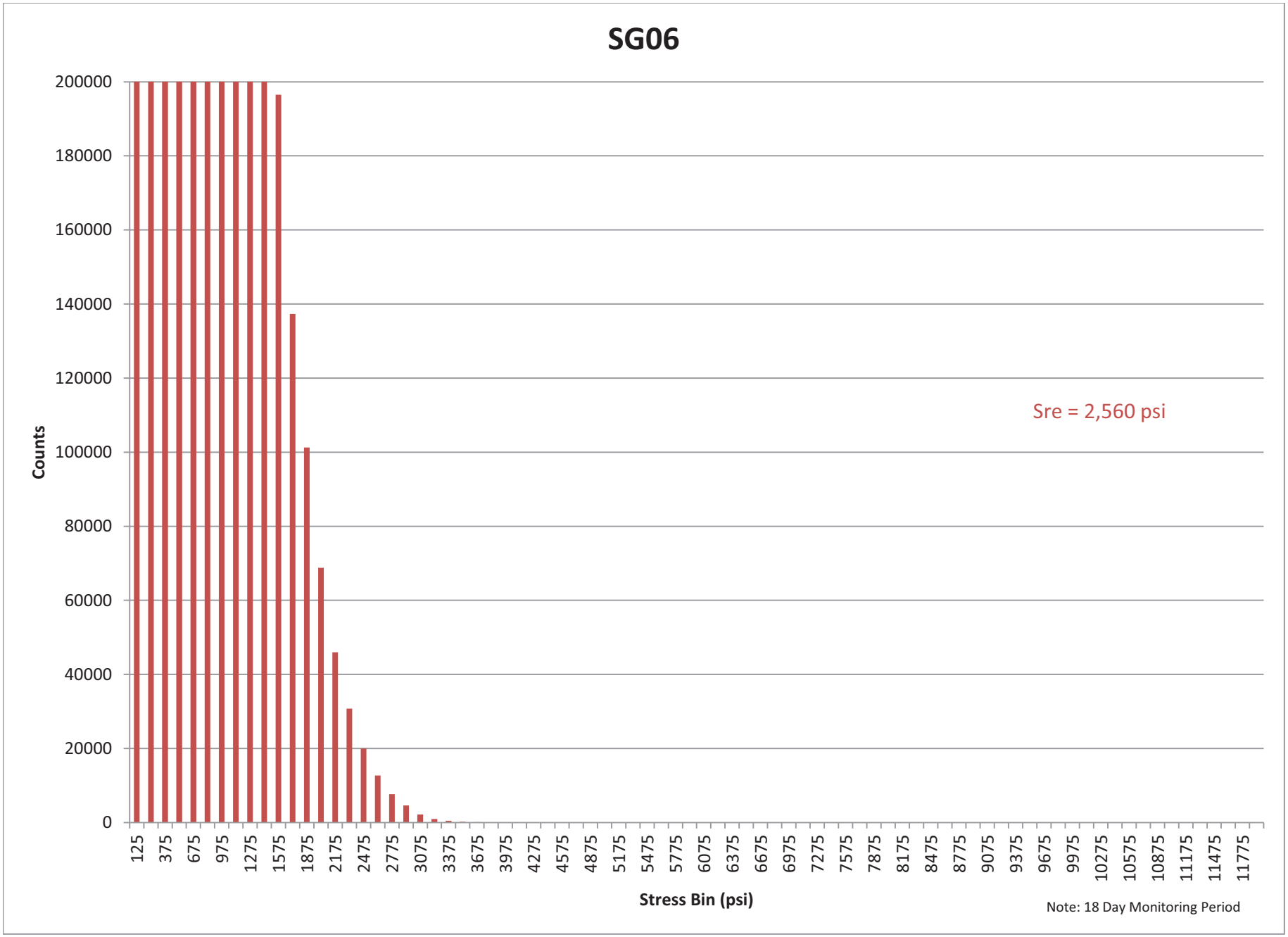
SG06
Counts
200000
180000
160000
140000
120000
100000
80000
60000
40000
20000
0
Sre = 2,560 psi
125
375
675
975
1275
1575
1875
2175
2475
2775
3075
3375
3675
3975
4275
4575
4875
5175
5475
5775
6075
6375
6675
6975
7275
7575
7875
8175
8475
8775
9075
9375
9675
9975
10275
10575
10875
11175
11475
11775
Stress Bin (psi)
Note: 18 Day Monitoring Period

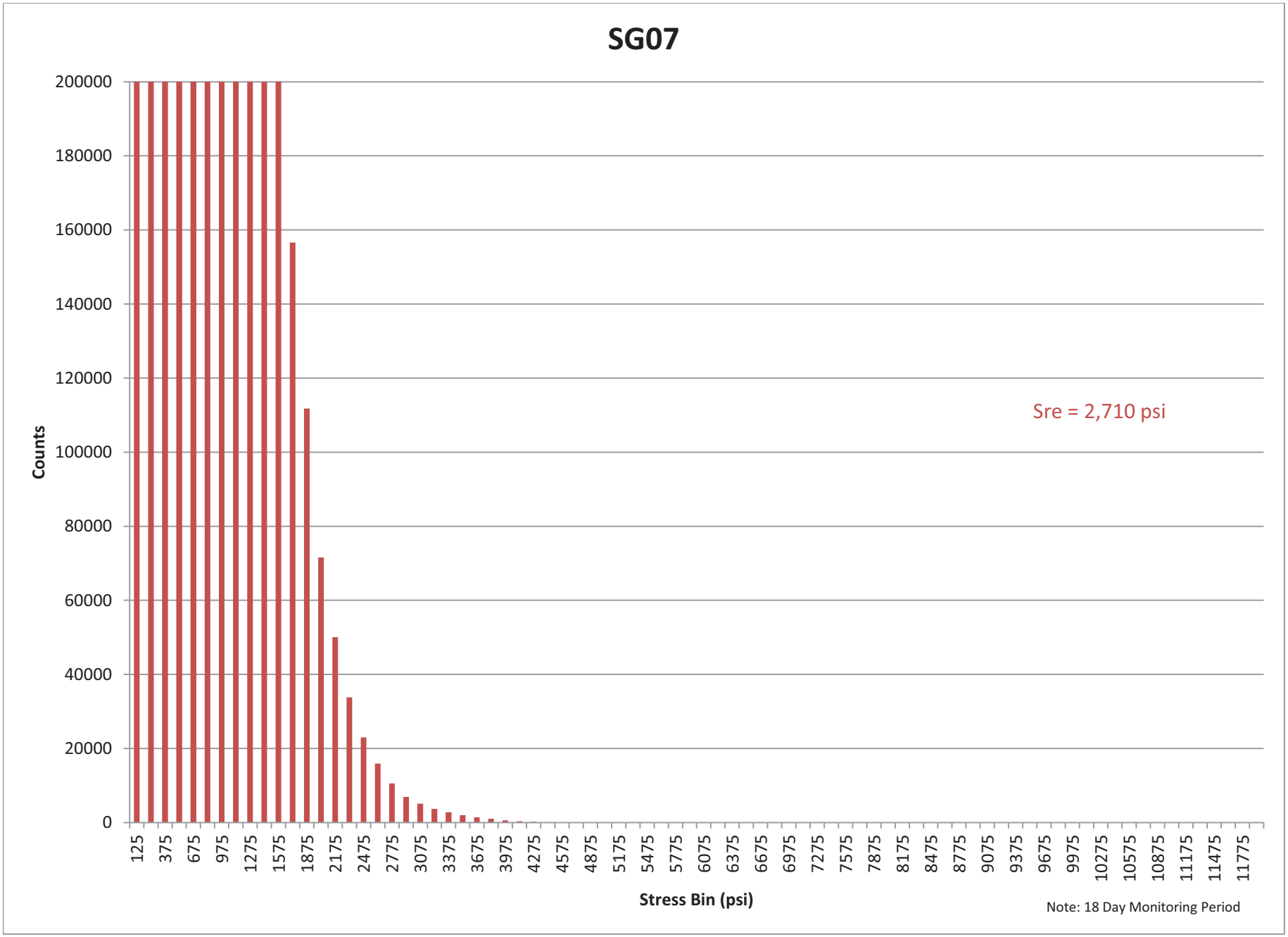
SG07
Counts
200000
180000
160000
140000
120000
100000
80000
60000
40000
20000
0
Sre = 2,710 psi
125
375
675
975
1275
1575
1875
2175
2475
2775
3075
3375
3675
3975
4275
4575
4875
5175
5475
5775
6075
6375
6675
6975
7275
7575
7875
8175
8475
8775
9075
9375
9675
9975
10275
10575
10875
11175
11475
11775
Stress Bin (psi)
Note: 18 Day Monitoring Period

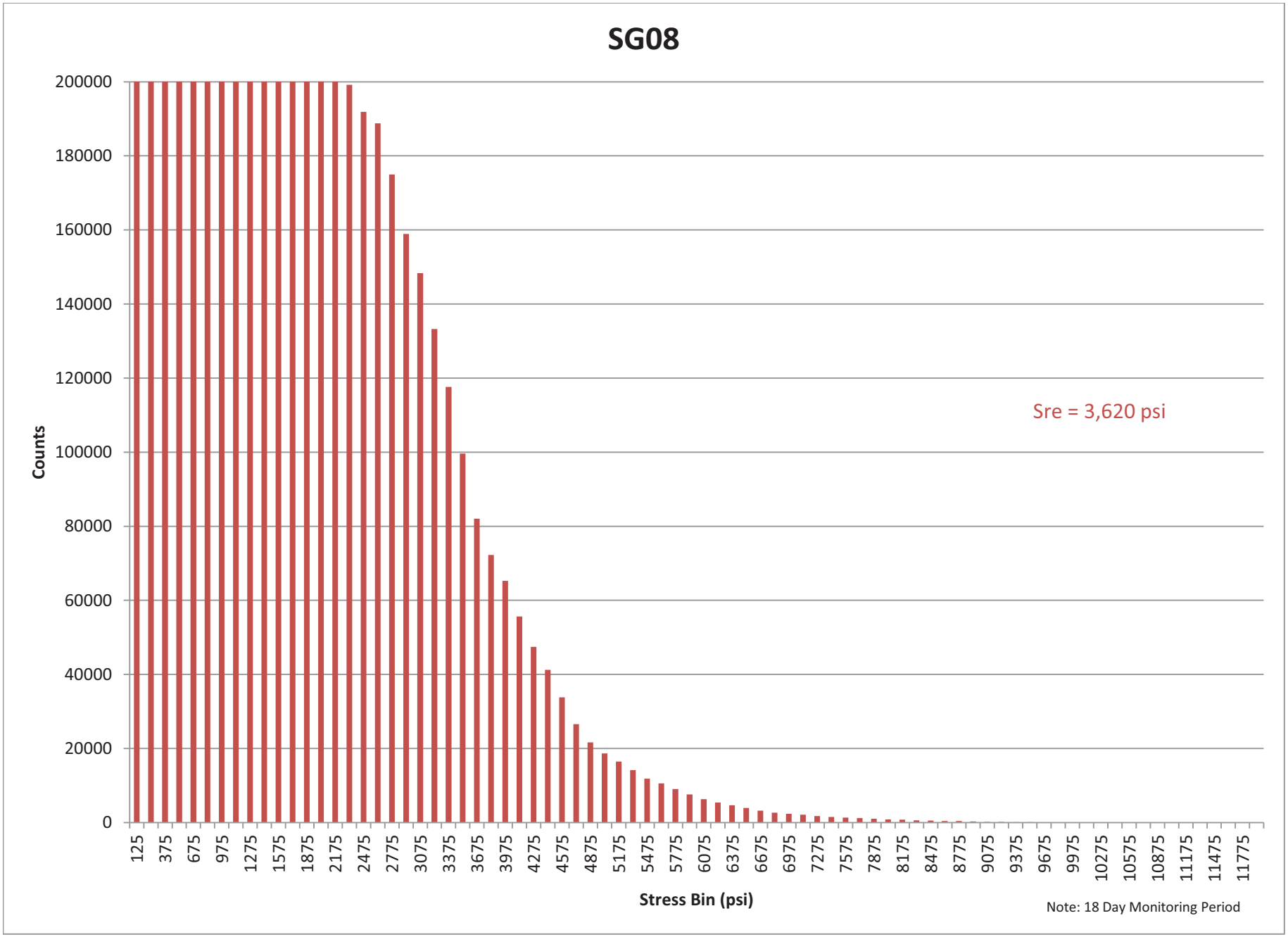
SG08
Counts
200000
180000
160000
140000
120000
100000
80000
60000
40000
20000
0
Sre = 3,620 psi
125
375
675
975
1275
1575
1875
2175
2475
2775
3075
3375
3675
3975
4275
4575
4875
5175
5475
5775
6075
6375
6675
6975
7275
7575
7875
8175
8475
8775
9075
9375
9675
9975
10275
10575
10875
11175
11475
11775
Stress Bin (psi)
Note: 18 Day Monitoring Period

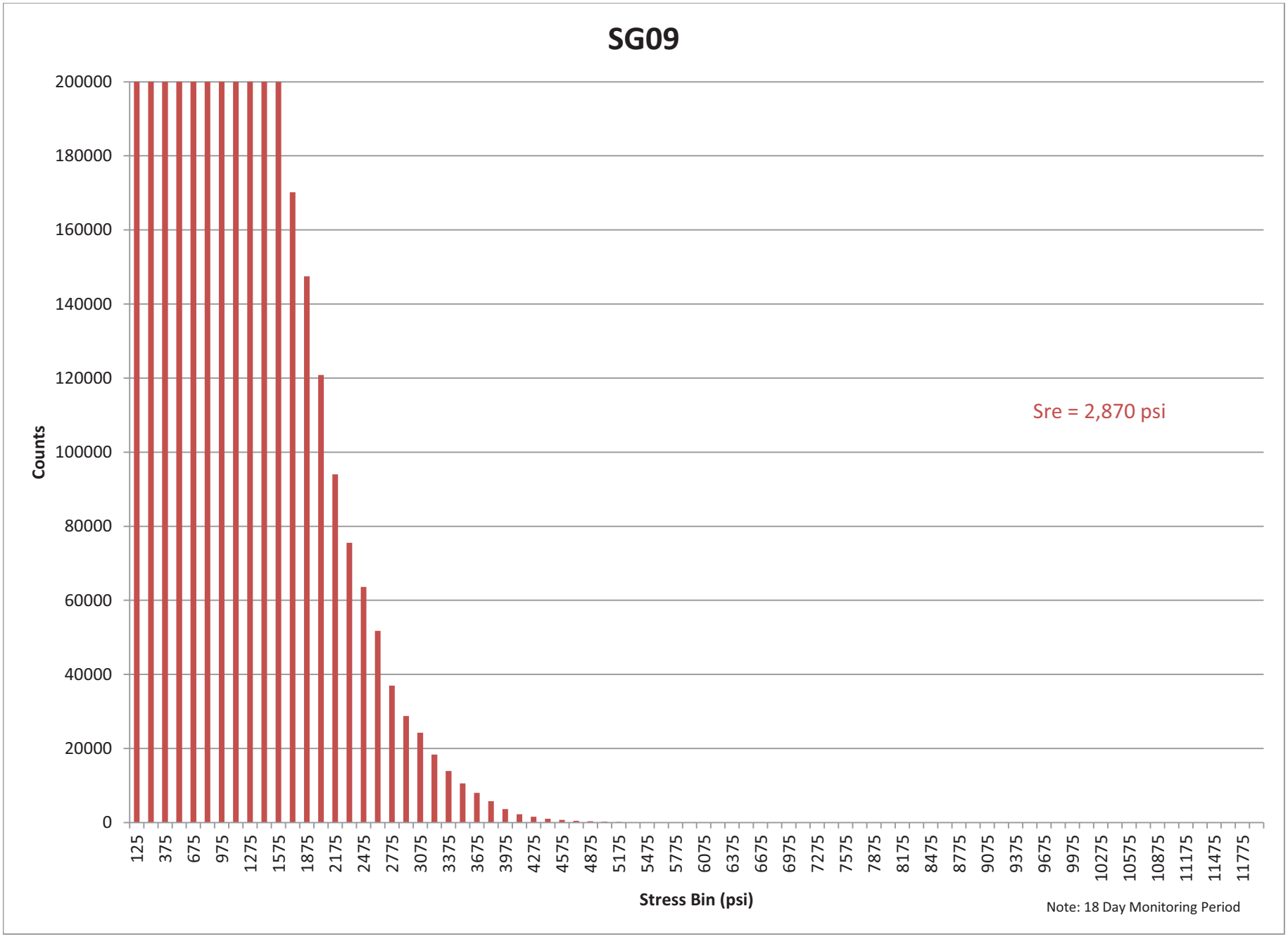
SG09
Counts
200000
180000
160000
140000
120000
100000
80000
60000
40000
20000
0
Sre = 2,870 psi
125
375
675
975
1275
1575
1875
2175
2475
2775
3075
3375
3675
3975
4275
4575
4875
5175
5475
5775
6075
6375
6675
6975
7275
7575
7875
8175
8475
8775
9075
9375
9675
9975
10275
10575
10875
11175
11475
11775
Stress Bin (psi)
Note: 18 Day Monitoring Period

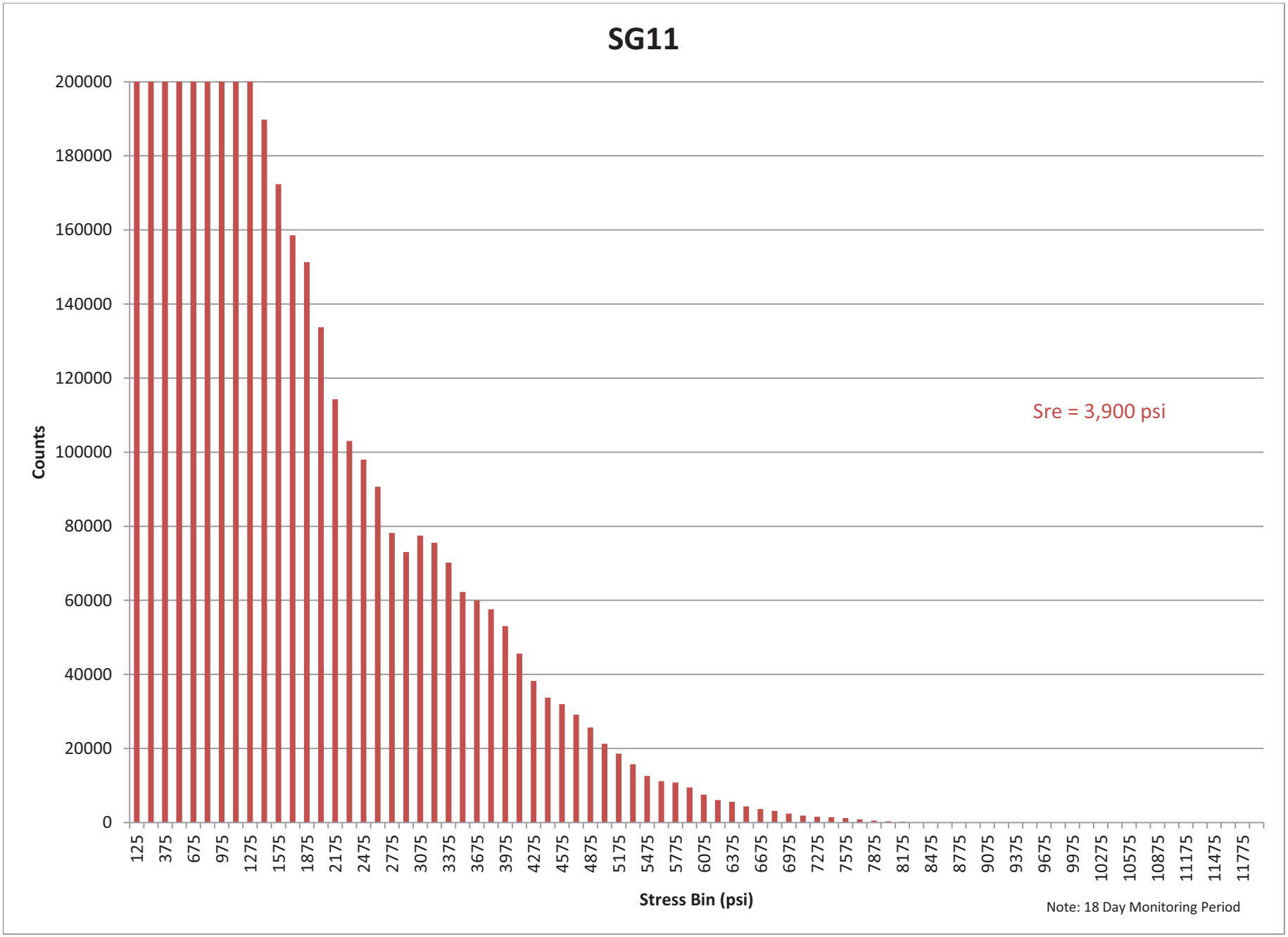
SG11
Counts
200000
180000
160000
140000
120000
100000
80000
60000
40000
20000
0
Sre = 3,900 psi
125
375
675
975
1275
1575
1875
2175
2475
2775
3075
3375
3675
3975
4275
4575
4875
5175
5475
5775
6075
6375
6675
6975
7275
7575
7875
8175
8475
8775
9075
9375
9675
9975
10275
10575
10875
11175
11475
11775
Stress Bin (psi)
Note: 18 Day Monitoring Period

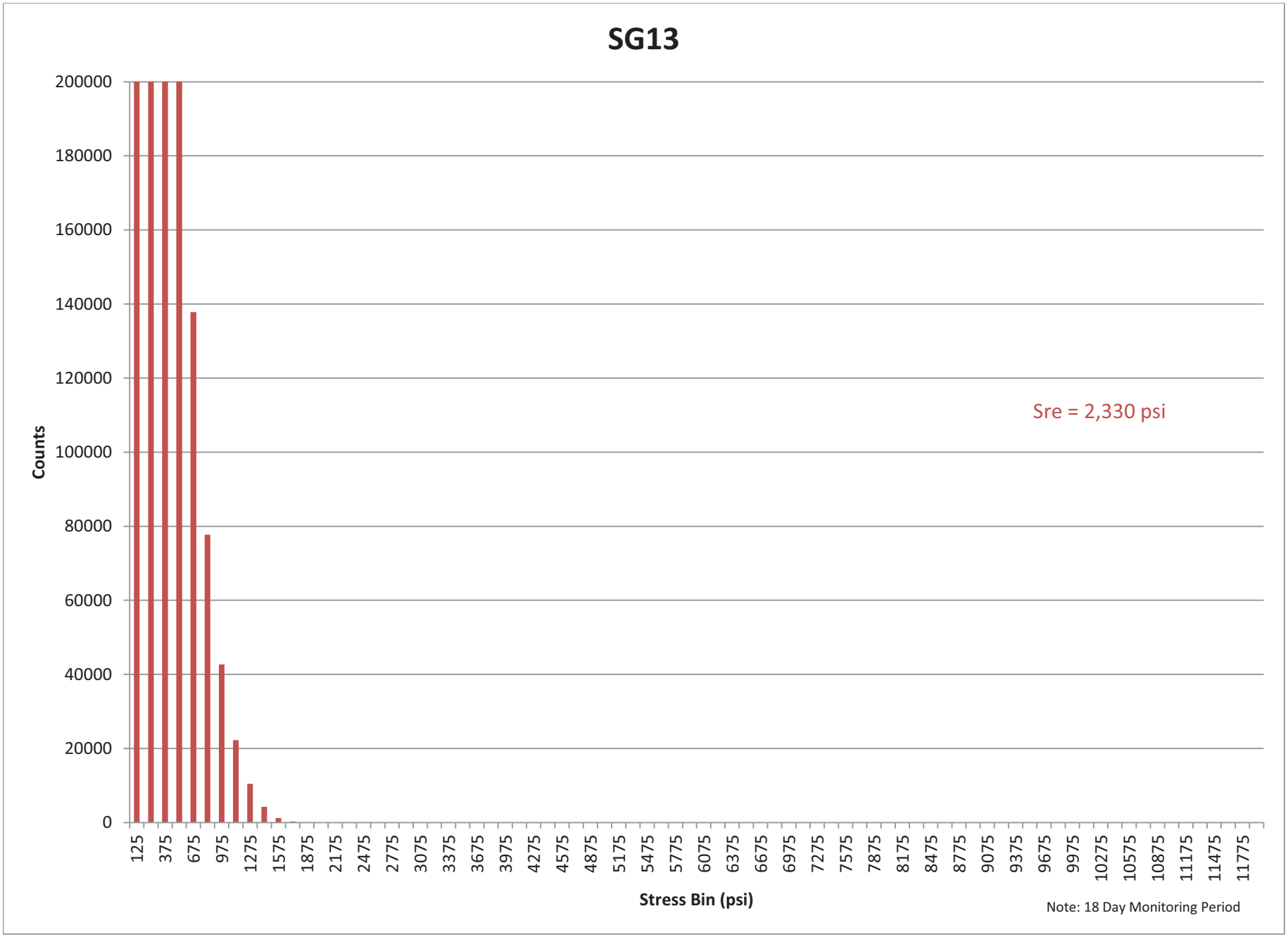
SG13
Counts
200000
180000
160000
140000
120000
100000
80000
60000
40000
20000
0
Sre = 2,330 psi
125
375
675
975
1275
1575
1875
2175
2475
2775
3075
3375
3675
3975
4275
4575
4875
5175
5475
5775
6075
6375
6675
6975
7275
7575
7875
8175
8475
8775
9075
9375
9675
9975
10275
10575
10875
11175
11475
11775
Stress Bin (psi)
Note: 18 Day Monitoring Period

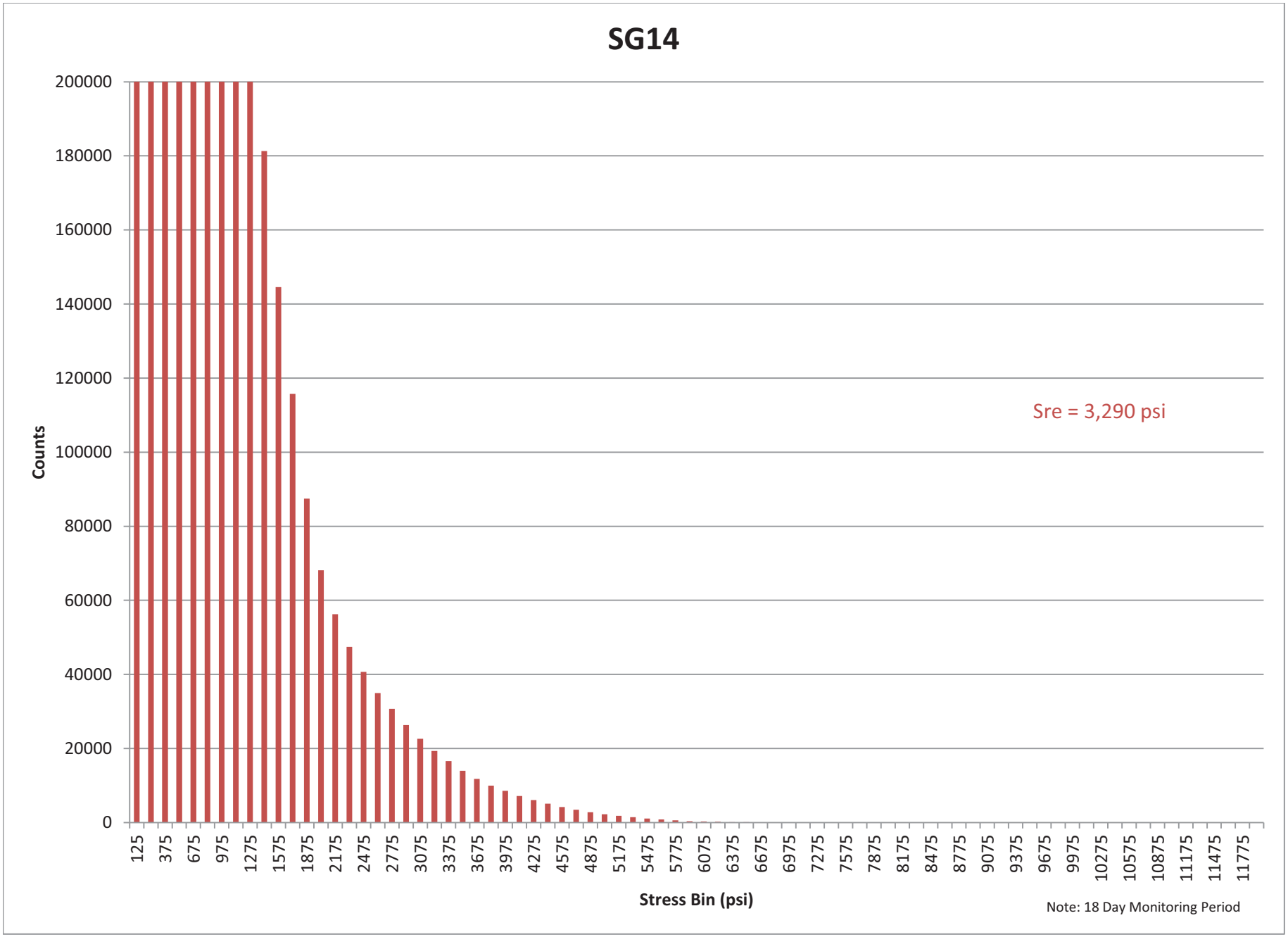
SG14
Counts
200000
180000
160000
140000
120000
100000
80000
60000
40000
20000
0
Sre = 3,290 psi
125
375
675
975
1275
1575
1875
2175
2475
2775
3075
3375
3675
3975
4275
4575
4875
5175
5475
5775
6075
6375
6675
6975
7275
7575
7875
8175
8475
8775
9075
9375
9675
9975
10275
10575
10875
11175
11475
11775
Stress Bin (psi)
Note: 18 Day Monitoring Period

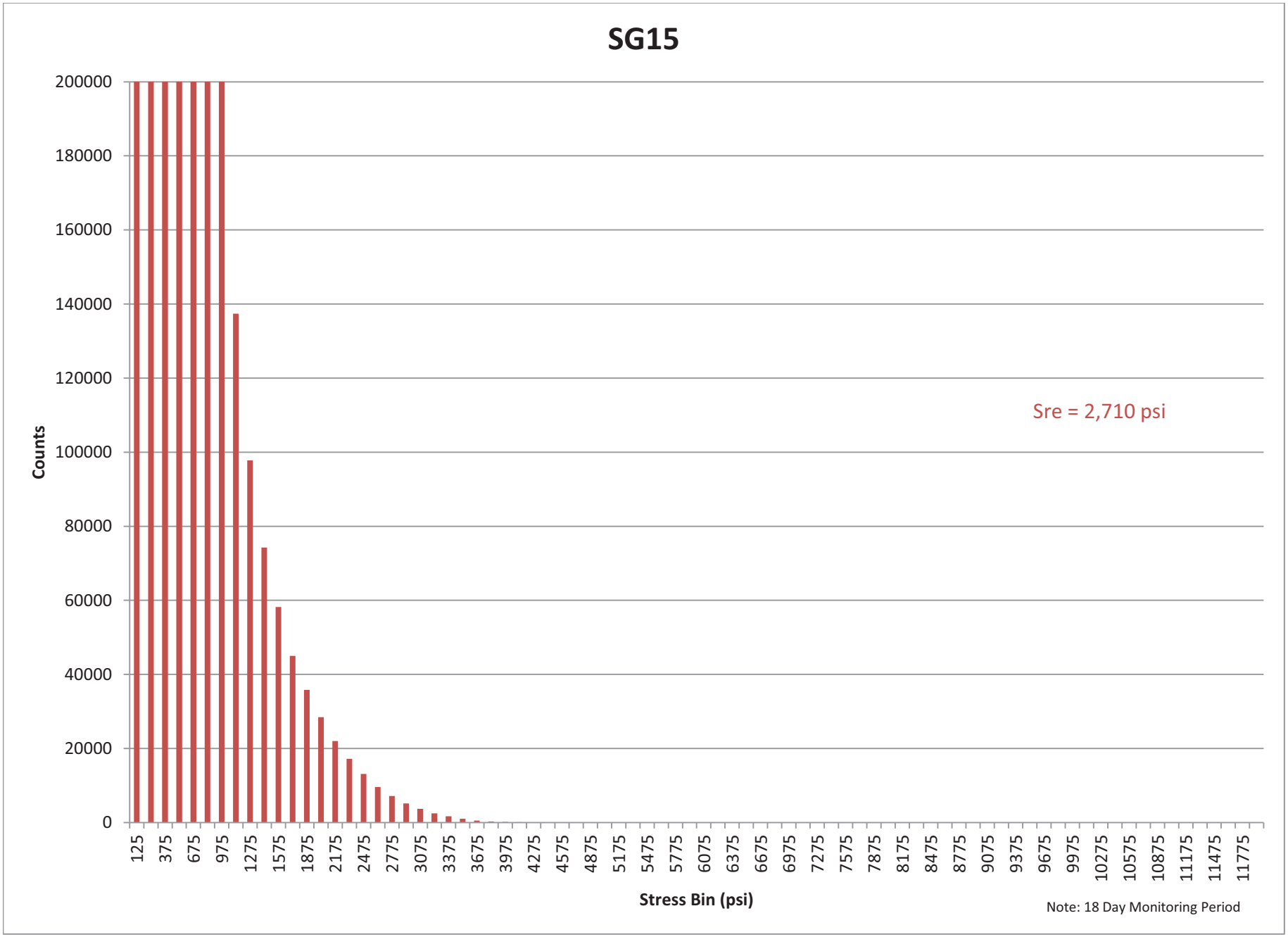
SG15
Counts
200000
180000
160000
140000
120000
100000
80000
60000
40000
20000
0
Sre = 2,710 psi
125
375
675
975
1275
1575
1875
2175
2475
2775
3075
3375
3675
3975
4275
4575
4875
5175
5475
5775
6075
6375
6675
6975
7275
7575
7875
8175
8475
8775
9075
9375
9675
9975
10275
10575
10875
11175
11475
11775
Stress Bin (psi)
Note: 18 Day Monitoring Period

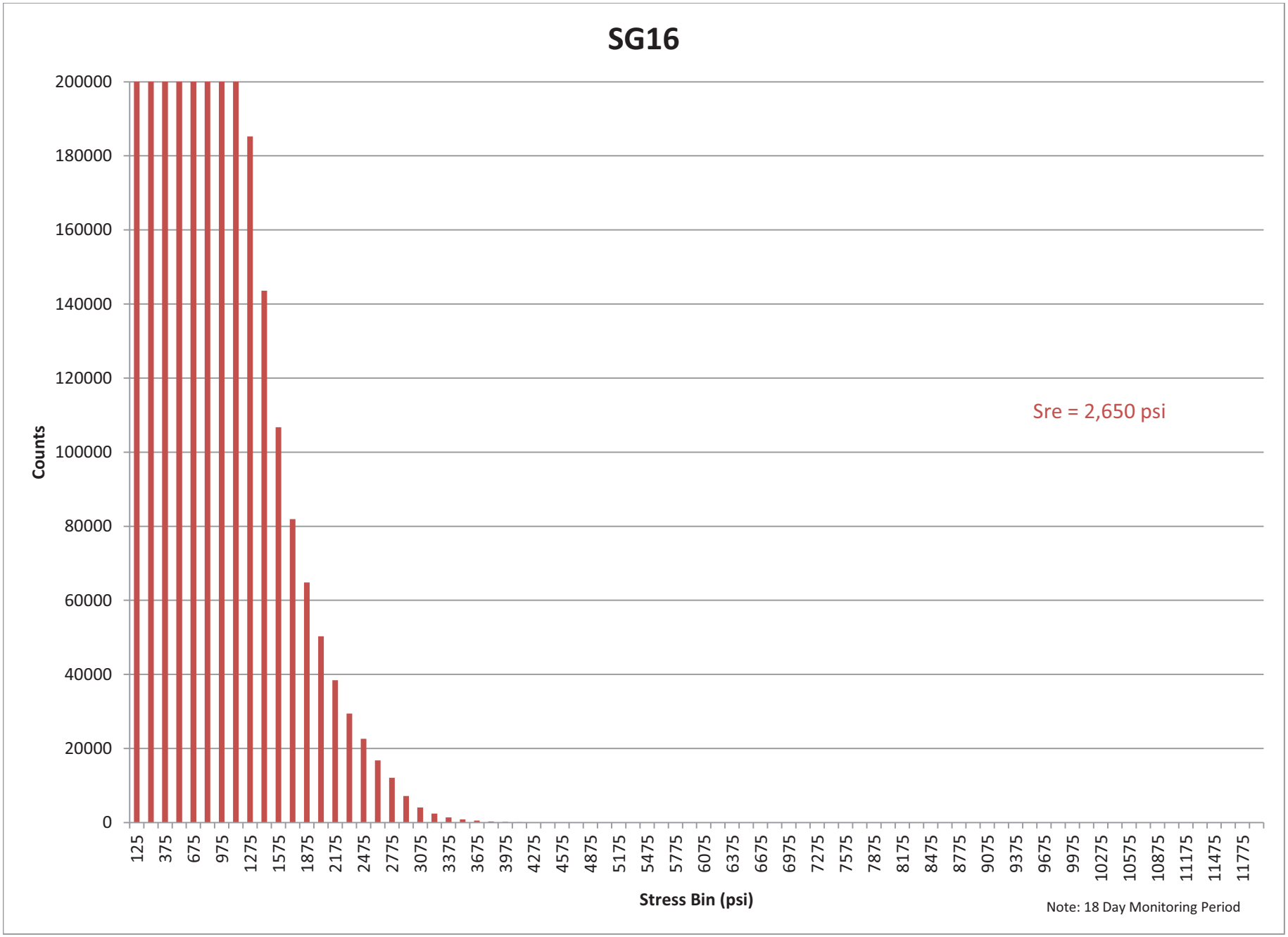
SG16
Counts
200000
180000
160000
140000
120000
100000
80000
60000
40000
20000
0
Sre = 2,650 psi
125
375
675
975
1275
1575
1875
2175
2475
2775
3075
3375
3675
3975
4275
4575
4875
5175
5475
5775
6075
6375
6675
6975
7275
7575
7875
8175
8475
8775
9075
9375
9675
9975
10275
10575
10875
11175
11475
11775
Stress Bin (psi)
Note: 18 Day Monitoring Period

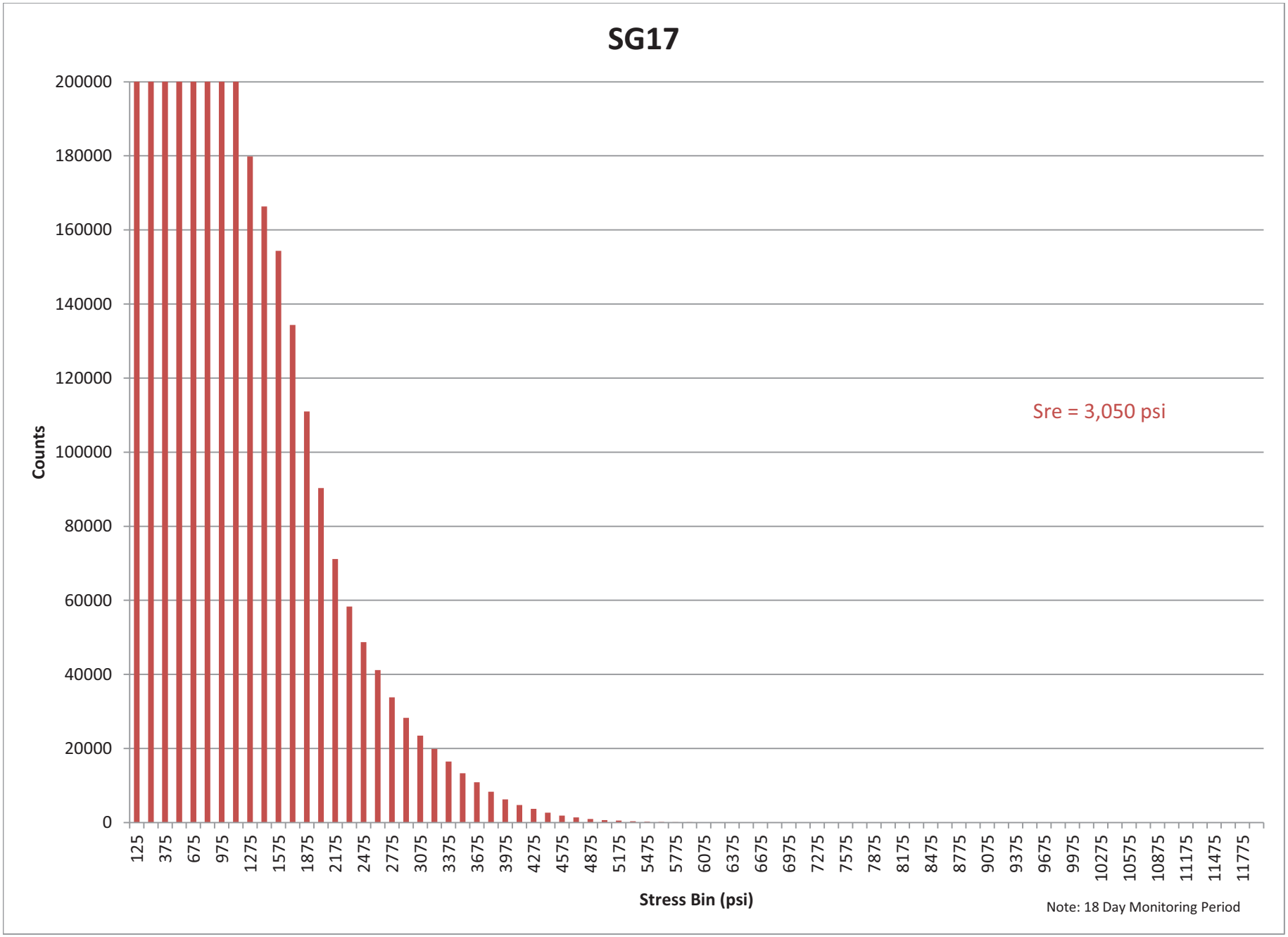
SG17
Counts
200000
180000
160000
140000
120000
100000
80000
60000
40000
20000
0
Sre = 3,050 psi
125
375
675
975
1275
1575
1875
2175
2475
2775
3075
3375
3675
3975
4275
4575
4875
5175
5475
5775
6075
6375
6675
6975
7275
7575
7875
8175
8475
8775
9075
9375
9675
9975
10275
10575
10875
11175
11475
11775
Stress Bin (psi)
Note: 18 Day Monitoring Period

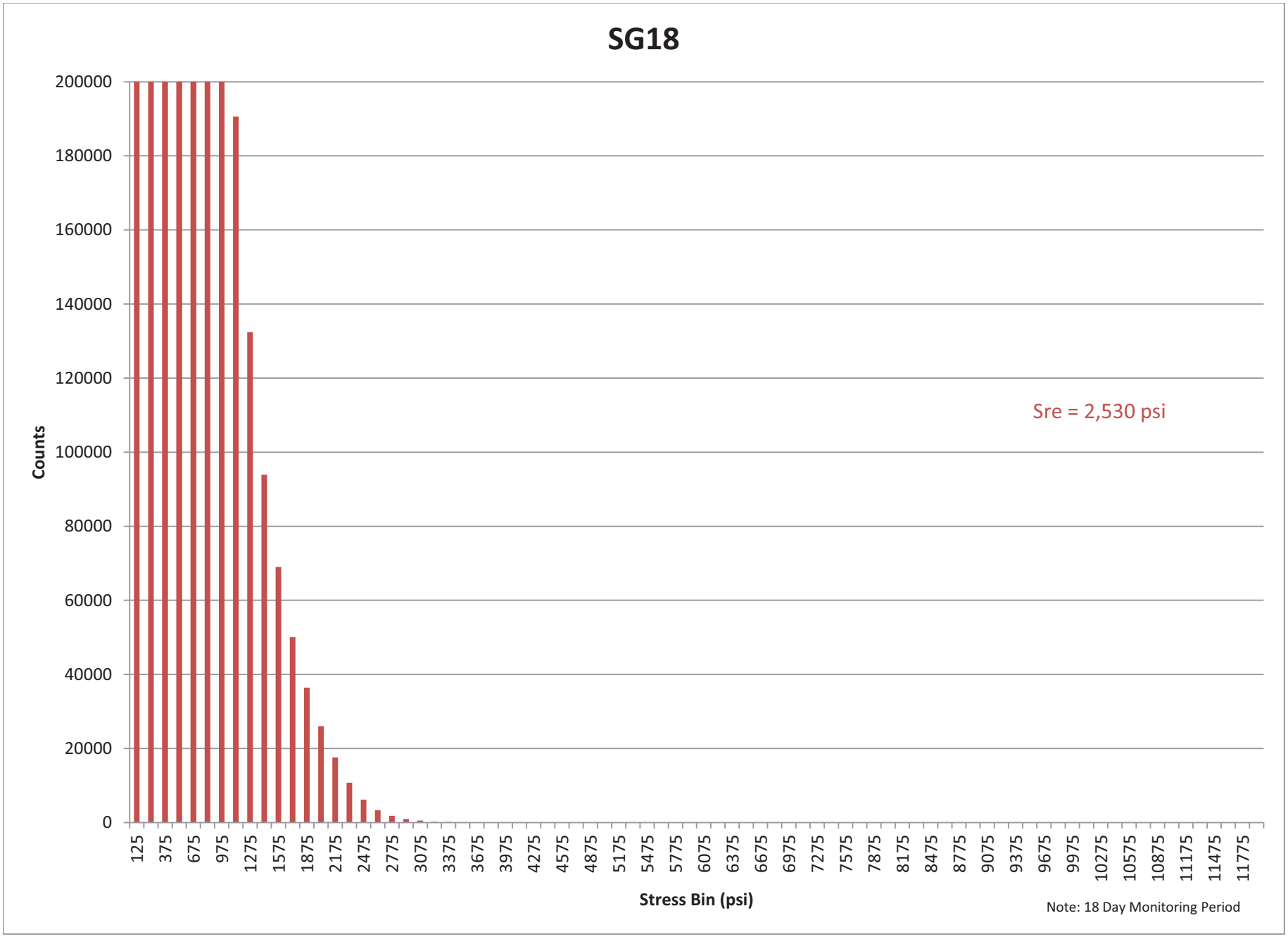
SG18
Counts
200000
180000
160000
140000
120000
100000
80000
60000
40000
20000
0
Sre = 2,530 psi
125
375
675
975
1275
1575
1875
2175
2475
2775
3075
3375
3675
3975
4275
4575
4875
5175
5475
5775
6075
6375
6675
6975
7275
7575
7875
8175
8475
8775
9075
9375
9675
9975
10275
10575
10875
11175
11475
11775
Stress Bin (psi)
Note: 18 Day Monitoring Period

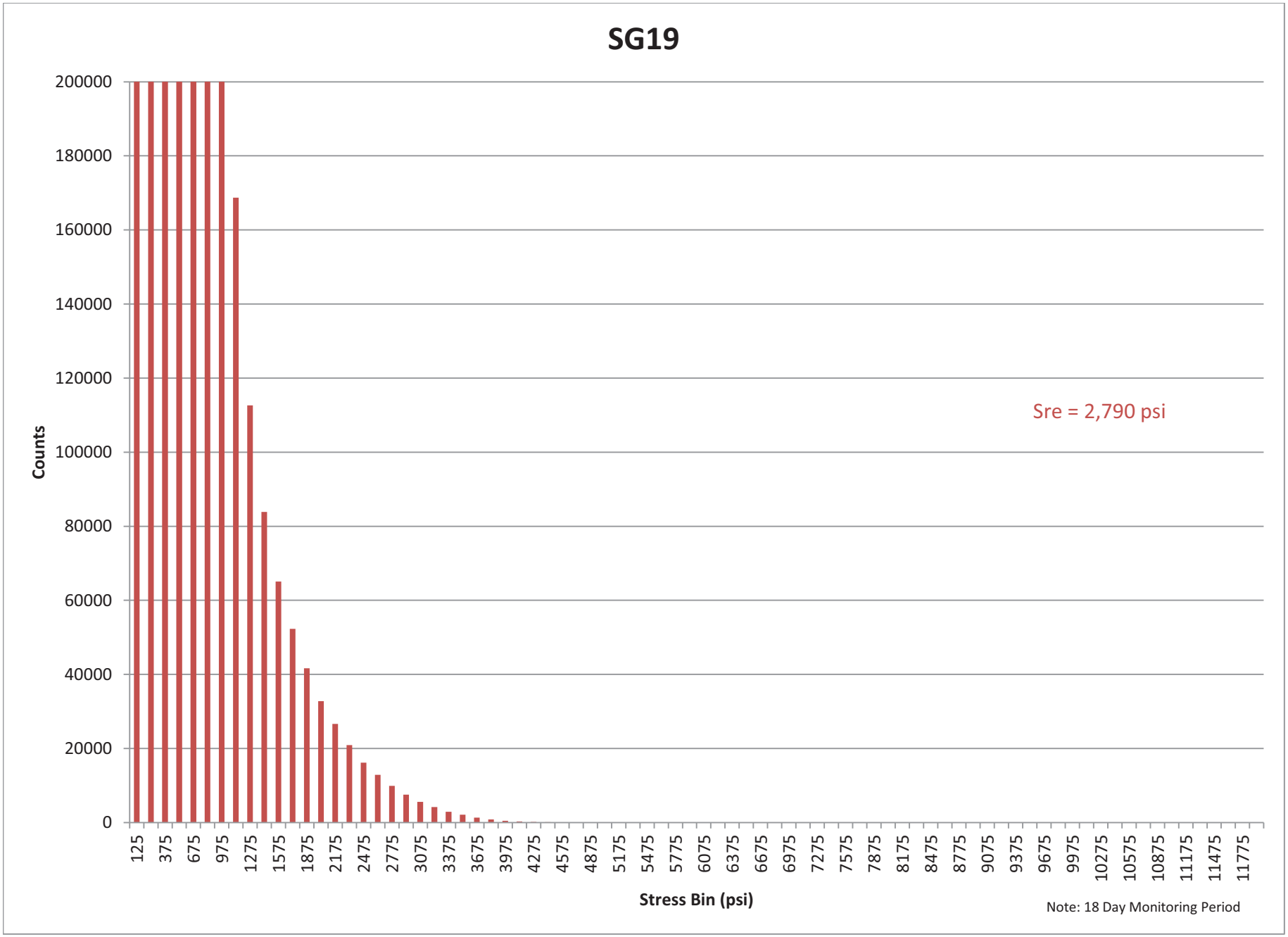
SG19
Counts
200000
180000
160000
140000
120000
100000
80000
60000
40000
20000
0
Sre = 2,790 psi
125
375
675
975
1275
1575
1875
2175
2475
2775
3075
3375
3675
3975
4275
4575
4875
5175
5475
5775
6075
6375
6675
6975
7275
7575
7875
8175
8475
8775
9075
9375
9675
9975
10275
10575
10875
11175
11475
11775
Stress Bin (psi)
Note: 18 Day Monitoring Period

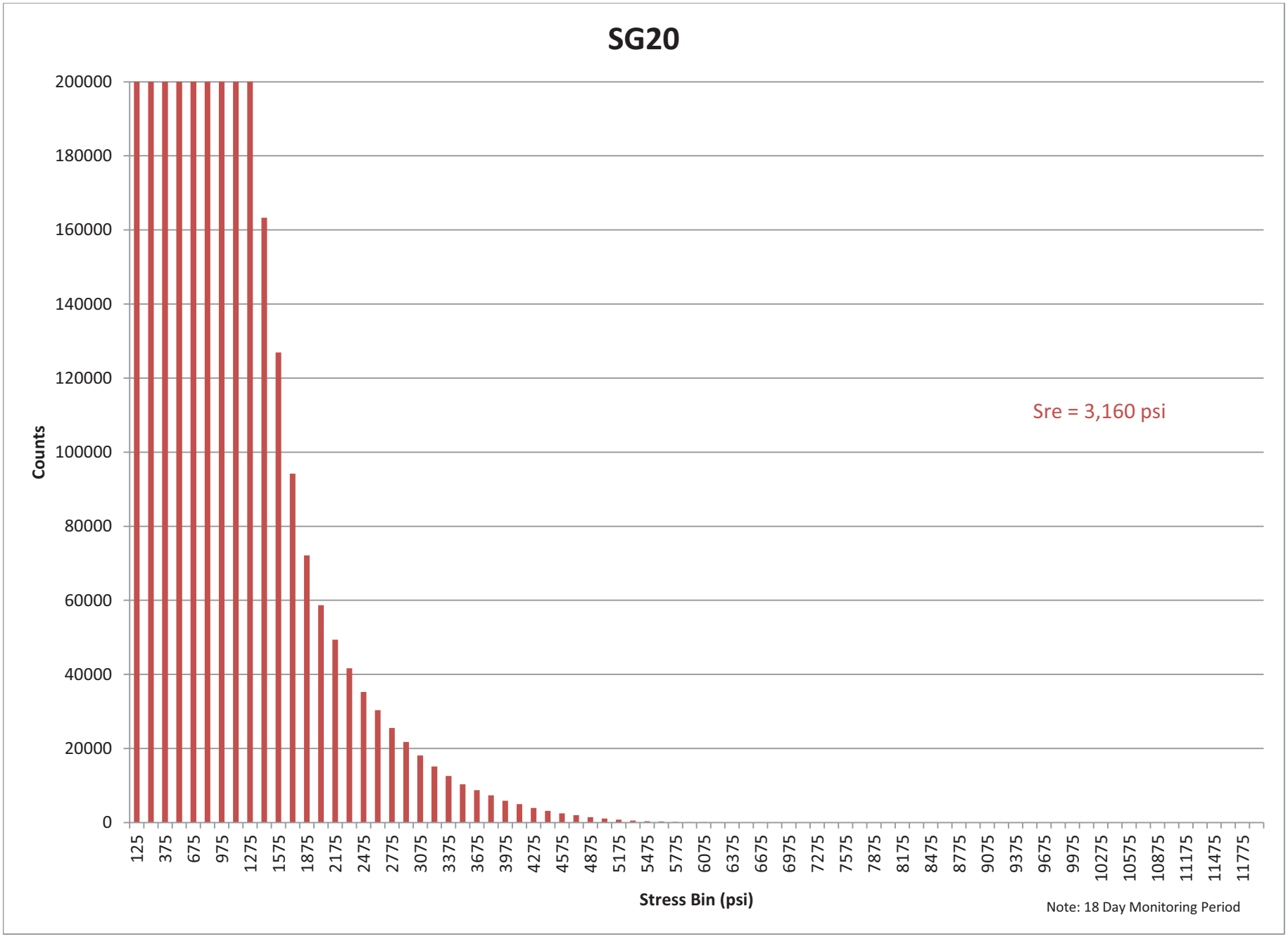
SG20
Counts
200000
180000
160000
140000
120000
100000
80000
60000
40000
20000
0
Sre = 3,160 psi
125
375
675
975
1275
1575
1875
2175
2475
2775
3075
3375
3675
3975
4275
4575
4875
5175
5475
5775
6075
6375
6675
6975
7275
7575
7875
8175
8475
8775
9075
9375
9675
9975
10275
10575
10875
11175
11475
11775
Stress Bin (psi)
Note: 18 Day Monitoring Period

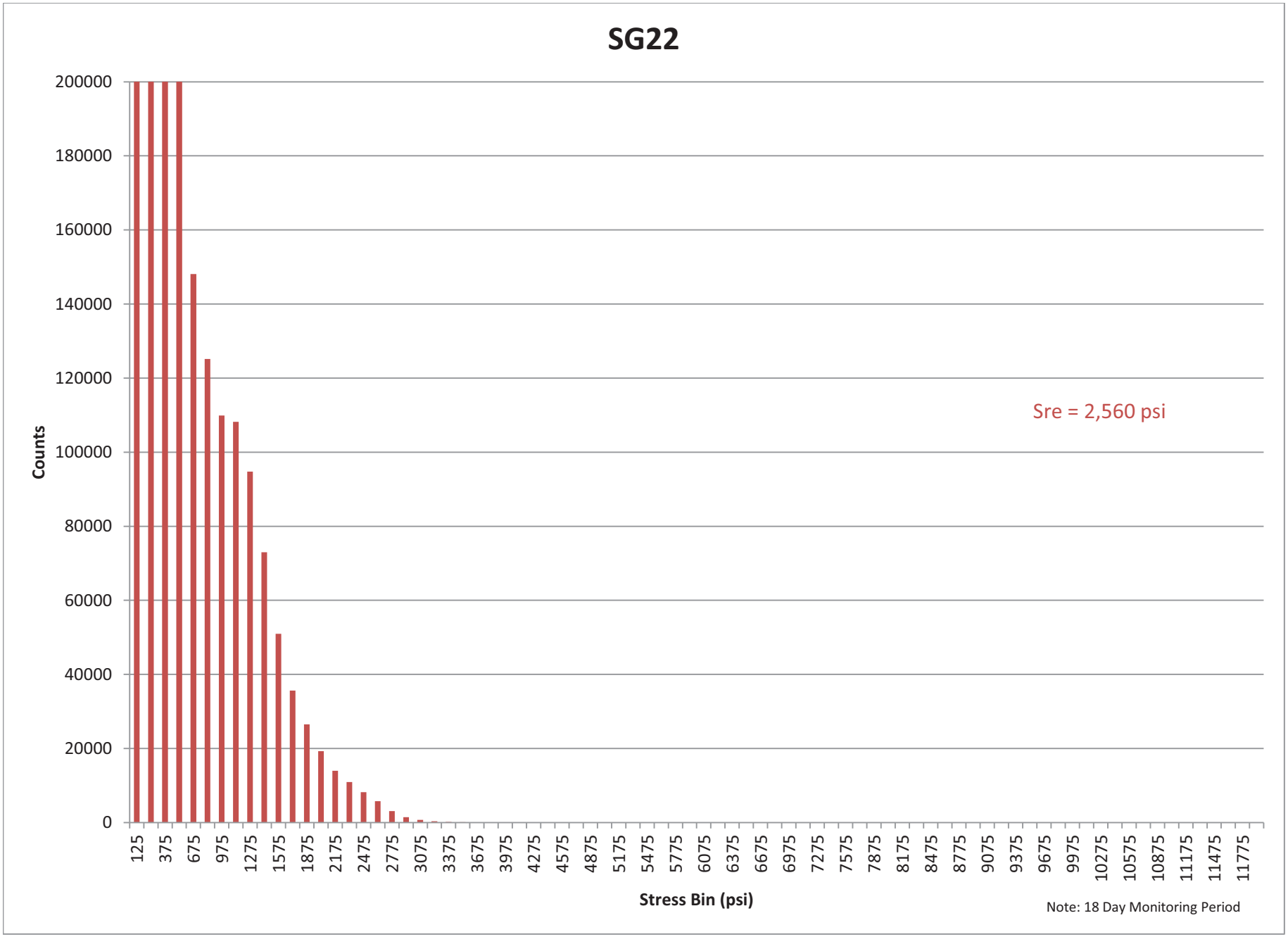
SG22
Counts
200000
180000
160000
140000
120000
100000
80000
60000
40000
20000
0
Sre = 2,560 psi
125
375
675
975
1275
1575
1875
2175
2475
2775
3075
3375
3675
3975
4275
4575
4875
5175
5475
5775
6075
6375
6675
6975
7275
7575
7875
8175
8475
8775
9075
9375
9675
9975
10275
10575
10875
11175
11475
11775
Stress Bin (psi)
Note: 18 Day Monitoring Period

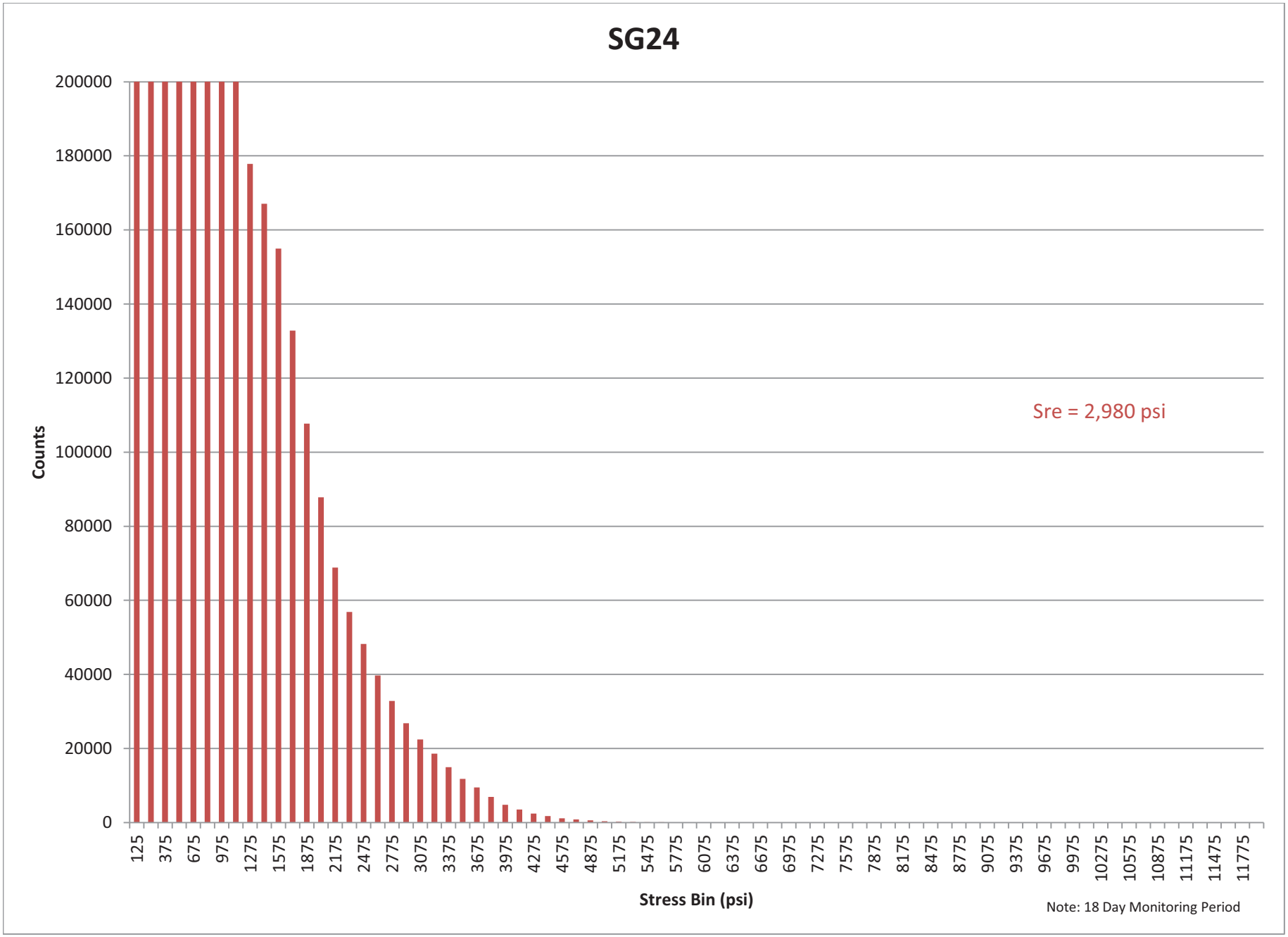
SG24
Counts
200000
180000
160000
140000
120000
100000
80000
60000
40000
20000
0
Sre = 2,980 psi
125
375
675
975
1275
1575
1875
2175
2475
2775
3075
3375
3675
3975
4275
4575
4875
5175
5475
5775
6075
6375
6675
6975
7275
7575
7875
8175
8475
8775
9075
9375
9675
9975
10275
10575
10875
11175
11475
11775
Stress Bin (psi)
Note: 18 Day Monitoring Period

WJE ENGINEERS ARCHITECTS MATERIALS SCIENTISTS

Appendix D

Preliminary Retrofit Drawings

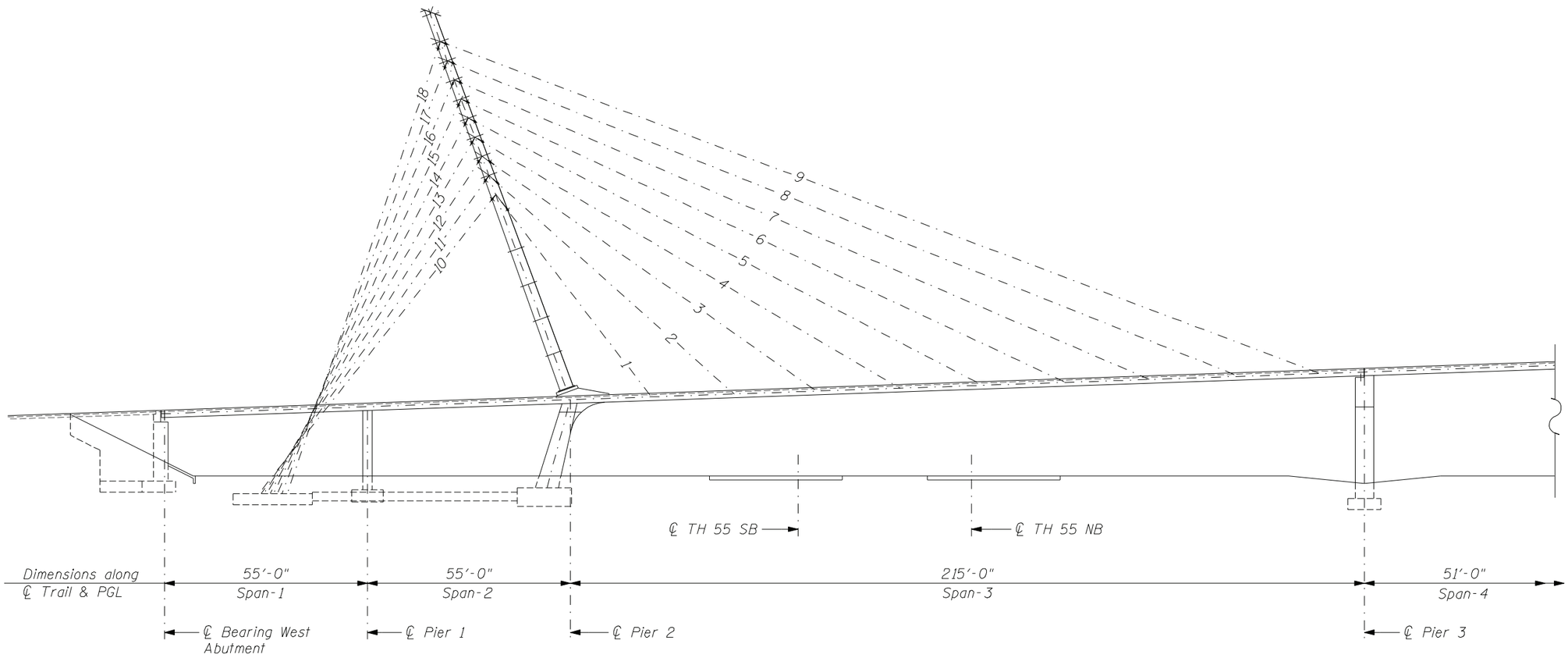

PARTIAL ELEVATION

WJE | ENGINEERS ARCHITECTS MATERIALS SCIENTISTS

Wiss, Janney, Elstner Associates, Inc.
330 Pfingsten Road
Northbrook, Illinois 60062
847.272.7400 tel | 847.291.9599 fax

Headquarters & Laboratories: Northbrook, Illinois
Atlanta | Austin | Boston | Chicago | Cleveland | Dallas | Denver | Detroit
Honolulu | Houston | Memphis | Minneapolis | New Haven | New York
Princeton | San Francisco | Seattle | Washington, D.C.

Seal

Consultants

Project

Martin Olav Sabo Pedestrian Bridge Over TH 55 and LRT Hennepin County Minneapolis, Minnesota

Owner

City of Minneapolis Department of Public Works

Mark	Date	Description

Project No.	2012.0901
Date	6/6/2012
Drawn	IMG
Checked	BJS
Scale	NTS

GENERAL ELEVATION

Sheet Title

Sheet No. **S-0**

DATE: 6/6/2012
FILENAME: p:\2012\0901-1000\2012.0901 - sabo bridge\drawings\retrofit plates\ELEVATION.dgn

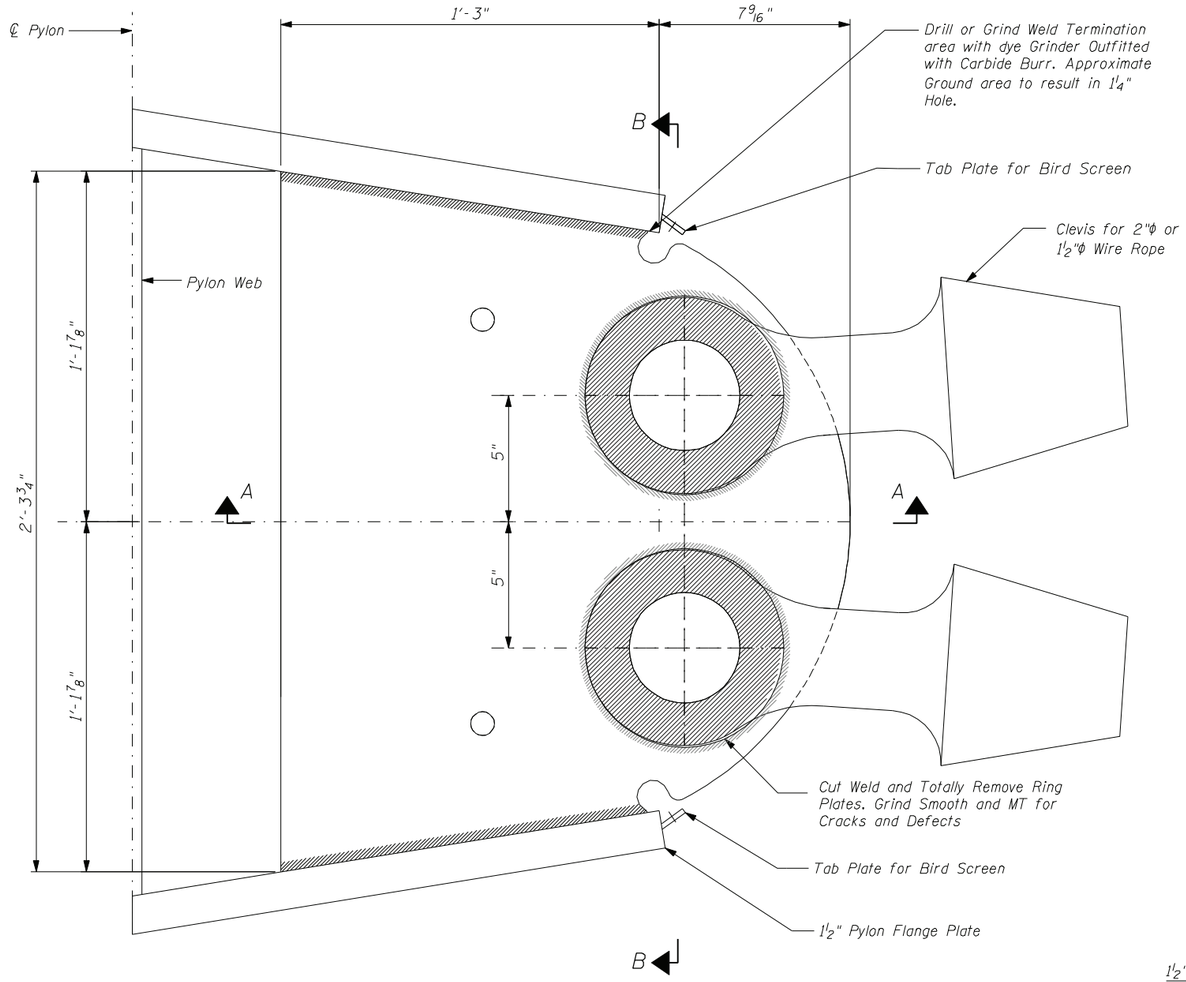

CABLE DIAPHRAGM PLATE 6

PROCEDURE:

1. Unload cable tension and disconnect clevises. Strap clevises to hold wire ropes in vicinity of the connection plate during strengthening retrofit.
2. Cut through fillet welds that connect ring plates to 3/4 in. diaphragm plate. Weld cutting may be accomplished using an angle grinder, sawzall, or carbide burrs in a dye grinder. Grinding operation shall totally remove the 4 ring plates. Following the removal, the 3/4 in. plate shall be ground smooth to a surface roughness of R_a 1000 or less. The ground 3/4 in. diaphragm plate must be magnetic particle tested (MT) to determine if any cracks or defects exist. Discuss cracks or defects with retrofit engineer for repair or modification.
3. If possible, drill a 1 in. diameter hole to initiate the modification at the weld termination. Following drilling, modify the weld terminations that connect the 3/4 in. diaphragm plate to the pylon flange plates by grinding. This grinding operation should be performed using a dye grinder outfitted with carbide ball-shaped burr to the shape shown. MT test the weld terminations for cracks or defects.
4. Blast clean all faying surfaces of strengthened connection and apply an approved AASHTO Class B coating.
5. Reference General Notes on S-2 for bolt location details.
6. Align a connection plate template on existing diaphragm plate for drilling. Drill all twelve 1-1/16 diameter holes in the plate center region of connection. Position the two 1-3/4 in. thick connection plates and fasten with 1 in. diameter bolts. Check alignment of pin holes through the 3 plates. If not perfectly aligned, pass hole cutter through holes to obtain proper pin placement.
7. Install the 4 connection angles between the connection plates and pylon flange plates. Clamp angles in position and begin drilling process. Pylon flange plate bolts will be countersunk to provide a smooth exterior surface. After all connection angle bolt holes are drilled, and installed in a snug tight condition, obtain approval of retrofit engineer. Remove connection angle bolts and connection angles. Clean off all contaminants due to drilling. Place sealant in gap between plates to totally fill gap. Reinstall the connection angles and bolts and tighten all bolts to snug tight condition.
8. Tighten all bolts to a minimum preload force of 51 kips.
9. Reinstall the wire rope clevises and jack proper lock-off force in the wire rope.

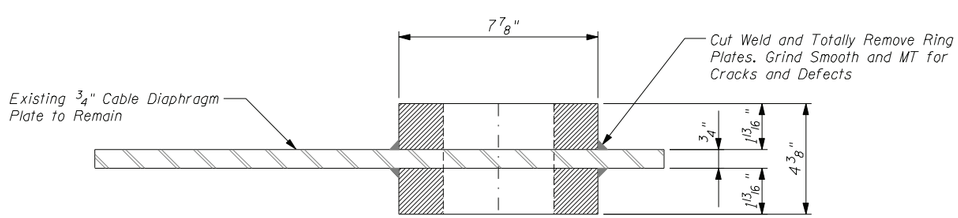

SECTION A-A

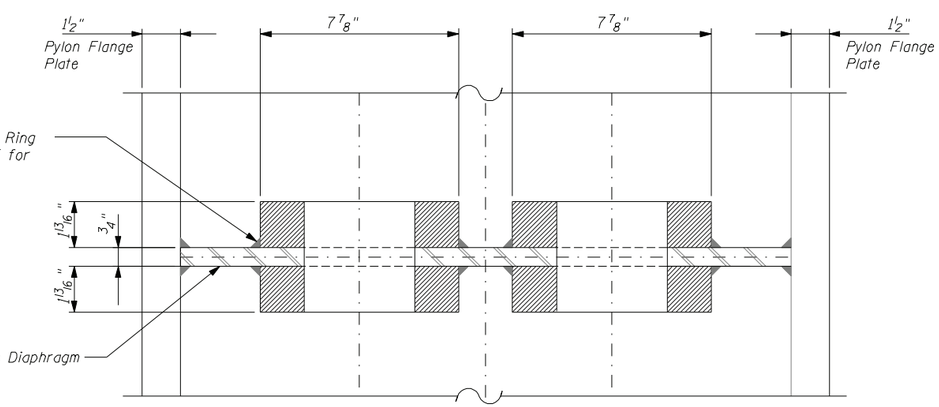

SECTION B-B

Legend:

Removal

WJE ENGINEERS ARCHITECTS MATERIALS SCIENTISTS

Wiss, Janney, Elstner Associates, Inc.
330 Pfingsten Road
Northbrook, Illinois 60062
847.272.7400 tel | 847.291.9599 fax

Headquarters & Laboratories: Northbrook, Illinois
Atlanta | Austin | Boston | Chicago | Cleveland | Dallas | Denver | Detroit
Honolulu | Houston | Memphis | Minneapolis | New Haven | New York
Princeton | San Francisco | Seattle | Washington, D.C.

Seal

Consultants

Project

Martin Olav Sabo Pedestrian Bridge Over TH 55 and LRT Hennepin County Minneapolis, Minnesota

Owner

City of Minneapolis Department of Public Works

Mark	Date	Description

Project No.	2012.0901
Date	6/6/2012
Drawn	IMG
Checked	BJS
Scale	NTS

Sheet Title: Cable Diaphragm Modification Plate 6

Sheet No.: Option 1 S-1

DATE: 6/6/2012
FILENAME: p:\2012\0901-10002012.0901 - sabo bridge\drawings\retrofit plates\Option 1 S-1PLATE6.dgn

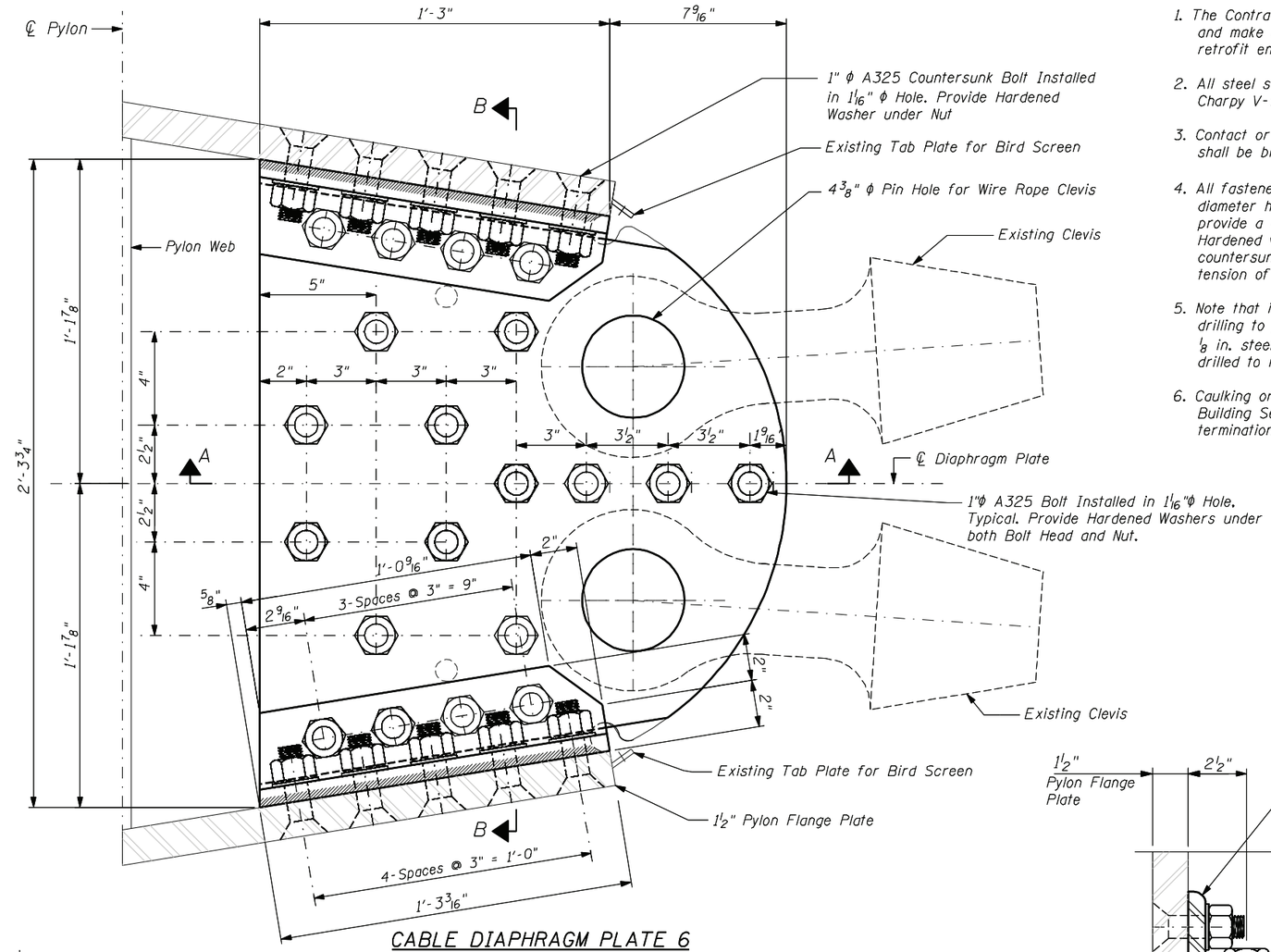

CABLE DIAPHRAGM PLATE 6

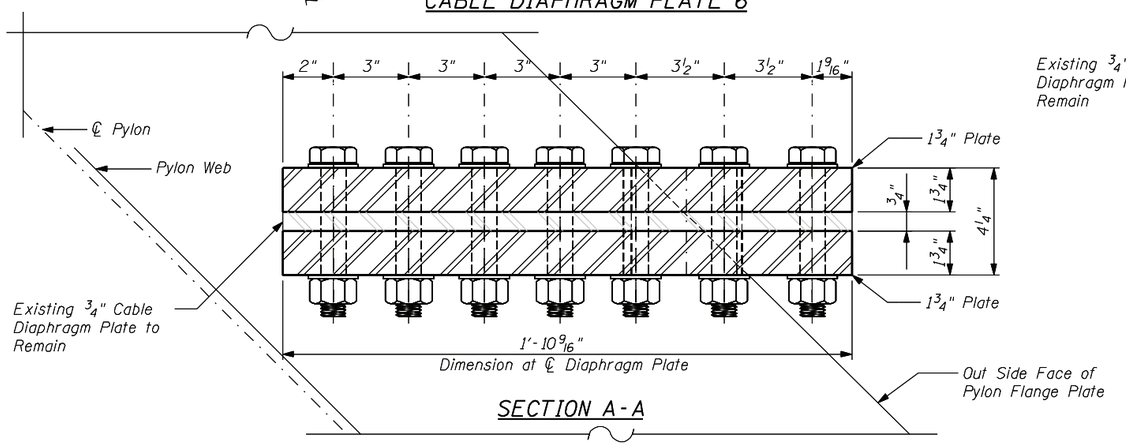

SECTION A-A

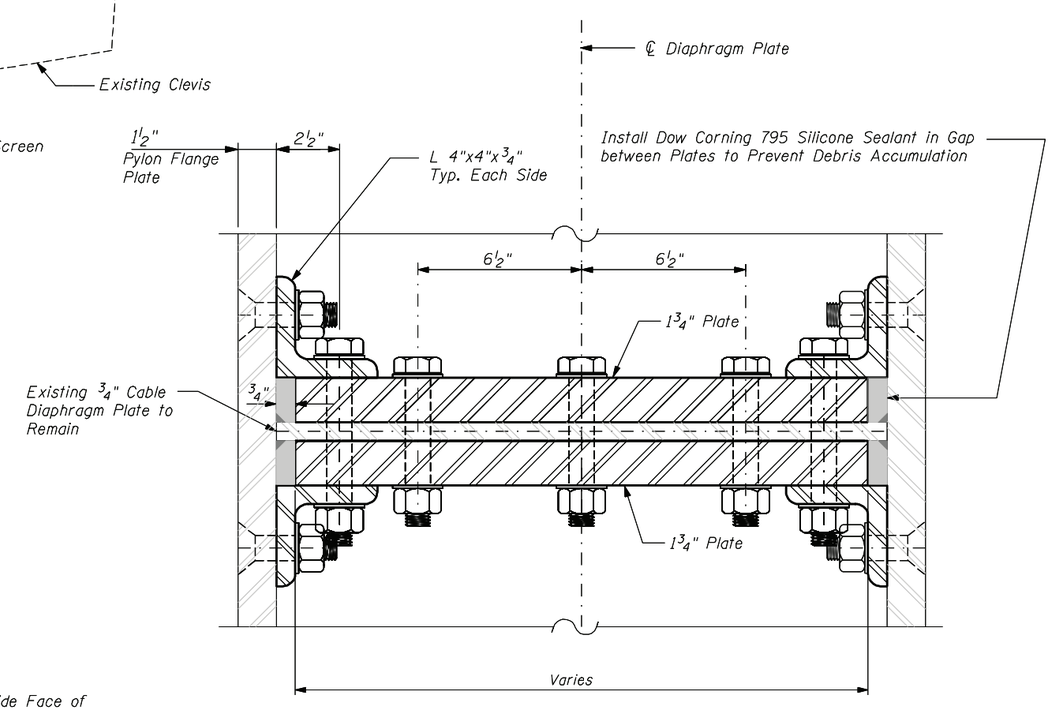

SECTION B-B

GENERAL NOTES:

1. The Contractor/Fabricator shall field verify all dimensions and details for the connection plates and make necessary adjustments prior to fabrication. All adjustments shall be approved by the retrofit engineer prior to fabrication.
2. All steel shall be AASHTO M270, Grade 50 (ASTM A709, Grade 50). All steel shall meet Zone 3 Charpy V-notch toughness requirements of 25 ft-lbs @ 10°F.
3. Contact or faying surfaces of the connection plates, pylon flange plates and connection angles shall be blast-cleaned and painted with an AASHTO Class B Coating.
4. All fasteners shall be AASHTO M164 (ASTM A325) bolts having a 1 in. diameter installed in 1 1/16 in. diameter holes. Bolts through the pylon flange plate shall have countersunk heads (A449 bolts) to provide a flush exterior surface. All other bolts will have standard heavy hex heads and nuts. Hardened washers shall be installed under bolt heads and nuts on standard bolts and under nuts on countersunk bolts. At completion of the connection, bolts shall be tightened to a minimum fastener tension of 51 kips.
5. Note that installation of connection plates and angles will require special alignment and match drilling to provide proper fit up. Templates of the connection plates should be fabricated using 1/8 in. steel plate for alignment and hole drilling. Connection angles will be positioned and match drilled to result in proper fit-up.
6. Caulking or sealant to fill gaps between plates shall be a high quality Dow Corning 795 Silicone Building Sealant or approved equal. Note the entire gap areas and around the existing weld terminations must be totally sealed.

WJE ENGINEERS ARCHITECTS MATERIALS SCIENTISTS

Wiss, Janney, Elstner Associates, Inc.
330 Pfingsten Road
Northbrook, Illinois 60062
847.272.7400 tel | 847.291.9599 fax

Headquarters & Laboratories: Northbrook, Illinois
Atlanta | Austin | Boston | Chicago | Cleveland | Dallas | Denver | Detroit
Honolulu | Houston | Memphis | Minneapolis | New Haven | New York
Princeton | San Francisco | Seattle | Washington, D.C.

Seal

Consultants

Project

Martin Olav Sabo Pedestrian Bridge Over TH 55 and LRT Hennepin County Minneapolis, Minnesota

Owner

City of Minneapolis Department of Public Works

Mark	Date	Description

Project No.	2012.0901
Date	6/6/2012
Drawn	IMG
Checked	BJS
Scale	NTS

Sheet Title

Cable Diaphragm Retrofit Plate 6

Sheet No.

Option 1 **S-2**

DATE: 6/6/2012
FILENAME: p:\2012\0901-1000\2012.0901 - sabo bridge\drawings\retrofit plates\Option 1 S-2 PLATE 6.dgn

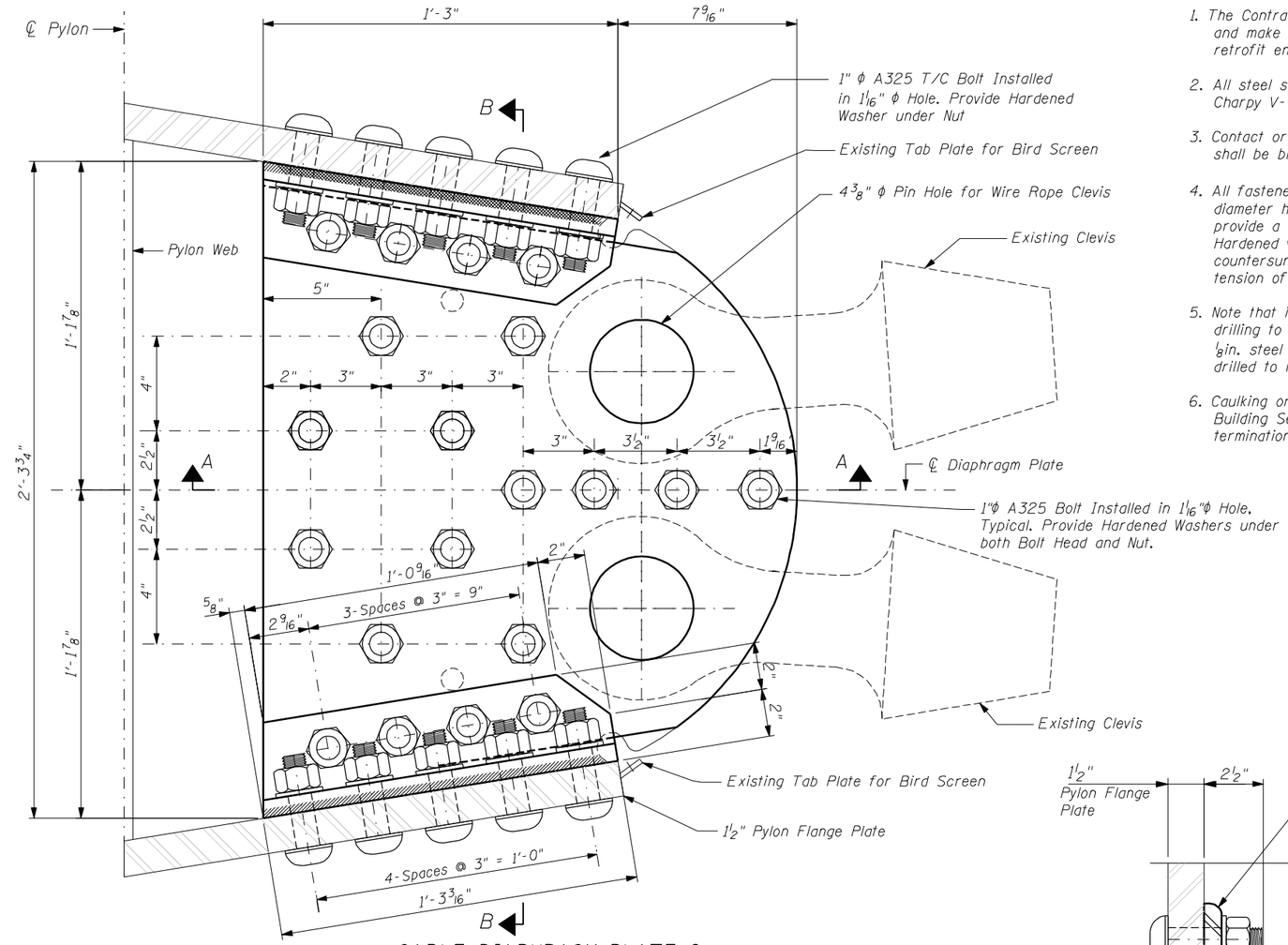

CABLE DIAPHRAGM PLATE 6

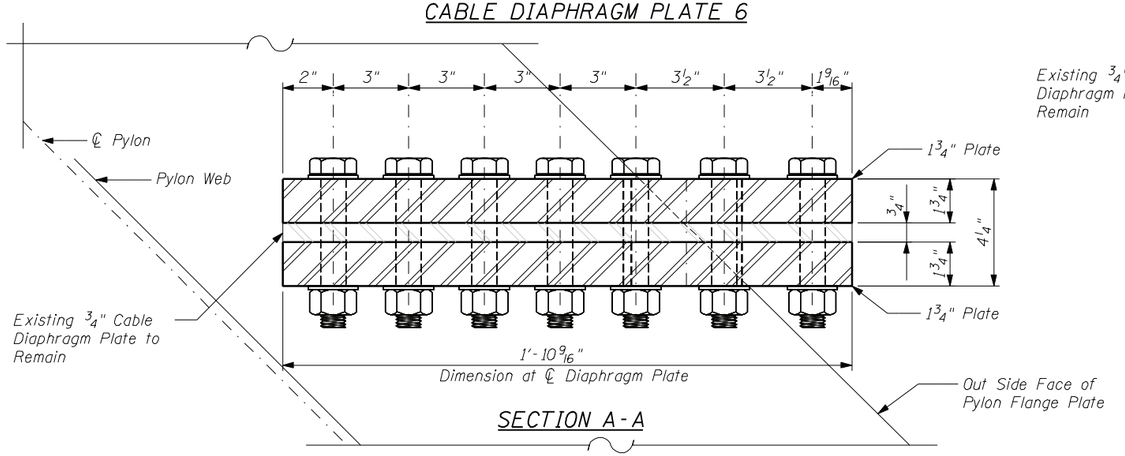

SECTION A-A

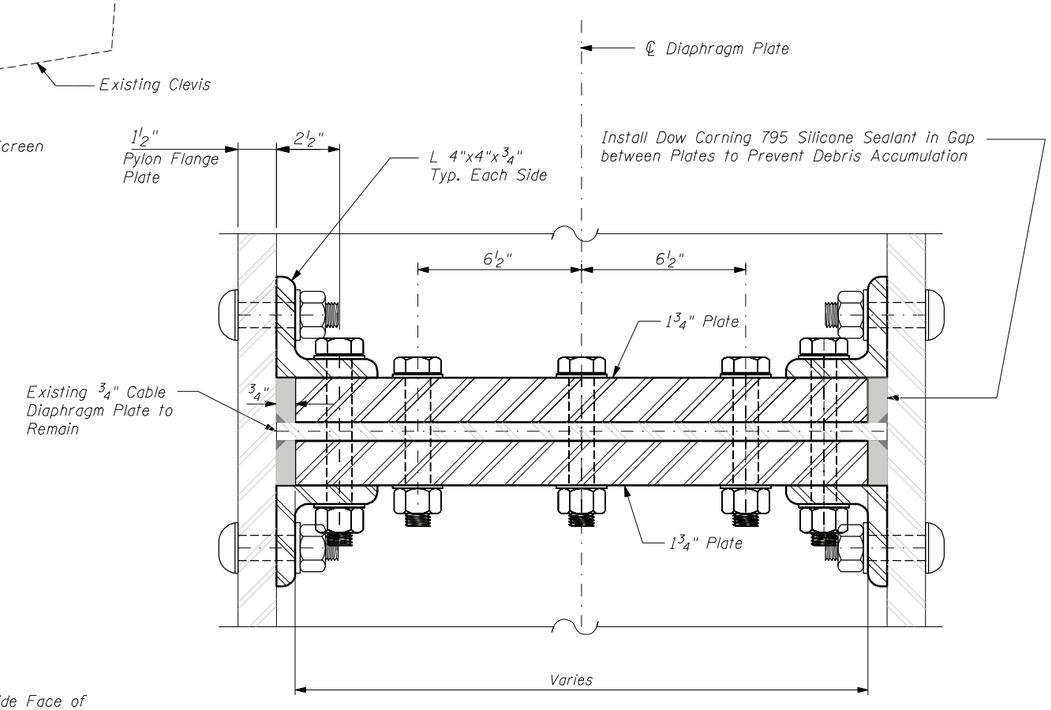

SECTION B-B

GENERAL NOTES:

1. The Contractor/Fabricator shall field verify all dimensions and details for the connection plates and make necessary adjustments prior to fabrication. All adjustments shall be approved by the retrofit engineer prior to fabrication.
2. All steel shall be AASHTO M270, Grade 50 (ASTM A709, Grade 50). All steel shall meet Zone 3 Charpy V-notch toughness requirements of 25 ft-lbs @ 10°F.
3. Contact or faying surfaces of the connection plates, pylon flange plates and connection angles shall be blast-cleaned and painted with an AASHTO Class B Coating.
4. All fasteners shall be AASHTO M164 (ASTM A325) bolts having a 1 in. diameter installed in 1 1/16 in. diameter holes. Bolts through the pylon flange plate shall have countersunk heads (A449 bolts) to provide a flush exterior surface. All other bolts will have standard heavy hex heads and nuts. Hardened washers shall be installed under bolt heads and nuts on standard bolts and under nuts on countersunk bolts. At completion of the connection, bolts shall be tightened to a minimum fastener tension of 51 kips.
5. Note that installation of connection plates and angles will require special alignment and match drilling to provide proper fit up. Templates of the connection plates should be fabricated using 1/8 in. steel plate for alignment and hole drilling. Connection angles will be positioned and match drilled to result in proper fit-up.
6. Caulking or sealant to fill gaps between plates shall be a high quality Dow Corning 795 Silicone Building Sealant or approved equal. Note the entire gap areas and around the existing weld terminations must be totally sealed.

WJE ENGINEERS ARCHITECTS MATERIALS SCIENTISTS

Wiss, Janney, Elstner Associates, Inc.
330 Pfingsten Road
Northbrook, Illinois 60062
847.272.7400 tel | 847.291.9599 fax

Headquarters & Laboratories: Northbrook, Illinois
Atlanta | Austin | Boston | Chicago | Cleveland | Dallas | Denver | Detroit
Honolulu | Houston | Memphis | Minneapolis | New Haven | New York
Princeton | San Francisco | Seattle | Washington, D.C.

Seal

Consultants

Project

Martin Olav Sabo Pedestrian Bridge Over TH 55 and LRT Hennepin County Minneapolis, Minnesota

Owner

City of Minneapolis Department of Public Works

Mark	Date	Description

Project No.	2012.0901
Date	6/6/2012
Drawn	IMG
Checked	BJS
Scale	NTS

Sheet Title

Cable Diaphragm Retrofit Plate 6

Sheet No.

Option 1

S-2A

DATE: 6/6/2012
FILENAME: p:\2012\0901-1000\2012.0901 - sabo bridge\drawings\retrofit plates\Option 1 S-2APLATE 6.dgn

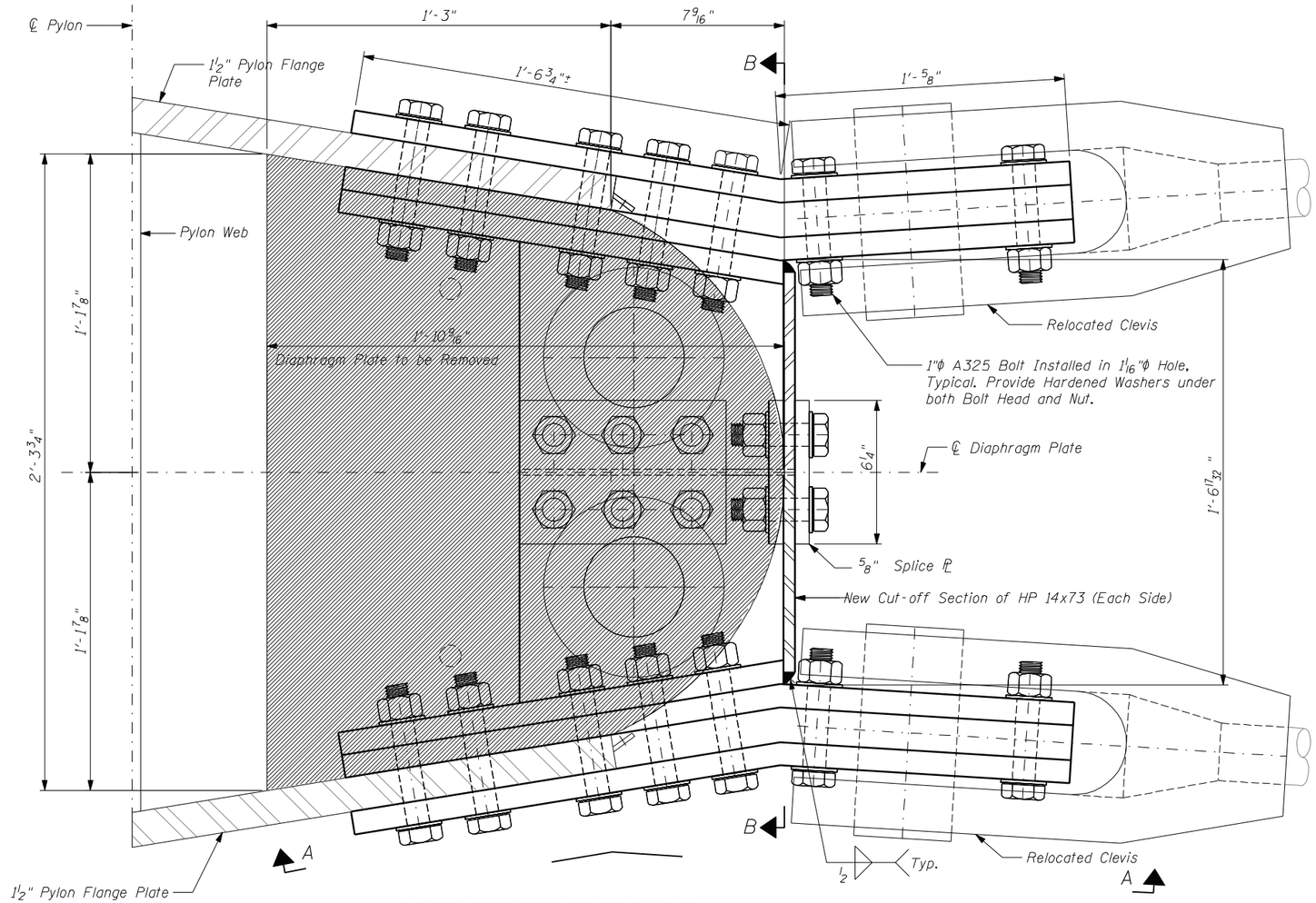

CABLE DIAPHRAGM PLATE 6

GENERAL NOTES:

1. The Contractor/Fabricator shall field verify all dimensions and details for the connection plates and make necessary adjustments prior to fabrication. All adjustments shall be approved by the retrofit engineer prior to fabrication.
2. All steel shall be AASHTO M270, Grade 50 (ASTM A709, Grade 50). All steel shall meet Zone 3 Charpy V-notch toughness requirements of 25 ft-lbs @ 10°F.
3. Contact or faying surfaces of the connection plates, pylon flange plates and connection angles shall be blast-cleaned and painted with an AASHTO Class B coating.
4. All fasteners shall be AASHTO M164 (ASTM A325) bolts having a 1 in. diameter installed in 1 1/16 in. diameter holes. Bolts through the pylon flange plate shall have countersunk heads (ASTM A449) in the exterior surface to provide a flush surface. All other bolts will have standard heavy hex heads and nuts. Hardened washers shall be installed under bolt heads and nuts on standard bolts and under nuts on countersunk bolts. At completion of the connection, bolts shall be tightened to a minimum fastener tension of 51 kips.
5. Note that connection plate bends must match at bend lines so that plates come in firm contact on either side of bend line. Once special alignment is achieved, match drill using 1/8 in. steel template for proper alignment of bolt holes and clevis pin hole. Similar template shall be used for drilling remaining holes in bracket and pylon flanges.
6. Weld inside flange plates to HP section.
7. After all holes are drilled and welding is completed and inspected in bracket halves, assemble bracket components to assure proper fit-up.
8. After completion of all hole drilling in the assembled field location and bolts installed in a snug tight condition, obtain approval of retrofit engineer. Remove connection material and clean-off all burrs and contaminants due to drilling. Reinstall the connection material and tighten all bolts to a snug tight condition.
9. Tighten all bolts to a minimum preload force of 51 kips.
10. Reinstall the wire rope clevises and jack the proper lock-off force in the wire cope.

Legend:
Removal

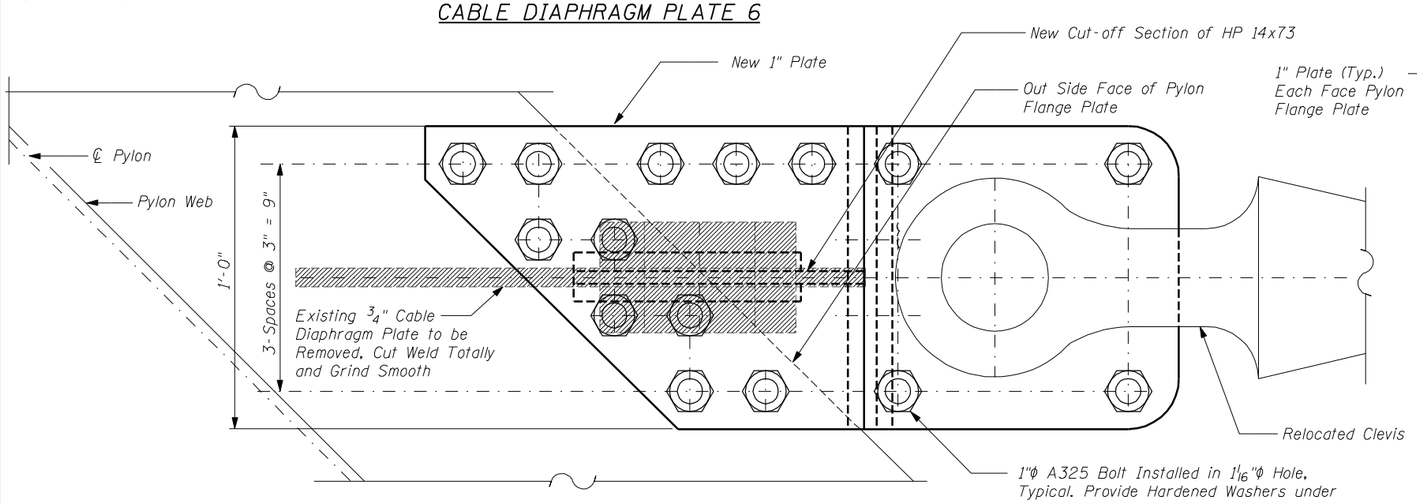

SECTION A-A

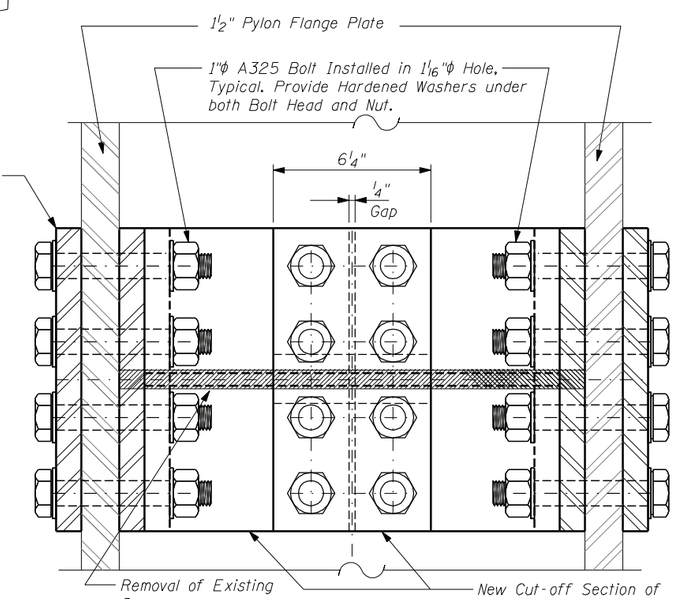

SECTION B-B

WJE ENGINEERS ARCHITECTS MATERIALS SCIENTISTS

Wiss, Janney, Elstner Associates, Inc.
330 Pfingsten Road
Northbrook, Illinois 60062
847.272.7400 tel | 847.291.9599 fax

Headquarters & Laboratories: Northbrook, Illinois
Atlanta | Austin | Boston | Chicago | Cleveland | Dallas | Denver | Detroit
Honolulu | Houston | Memphis | Minneapolis | New Haven | New York
Princeton | San Francisco | Seattle | Washington, D.C.

Seal

Consultants

Project

Martin Olav Sabo Pedestrian Bridge Over TH 55 and LRT Hennepin County Minneapolis, Minnesota

Owner

City of Minneapolis Department of Public Works

Mark	Date	Description

Project No.	2012.0901
Date	6/6/2012
Drawn	IMG
Checked	BJS
Scale	NTS

Sheet Title

Cable Diaphragm Retrofit Plate 6

Sheet No.

Option 2 **S-3**

DATE: 6/6/2012
FILENAME: p:\2012\0901-1000\2012.0901 - sabo bridge\drawings\retrofit plates\Option 2 S-3PLATE 6.dgn

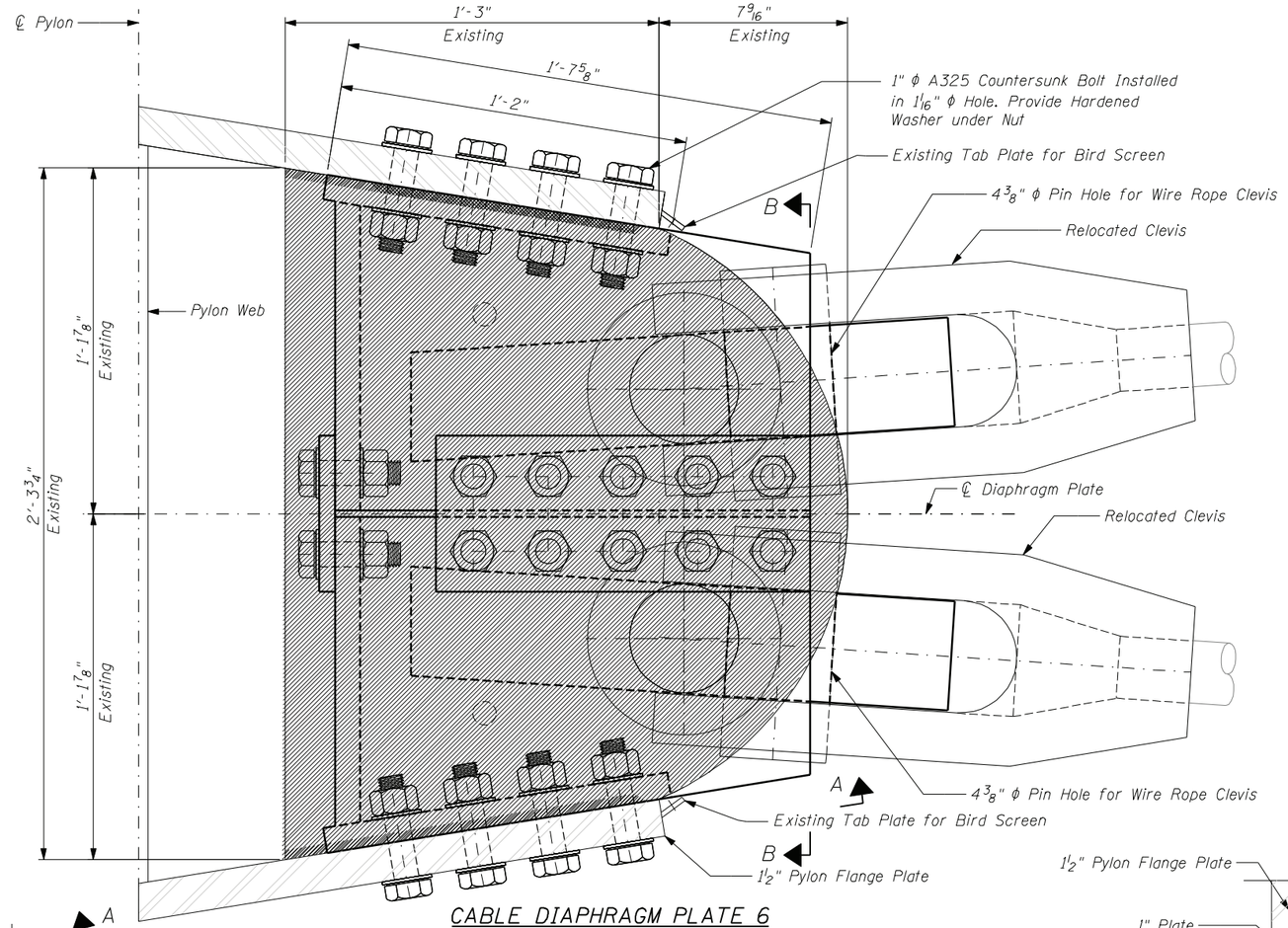

CABLE DIAPHRAGM PLATE 6

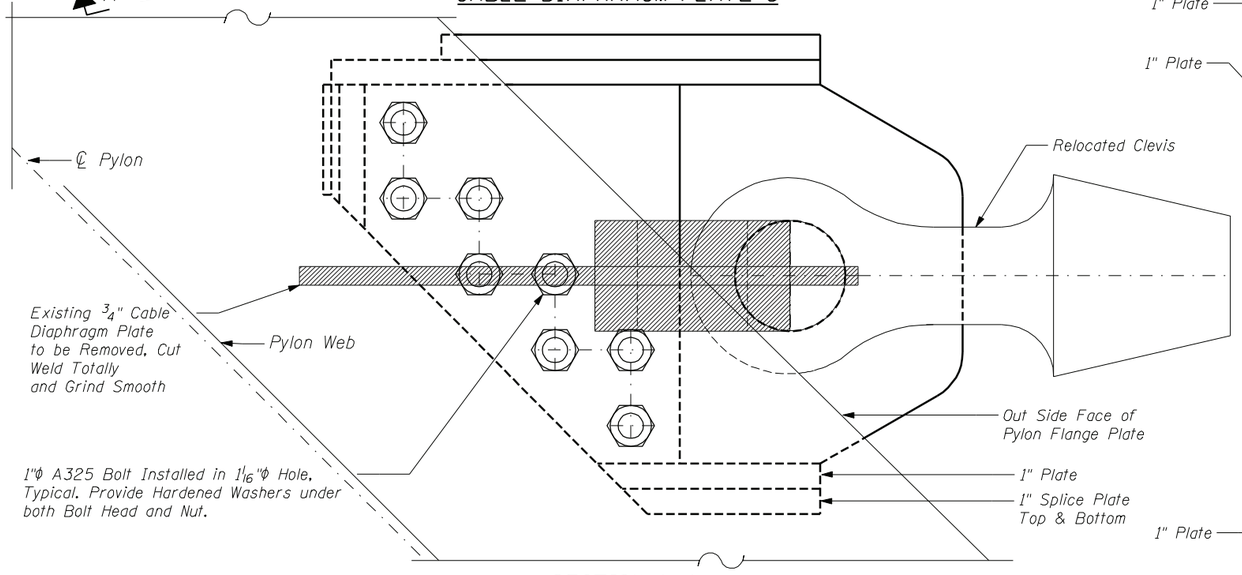

SECTION A-A

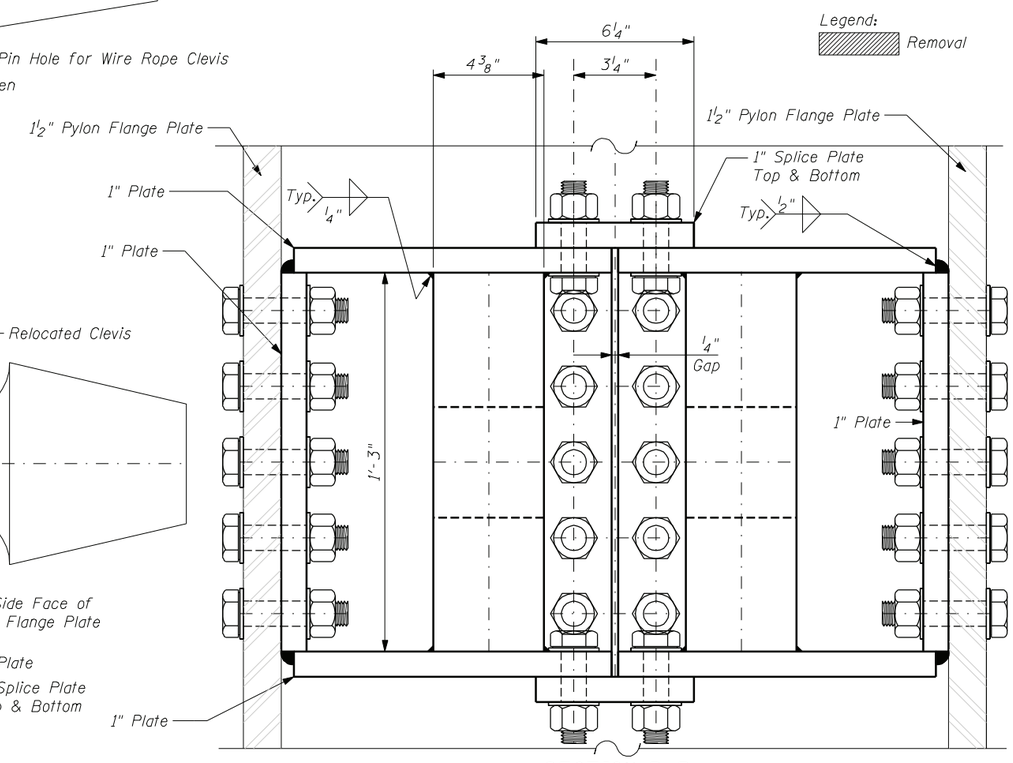

SECTION B-B

GENERAL NOTES:

1. The Contractor/Fabricator shall field verify all dimensions and details for the connection plates and make necessary adjustments prior to fabrication. All adjustments shall be approved by the retrofit engineer prior to fabrication.
2. All steel shall be AASHTO M270, Grade 50 (ASTM A709, Grade 50). All steel shall meet Zone 3 Charpy V-notch toughness requirements of 25 ft-lbs @ 10°F.
3. Contact or faying surfaces of the connection plates, pylon flange plates and connection angles shall be blast-cleaned and painted with an AASHTO Class B coating.
4. All fasteners shall be AASHTO M164 (ASTM A325) bolts having a 1 in. diameter installed in 1 1/16 in. diameter holes. Bolts through the pylon flange plate shall have countersunk heads (ASTM A449) in the exterior surface to provide a flush surface. All other bolts will have standard heavy hex heads and nuts. Hardened washers shall be installed under bolt heads and nuts on standard bolts and under nuts on countersunk bolts. At completion of the connection, bolts shall be tightened to a minimum fastener tension of 51 kips.
5. Note that the clevis plates must extend beyond the pylon flange plates to allow clearance for installing pins. Top and bottom plates extend only to the pylon flange plate line. Once special alignment is achieved, match drill using 1/8 in. steel template for proper alignment of bolt holes and clevis pin hole. Similar template shall be used for drilling remaining holes in bracket and pylon flanges.
6. Weld clevis plates to top and bottom plates with 1/4 in. fillet weld and minimum 6 in. length.
7. After all holes are drilled and welding is completed and inspected in bracket halves, assemble bracket components to assure proper fit-up.
8. After completion of all hole drilling in the assembled field location and bolts installed in a snug tight condition, obtain approval of retrofit engineer. Remove connection material and clean-off all burrs and contaminants due to drilling. Reinstall the connection material and tighten all bolts to a snug tight condition.
9. Tighten all bolts to a minimum preload force of 51 kips.
10. Reinstall the wire rope clevises and jack the proper lock-off force in the wire cope.

WJE ENGINEERS ARCHITECTS MATERIALS SCIENTISTS

Wiss, Janney, Elstner Associates, Inc.
330 Pfingsten Road
Northbrook, Illinois 60062
847.272.7400 tel | 847.291.9599 fax

Headquarters & Laboratories: Northbrook, Illinois
Atlanta | Austin | Boston | Chicago | Cleveland | Dallas | Denver | Detroit
Honolulu | Houston | Memphis | Minneapolis | New Haven | New York
Princeton | San Francisco | Seattle | Washington, D.C.

Seal

Consultants

Project

Martin Olav Sabo Pedestrian Bridge Over TH 55 and LRT Hennepin County Minneapolis, Minnesota

Owner

City of Minneapolis
Department of Public Works

Mark	Date	Description

Project No.	2012.0901
Date	6/6/2012
Drawn	IMG
Checked	BJS
Scale	NTS

Sheet Title

Cable Diaphragm Retrofit Plate 6

Sheet No.

Option 3 S-4

DATE: 6/6/2012
FILENAME: p:\2012\0901-1000\2012.0901 - sabo bridge\drawings\retrofit plates\Option 3 S-4PLATE.dgn